Impacts and Adaptation Subcomponent of the Climate Change Action Fund (CCAF)

Canada

Assessment of the Impact of Climate Variability and Change on the Reliability, Resiliency and Vulnerability of Complex Flood Protection Systems

Project no. A145

Slobodan P. Simonovic, Professor
Department of Civil and Environmental Engineering
The University of Western Ontario
London, ON
N6A 5B9

London, ON
June 2001

Project participants:

Dr. Lanhai Li, Postdoctoral Fellow, Department of Civil and Environmental Engineering, University of Western Ontario
Mr. Sajjad Ahmad, PhD candidate, Department of Civil and Environmental Engineering, University of Western Ontario
Mr. Sandu Karampul, Research assistant, Department of Civil and Geological Engineering, University of Manitoba

Starting date: April 1, 1999

Ending date: March 31, 2001

Project summary:

An original modeling framework (DYHAM*)* for assessment of climate variation and change impacts on the performance of complex flood protection system has been developed and tested using the Red River basin (Manitoba) as a case study. Modeling framework allows for evaluation of different climate change scenarios generated by the global climate models. Temperature and precipitation are used as the main factors affecting flood flow generation. System dynamics modeling approach proved to be of great value in the development of system performance assessment model.

The most important impact of climate variability and change on hydrologic processes is reflected in the change of flood patterns: flood starting time, peak value and timing. Floods in the Red River basin generally occur in spring when the increase in temperature initiates snowmelt that usually coincides with heavy rain. In this study more than 90% of floods (at Shellmouth reservoir on the Assiniboine River and at Ste. Agathe on the Red River) generated using three different climate models started earlier in March and April. We conclude that the increase in temperature from climate variation and change results in an earlier flood starting time in the Red River basin.

The DYHAM assessment of the performance of Red River flood protection system is based on the flood flows, the capacity of flood control structures and failure flow levels at different locations in the basin. In the Assiniboine River basin, higher reliabilities at downstream locations are obtained indicating that Shellmouth reservoir plays an important role in reducing downstream flooding. However, a different trend was identified in the Red River basin. The study results show that flood protection capacity of the Red River infrastructure is sufficient under low reliability criteria but may not be sufficient under high reliability criteria.

Table of content

List of figures

List of tables

1. Introduction

The changes in land use and the concentration of greenhouse gases in the atmosphere are thought to be the two major anthropogenic causes of climate change. Widespread urbanization and deforestation have changed the earth's coverage, the soil moisture level, and the topographic features of landmasses, altering the regional radiation exchange and circulation patterns (Lewis, 1989). Recent concerns about climate change have been focused primarily on the emission of greenhouse gases into the atmosphere. The strong evidence exists which shows that greenhouse gases, such as carbon dioxide, methane, nitrous oxide and tropospheric ozone are trapping the long-wave radiation energy emitted by the earth's surface, causing surface temperature to increase. An increase in global temperature may affect the hydrologic cycle (Houghton et al., 1996) and influence water resources (Brent and Yu, 1999). This phenomenon has been regionally observed through changes in rainfall (Karl et al., 1996) and river flow (Lettenmier et al., 1994).

Changes in temperature and precipitation under climate variation have serious impact on the hydrologic processes related to floods that are caused by snowmelt. Usual changes are observed in the shift of flood starting time and the magnitude of flood peak. Therefore, serious consequences may be expected in the ability of existing large-scale flood protection systems to serve their function (Klemes, 1985; Burn and Simonovic, 1996). Red and Assiniboine Rivers in Manitoba are the two main rivers flowing through the City of Winnipeg. Floods in both river basins often occur in the spring. The well-known causal parameters producing floods in Manitoba include: (a) soil moisture at freeze-up time (previous autumn); (b) total winter precipitation; (c) rate of snowmelt; (d) spring rain amount; and (e) timing factor (Warkentin, 1999). Temperature and precipitation are the two major variables that affect the above five parameters. Annual distribution patterns of the temperature and precipitation have significant influence on the flood starting time, flood magnitude and occurrence interval of floods.

Situated in the geographic centre of North America, the Red River originates in Minnesota and flows north (one of eight rivers in the world that flow north). The Red River basin covers 116,500 km^2 of which nearly 103,600 km^2 are in the United States. The basin is remarkably flat. The elevation at Wahpeton, North Dakota, is 287 meters above sea level. At Lake Winnipeg, the elevation is 218 meters. The basin is about 100 km across at its widest. When the conditions are right and the river floods, nothing holds it back. During major floods, the entire valley becomes the floodplain. In 1997, the Red River spread to a width of about 40 km in Manitoba.

The main tributary of the Red River and part of our study area (Figure 1) is the Assiniboine River. It originates in the middle northwest Saskatchewan and drains the area from eastern part of Saskatchewan to the western part of Manitoba. Its major tributaries include Qu'Appelle River and Souris River. The Assiniboine River flows from Northwest to Southeast and enters into the Red River at Winnipeg in Manitoba. Since the lower reach is below Shellmouth Dam that can significantly reduce flow rates and downstream water levels, the case study area for the Assiniboine River focuses on its surface basin from headwaters to the Shellmouth Reservoir. Study area covers 16,496

km^2. Topographically, the basin is gently to moderately undulating with higher relief evident in the Northeast portion. Northeast part of the basin is located within the Boreal Plains Ecozone with characteristics of groves of brush, wooded bluffs and steeper flow gradient, while south part lies within the Prairie Ecozone, a flatter terrain characterized by less brush and few trees. Climatologically, the basin is continental sub-humid characterized by long, cold winter and short, warm summer. The frost-free season varies from 90-110 days. Annual precipitation averages about 450 mm of which 27% is snow, but it has wide variations from 140 to 550 mm. The streamflow in the basin is highly variable on daily basis. During spring, water levels on the Assiniboine River reach peak due to snowmelt, and rapidly decline to a base level. About 63% of annual total flow is contributed by the mouths of April and May, while only 3% by December to March. Variation of year-to-year flows is also high due to climate variations.

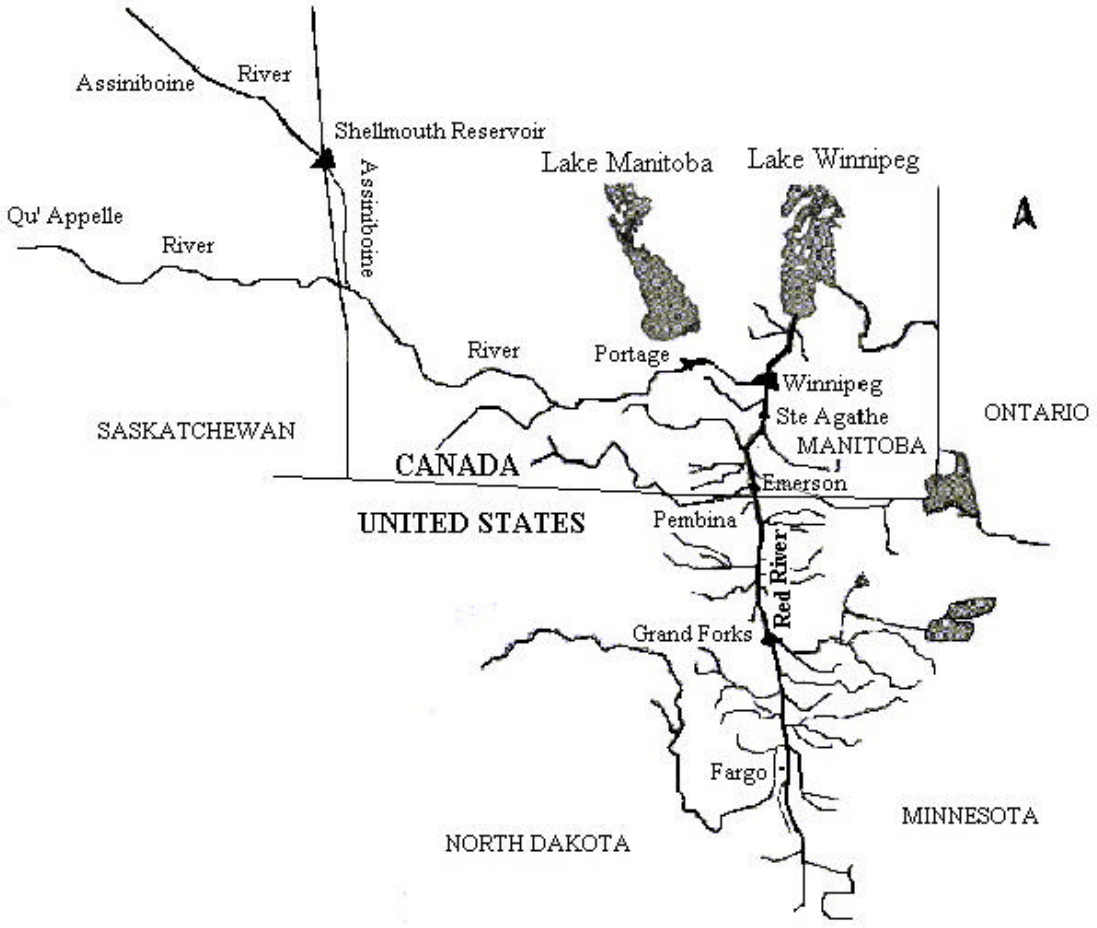

Figure 1. Study area

The Red River/Assiniboine basin floods regularly. Early records show several major floods in the 1800s, the most notable being those of 1826, 1852 and 1861. This century, major floods occurred in 1950, 1966, 1979, 1996 and 1997. The Red River basin has 25 subbasins, which have different topography, soils and drainage that result in different responses during flood conditions. One common characteristic is overland flow during

times of heavy runoff. Water overflows small streams and spreads overland, returning to those streams or other watercourses downstream. Existing monitoring and forecasting systems do not track these flows well, leading to unanticipated flooding.

In Manitoba, almost 90 percent of the residents of the Red River/Assiniboine basin live in urban centres. Metropolitan Winnipeg contains 670,000 people, and another 50,000 live along the Red River north and south of the city. The Red River valley is a highly productive agricultural area serving local, regional and international food needs.

The earliest recorded flood in the basin was in 1826, although anecdotal evidence refers to larger floods in the late 1700s. Some communities south of Winnipeg were flooded regularly, but this flooding was regarded as local rather than systemic, often caused as much by the flooding of tributary rivers as the main stem. The valley inhabitants appreciated the risks of flooding, but they appear to have regarded high water as a part of life in the region. Most of the communities in the basin simply evacuated low-lying lands and rebuilt after each inundation. The 1826 flood remains the largest on record. The floods of 1852 and 1861 were exceeded by the 1997 event.

Most of the flood management planning in Manitoba was initiated after the 1950 flood. This flood was the turning point in the history of flooding and flood control in Manitoba's portion of Red River basin. Construction of elevated boulevards (dikes) within the City of Winnipeg and associated pumping stations was initiated in 1950. The current flood control works for the Red River valley consist of the Red River Floodway, the Portage diversion and Shellmouth Dam on the Assiniboine River, the primary diking system within the City of Winnipeg, and community diking in the Red River valley. Following the 1950 flood on the Red River, the federal government and the Province of Manitoba set up a fact-finding commission to appraise the damages and make recommendations. The commission recommended in 1958 the construction of the Red River Floodway (completed in 1966), the Portage Diversion (completed in 1970) and the Shellmouth Reservoir (completed in 1972). As a consequence of the concern over flood protection for the Red River Valley, a federal-provincial agreement led to the construction in early 1970s of a series of ring dikes around communities in the Valley. Moreover, financial aid programs encouraged rural inhabitants to raise their homes, as well as to create individual dikes around their properties. All the decisions regarding the capacity of current flood control works were based primarily on economic efficiency, getting the largest return for the investment. Existing facilities effectively protected the City from the floods in last decades. However, there still exists an uncertainty on their ability to protect the City from floods under the future climate change.

In order to assess the performance of complex flood protection system under climate variability and change, taking into consideration the way continuous atmospheric variations will influence basin hydrology, requires modeling both, climatic factors (temperature and precipitation) and river flow. Under the leadership of the Intergovernmental Panel on Climate Change (IPCC) a considerable progress has been made in developing high-resolution forecasts of temperature and precipitation using General Circulation Models (GCM). Use of GCM forecasts is of assistance in assessing

possible impacts of climate change on the regional level. Using available GCMs a number of different climate change scenarios have been developed providing yearly, monthly and daily temperature and precipitation data for the next 100 years.

A large body of knowledge exists that allows sophisticated modeling of hydrologic processes on the watershed-scale. There are many exiting models that have been developed to analyze the hydrologic processes and predict the runoff. Integration of climate change scenarios obtained by GCMs with hydrologic models that can predict river flow on the watershed-scale provides sufficient information that can be utilized by water resources management models (Bicknell et al., 1997; Leavesley et al., 1983; Manley, 1978; Kite, 1998; Ahmad and Simonovic, 2000) in order to assess the impact of climate change on the performance of existing water resources management infrastructure.

This study has developed a comprehensive methodology and the regional assessment model that can analyse the performance of existing large-scale flood protection system in the Red River basin under different climate change scenarios. The main objective of the study was to develop a regional dynamic hydroclimatologic assessment model (DYHAM). More specific objectives include:

- Development of a hydrologic model component to simulate river flow under historical and predicted conditions;
- Identification of the magnitude and likelihood of floods under different climate change scenarios;
- Development of system dynamics model for assessing the performance of flood control works; and
- Identification of statistical indices of the Red River flood protection system performance under different climate change scenarios.

1.1 Research methodology

Research conducted in this study was performed in three steps: (a) Development of climate change scenarios; (b) Modeling of hydrologic processes; and (c) Development and application a system dynamics assessment model.

In the first step temperature and precipitation data was generated that are used as input onto the step (b). Hydrologic modeling task generates river flows for assessing the performance of flood protection system in step (c). A schematic presentation of the research framework is shown in Figure 2.

In the first step a comprehensive investigation of Climate Change Models has been conducted to develop climate change scenarios and generate climate data. Literature indicates the existence of numerous hydrologic models that are used for generating river flows and predicting flood events on the basis of climate data and hydrologic parameters. However, only a few models integrate climate change scenarios with snowmelt, annual variation of canopy size, physical soil conditions (freezing and defrosting) and

groundwater. In step (b) a dynamic model is developed for simulating watershed-based hydrologic processes using. Model development is done using principles of system dynamics. System Dynamics employs feedback to describe important relationships among system elements and endogenous structure of the system that generate the system behavior. The model focuses on both, endogenous structure and exogenous variables that are relevant for an accurate description of hydrologic processes. The model is calibrated and verified using historic data and flood events. The simulated model performance data are statistically compared with historical values.

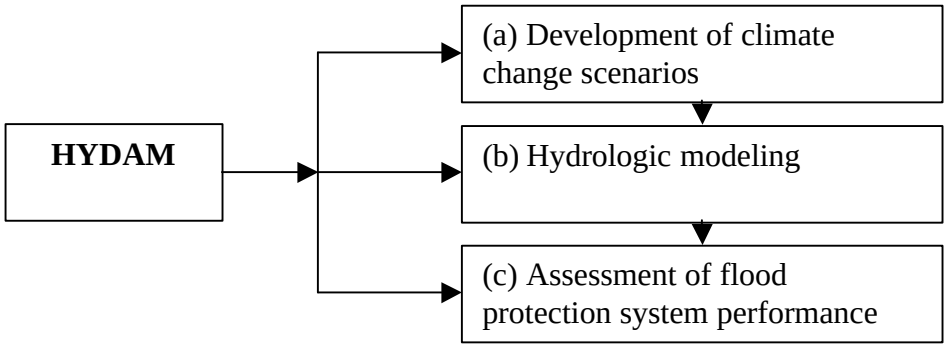

Figure 2. Research framework of the study

The performance of flood protection system is assessed using system dynamics simulation model and the input data (river flow) generated using hydrologic model. The reliability, resilience and vulnerability of system performance is used to describe the protection system performance under different climate change and variability scenarios.

In the next section of the report we provide the detailed descriptions of the development of DYHAM, choice of climate change scenarios, hydrologic model development and analysis, and assessment model development and analysis. Following section presents the results of DYHAM model application in the Red River basin. Report ends with conclusions and recommendations for further research.

2. Climate change scenarios

The effect of climate change, although gradual, is having an increasing impact on the weather experienced in Canada. According to Environment Canada's Climate Research Branch, Canada as a whole experienced above average temperatures for the year 2000. Since comparable nationwide records began in 1948, the year 2000 was the 7th warmest, at 0.9 ^{o}C above normal, based on the preliminary data. The warmest year was 1998 (+2.5 ^{o}C). Temperatures over the last three years have been well above normal, and a linear trend shows an increase of 0.9 ^{o}C over the 53 year period. On a regional scale such as the Prairies where the Red River basin is, climate change has definite impacts on areas such as crop production, forestry, energy sector, and water resources sector, to name a few. It therefore becomes crucial to be able to determine what climate scenarios can be expected in the future.

Different techniques are used to predict the climatic change, including the paleoclimate analogue, the recent climate analogue and the general circulation modeling (GCM). The paleoclimate analogue and the recent climate analogue techniques reconstruct past climatic events using records such as pollen deposits, tree rings, trapped gases in ice cores and historical rainfall and runoff data (Gleick, 1989). The general circulation models are based on the fundamental conservation laws of mass, momentum and energy which describe the apportioning and transport of heat and moisture by the atmosphere and the oceans (Cubasch and Cess, 1990). GCM models provide a digital-analogue way to predict the climatic change. These are models of the climate system that have been developed and are used both to gain physical insight into major features of the behaviour of the climate system, and to produce climate projections for a range of assumptions about emissions of carbon dioxide and other greenhouse gases. These models simulate the evolution of the atmosphere through time from some initial state. GCMs have the ability to model the evolution of the atmosphere in response to external forcing mechanisms – for example, a doubling of carbon dioxide. Although the GCMs use coarse discretization grids and static boundary conditions, they provide the clearest picture of potential climatic change on the global scale.

Currently, Data Distribution Centre (DDC) of the IPCC provides various GCMs related scenarios for impacts assessments (http://ipcc-ddc.cru.uea.ac.uk/). In order to construct scenarios and generate precipitation and temperature data, this study chose three climate change models: HadCM3 (http://ipcc-ddc.cru.uea.ac.uk/dkrz/hadcm2_index.html) which was developed at the Hadley Centre, Bracknell, UK, CGCM1 (http://ipcc-ddc.cru.uea.ac.uk/dkrz/cccma_index.html) which was developed at the Canadian Centre for Climate Modeling and Analysis, and ECHAM4 (http://ipcc-ddc.cru.uea.ac.uk/dkrz/echam4_index.html) which was developed in co-operation between the Max-Planck-Institut für Meteorologie (MPI) and Deutsches Klimarechenzentrum (DKRZ) in Hamburg, Germany. Three models are used in order to evaluate the reliability of the predictions and to eliminate bias associated with data simulated from a sole model.

Although a large number of variables are simulated by the models (i.e., soil moisture, evaporation, wind speed), this study focuses on two variables: temperature and precipitation. These variables are considered to be the major climatological variables affecting the hydrology/water resources sensitivity of the Red River basin.

Models commonly generate data for two main scenarios: Scenario 1, which assumes a 1% CO_2 increase from a baseline of 1961 – 90, and Scenario 2, which assumes a 1% CO_2 + Sulfate Aerosol increase from the same baseline.

Two general scenarios are examined for effects on precipitation and temperature. Scenario 1 (S1) assumes 1% increase in CO_2 concentration, while Scenario 2 (S2) assumes 1% increase in CO_2 concentration plus Sulphate Aerosols. As a reference, a control scenario with constant CO_2 is used. The selected models currently provide yearly and monthly temperature and precipitation data. However, daily temperature and precipitation are not readily available for all scenarios. Scenarios that were available with daily data are presented in Table 1. Predicted daily temperature and precipitation from selected scenarios of the models is used as input into our study. As it can be seen from the Table 1 only limited comparative analysis is possible to assess the choice of GCM model and its impact on final system performance assessment.

Table 1. Selected GCMs and scenarios for the study

Scenarios	Control (without change in CO2)	S1 (1% increase in CO2)	S2 (1% increase in CO2 + Sulfate Aerosols)
Canadian Model (CGCM1)			X
British Model (HadCM3)	X	X	
German Model (ECHAM4)		X	

The three dimensions of space can be accounted for in various ways in climate prediction models. Most models are grid models, in which variables are computed at discrete grid points in the horizontal and vertical directions. The model resolution refers to the (horizontal) spacing between gridpoints. The grid spacing is not necessarily equidistant. For instance, some models use a longitude difference as zonal grid spacing, so near the poles the zonal grid spacing becomes zero. Other models are spectral models. These transform the variation of some variable (e.g. temperature) with latitude and longitude into a series of waves; i.e., atmospheric fields are held and manipulated in the form of waves. The variation of any quantity around a latitude zone can be represented as a summation of a number of waves. Model resolution is governed by the wave number,

with the truncation number representing the number of waves that are resolved around a latitude zone. The 'R' and 'T' refer to the method of truncation, rhomboidal and triangular, respectively, whilst the number indicates the number of waves in each latitude zone, e.g., R15 indicates that there are 15 waves in the latitude zone and rhomboidal truncation has been used.

The equilibrium climate sensitivity of HadCM3, which is the global-mean temperature response to a doubling of effective CO_2 concentration, is approximately 2.5^0C. This is somewhat lower than most other GCMs. The climate sensitivity of HadCM3 is therefore approximately 2.5^0C. HadCM3 is a coupled atmosphere-ocean GCM. It has stable control climatology and does not use flux adjustment. The atmospheric component of the model has 19 levels with a horizontal resolution of 2.5 degrees of latitude by 3.75 degrees of longitude, which produces a global grid of 96 x 73 grid cells. This is equivalent to a surface resolution of about 417 km x 278 km at the Equator, reducing to 295 km x 278 km at 45 degrees of latitude. A new radiation scheme is included with 6 and 8 spectral bands in the short wave and long wave. The radiative effects of minor greenhouse gases as well as CO_2, water vapor and ozone are explicitly represented. A simple parameterization of background aerosol is also included. A new land surface scheme includes a representation of the freezing and melting of soil moisture, as well as surface runoff and soil drainage; the formulation of evaporation includes the dependence of stomatal resistance to temperature, vapor pressure and CO2 concentration. The surface albedo is a function of snow depth, vegetation type and also of temperature over snow and ice. Two scenarios of HADCM3: Control run and greenhouse gas integration, provide daily temperature and precipitation data for our study. We used data for three grid points in the Red River basin (located approximately at 45.5-50.5°N, 94-100.5°E), and one grid point for the Assiniboine River basin (which is located approximately at 51.0-52.1°N, 101.5 to 103.6°E).

The CGCM1 model uses a spectral T32 resolution, equivalent to a grid resolution of 3.75 deg. X 3.75 deg., producing a global grid of 96 x 48 grid cells. The climate sensitivity of CGCM1 is about 3.5^0C. The model uses heat and water flux adjustments obtained from uncoupled ocean and atmosphere model runs (of 10 years and 4000 years duration respectively), followed by an `adaptation' procedure in which the flux adjustment fields are modified by a 14year integration of the coupled model. A multi-century control simulation with the coupled model has been performed using the present-day CO2 concentration to evaluate the stability of the coupled model's climate, and to compare the modeled climate and its variability to that observed. One of the simulations used as input to our study uses an effective greenhouse gas forcing change corresponding to that observed from 1850 to the present, and a forcing change corresponding to an increase of CO_2 at a rate of 1% per year (compounded) thereafter until year 2100. The direct forcing effect of sulphate aerosols is also included by increasing the surface albedo based on loadings from the sulphur cycle model. Only CGCM1 could provide daily temperature and precipitation data for our study. We used data for two grid points in the Red River basin (located approximately at 45.5-50.5°N, 94-100.5°E), and one grid point for the

Assiniboine River basin (which is located approximately at 51.0-52.1°N, 101.5 to 103.6°E).

The ECHAM4 model uses a spectral T42 resolution, equivalent to a grid resolution of 2.8 deg. X 2.8 deg., producing a global grid of 128 x 64 grid cells. The climate sensitivity of ECHAM4 is about 2.6^0C. The model is a spectral transform model with 19 atmospheric layers. The initial sea surface temperature and sea-ice data is the COLA/CAC AMIP SST and sea-ice data set. The mean terrain heights are computed from high resolution US Navy data set. The fraction of grid area covered by vegetation based on the Wilson and Henderson-Sellers data set. The ocean albedo is a function of solar zenith angle and the land albedo from the satellite data. A diurnal cycle and gravity wave-drag is included. The time-step of the model is 24 minutes, except for radiation which uses two hours. The ocean model is an updated version of the isopycnal model. The concept to use isopycnals as the vertical co-ordinate system for an ocean model is based on the observation that the interior ocean behaves as a rather conservative fluid. Even over long distances the origin of water masses can be traced back by considering the distribution of active or passive tracers. Treating the ocean as a conservative fluid fails in areas of significant turbulence activity such as the surface boundary layer. A surface mixed-layer is therefore coupled to the interior ocean in order to represent near-surface vertical mixing and to improve the response time-scales to atmospheric forcing which is controlled by the mixed-layer thickness. Since the model is designed for studies on large scales, a sea ice model with rheology is included and serves the purpose of de-coupling the ocean from extreme high-latitude winter conditions and promotes a realistic treatment of the salinity forcing due to melting or freezing sea ice. The experiment from which daily results are used here is based on the greenhouse gas forcing from 1860 to 1990 followed by a 1 per cent annum increase in radiative forcing from 1990 to 2099. Since the Assiniboine River basin (approximately at 51.0-52.1°N, 101.5 to 103.6°E) is located between two grid points, we used the average data from two grid points. In the Red River basin (located approximately at 45.5-50.5°N, 94-100.5°E), two grid points cover upstream area, and two grid points the downstream. The average of each of the two grid points were used for upstream and downstream.

3. Hydrologic modeling

Flood is a hydrologic phenomenon that is characterized by both precipitation and soil-water contributions. However, snow pack accumulation and melt are in many regions of North America regarded as important sources of runoff and contribute significantly to cause of floods (World Meteorological Organization, 1970; Gray and Male, 1981). In order to forecast snowmelt runoff, understanding of hydrologic processes is equally important as the knowledge of the watershed carrying capacity available to respond to external inputs. Both, processes and carrying capacity are affected by the internal structure of the watershed system as well as the external disturbances. Estimation of snowmelt and carrying capacity of the watershed system is a complex problem that requires climatic and physical data. Understanding of dynamic processes and interactions within surface and subsurface components of the watershed system can be improved. A difficulty may also arise from availability of climatic and landscape data required for snowmelt runoff computation. Hence, proper system description methodology and appropriate predicting techniques are required for practical use in estimating snowmelt runoff.

Considerable effort has been made to investigate and describe runoff generation process. Accompanying rapid progress in computer analysis techniques, the development and application of detailed simulation models are playing important role in runoff prediction. Simulation models have been utilized either for generating streamflow or to determine how runoff responds to the change in climate, landscape and soil-water saturation. A simple way to predict water flow is based on the use of statistical techniques (Thomas and Megahan, 1998). These methods are capable of describing relationships between water flow and relevant conditions in simpler watershed systems. However, they are incapable of capturing more complex non-linear hydrologic processes. More complex runoff models (Arp and Yin, 1992; Bobba and Lam, 1990; Kite et al., 1994) were developed to route water through different land-use, soil-levels and evapotranspiration processes. They can test how water flow responds to the varying conditions. They also require large amount of information that is not always available. Neural networks as predictive tools are also used in runoff prediction (Hsu et al., 1995; Lealand et al., 1999; Zealand et al., 1999; Ehrman et al., 2000). Neural network technique is a mathematically valid, pattern recognition procedure that can utilize complex algorithms for describing the relationships among a number of input and output variables (Rumelhardt and McClelland, 1986). This approach is very powerful when abundant data is available that contains non-linear and seasonal tendencies. However, it is more difficult for application that requires analyses of cause-effect relationships (Rumelhardt and McClelland, 1986).

Group of existing hydrologic models is addressing snow pack accumulation and melt. Examples include Hydrologic Simulation Program—Fortran (HSPF) (Bicknell et al., 1997), Precipitation-Runoff Modeling System (PRM) (Leavesley et al., 1983), Hydrologic Simulation Model (HYSIM) (Manley, 1978) and the SLURP hydrologic model (Kite, 1998). These models integrate climatic factors with surface and subsurface watershed components. They are considering detailed processes of water flow through different soil layers, and require a large amount of data (climate, land use, soil properties,

and other). In calibrating these models, a usually difficulty arises in adjusting parameters related to land use and soil properties.

Degree-day method is generally considered to be a straightforward and reliable approach to snowmelt calculation (US Army Corps of Engineers, 1971; Anderson, 1973). It provides a simple way to estimate snowmelt on the basis of air temperature. The method has been applied to estimate the streamflow from snowmelt (Martinec, 1960, 1970, 1975; Anderson, 1973; Singh and Kumar, 1996). In most of these models, runoff is routed as one component of snowmelt, but the dynamics of moisture movement and soil saturation is ignored.

The contribution of snowmelt to runoff is described by the interaction among climatic factors, vegetation, physical properties of soil, and soil moisture saturation. Most major floods occur following heavy precipitation in the previous fall, substantial snowfall, sudden thaws in association with heavy rainfall or wet snow conditions during the spring breakup. Precipitation and temperature are the two key indicators of these flood events. Snowmelt water and/or rainfall will partially be intercepted by vegetation, and some infiltrated into the soil. Surplus water, after interception and infiltration, is routed as streamflow. Interception capacity is subject to seasonal change of vegetation. Vegetation growth within a year accumulates in time and space until reaching a maximum biomass and cover consistent with the local physical environment (Gutierrez and Fey, 1980). Vegetation growth is very rapid during the spring season. It reaches its maximum value and eventually starts decreasing as the growth rate approaches zero. Infiltration rate and surface storage capacity, both depend on the physical state of the soil. In snowmelt active season, vegetation is rare and infiltration rate is limited due to the frozen surface soil. These conditions often result in flooding. Active temperature (≥0°C) and its duration are important for vegetation growth and defrosting and refreezing of surface soil.

This section of the report describes a hydrologic model developed for flood generation. System Dynamics modelling methodology (Forester, 1968) is applied to capture all essential dynamic characteristics of hydrologic processes occurring between surface and subsurface watershed system components. The model is able of examining the impact of active temperature on the seasonal change of flood patterns and infiltration rate. Based on the analysis and integration of existing information available on hydrologic processes occurring in a watershed, the report first outlines the general structure of a watershed system. Then, a dynamic hypothesis is developed to describe hydrologic system dynamics using feedback relations among the system components. Relaying on the existing knowledge and information, a mathematical model formulation is developed and implemented using STELLA II simulation tool (High Performance System Inc., 1997). The model is calibrated and verified using historical flood events occurring in the Assiniboine and the Red River basins, Manitoba, Canada. The section ends with the discussion of model applications.

3.1 Hydrologic model description

Hydrologic simulation models that consider surface-subsurface water interactions have been in existence for quite some time. Various approaches have been applied to simulate

the hydrologic cycle on a continuous basis. Runoff records, long and reliable records of precipitation and temperature are easily available in flood-prone watersheds. However, data is all in terms of daily values, and limited information is available concerning hydrologic parameters of the soil mantle. Given the purpose of our study and the data availability for the Red River basin, the best choice is a lumped-parameter conceptual hydrologic model, capable of simulating various components of the streamflow. In this research we build on the existing models. Our main contribution is in integration of the key climate change indicators (temperature and precipitation) complex hydrologic processes occurring in the watershed of that size. Model parameters are defined for the whole watershed and simulation of vertical water balance is performed using five tanks to describe watershed system: (a) snow storage; (b) canopy storage; (c) surface soil storage, (d) subsurface storage and (e) groundwater storage. Schematic presentation of the hydrologic model is in given in Figure 3.

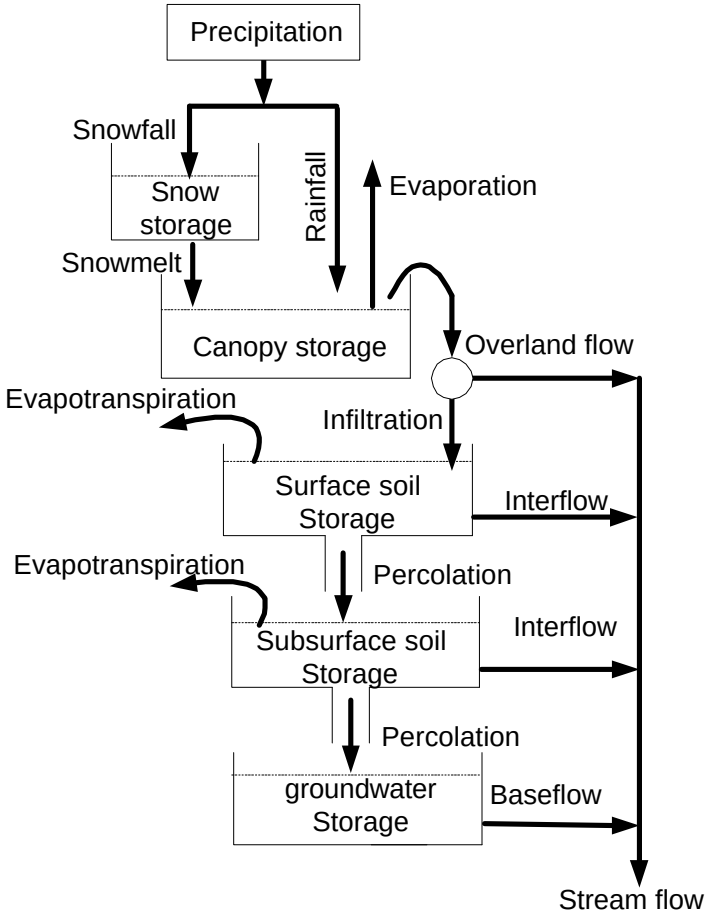

Figure 3. A schematic representation of the vertical water flow

Precipitation falling as snow is accumulated in the snow storage. The rate of release by snowmelt is equal to the potential snowmelt rate. Rainfall and water from snowmelt first

enter into the canopy storage. Canopy storage represents the interception of moisture by vegetation, i.e. trees leaves, grass, etc. Canopy storage capacity varies seasonally due to the different intensity of vegetation growth. The loss from this storage is due to evaporation. Any moisture in excess of the maximum canopy storage capacity is passed to the surface soil storage.

Surface soil storage represents moisture held in the upper soil layer. It has a finite capacity equal to the depth of this layer multiplied by its porosity. Excess water from the canopy storage enters into this zone. Potential infiltration rate limits the rate at which moisture enters this storage. Potential infiltration rate is a function of soil permeability and land slope, as well as a function of surface soil conditions and soil moisture content. Temperature determines the physical state of the soil. Existing level of soil water saturation in the form of feedback affects the infiltration. The difference between the volume of water from the canopy storage and the amount infiltrated into the soil becomes overland flow. This is a fast response component of the runoff.

Losses from the surface soil storage are due to the evapotranspiration, percolation into the lower soil storage and the interflow. Evapotranspiration flux aggregates physical (evaporation) and biological loss (evapotranspiration). It depends on the moisture saturation and weather conditions. The next transfer of moisture is due to the interflow (i.e. lateral flow). The rate of interflow is a very complex function of the effective horizontal permeability, water saturation, gradient of the layer and the distance from the channel or land drain. The final transfer from the surface layer is through the percolation into the lower layer. Percolation rate depends on the water saturation within surface and lower soil layers.

Subsurface storage represents moisture below the surface layer but still in the root zone. Water enters this storage by percolation from the surface layer. Similar losses, to those from the surface soil storage, exist in lower soil storage: evapotranspiration, interflow runoff and percolation into the groundwater. Evapotranspiration from the lower soil layer depends upon vegetation transpiration and varies with the type of vegetation, the root depth, the density of vegetation cover, the stage of plant growth and the moisture characteristics of the soil layer. Interflow and percolation to groundwater storage may be affected by moisture saturation.

Groundwater storage is an infinite linear reservoir, assumed to have a constant discharge coefficient.

Temperature is an important climate indicator that affects a snow pack accumulation and the snowmelt. The runoff from snowmelt may follow a general pattern of temperature change during active period of snowmelt. In winter, precipitation is accumulated as snow pack due to the low temperature. The winter runoff is dominated by the flow originating from the groundwater storage and the lower soil storage due to the frozen surface soil. As temperature reaches to active point in early spring, snow starts melting. Most of the snowmelt is transformed into the overland flow due to the small canopy storage and the frozen surface soil. As temperature increases, snowmelt provides more water that

contributes to the rapid increase in streamflow and gradually leads to flood conditions. In the same time, active temperature also gradually defrosts the soil. That process results in the increase of infiltration rate and the surface soil storage capacity. Consequently, the streamflow starts declining. If heavy rain occurs during the snowmelt period, streamflow will even more rapidly reach the peak value and the magnitude of the peak will be larger. As accumulated snow pack melts, streamflow gradually returns to the normal level. After the snowmelt period, water from the groundwater storage and the soil storage provides the main contribution to the streamflow, and the fluctuation of streamflow is strongly dependent on the rainfall intensity variation. This pattern has been clearly observed at different locations along the Assinibione and the Red River in Southern Manitoba.

3.2 Hydrologic model development

Dynamic hypothesis

Mathematical simulation model can increase the understanding of hydrologic dynamics and contribute to the better prediction of the flood behavior. System Dynamics (SD), a feedback-based methodology, is applied to develop the hydrologic model and capture the dynamics of hydrologic processes presented in the previous section. System dynamics provides a conceptual framework useful in the assembly of nonlinear differential equations with complex feedback (Forrester, 1968). It recognizes that the dynamic behavior of systems is controlled by feedback structure (Senge, 1990; Richardson, 1991). The positive feedback stimulates all factors in a positive feedback loop to increase or decrease. However, the negative feedback loop tends to keep the system in equilibrium. If any system element that is a part of the negative feedback loop is moved from the equilibrium, the negative feedback will push it to return into the steady state. System dynamics approach helps in identification of sources of problematic system behavior and understanding of feedback structure of the system. Dynamic behavior of the hydrologic systems is dominated by feedback loop structures that control change in the watershed. Based on the hydrologic processes in the surface and the subsurface layers, a basic dynamic hypothesis for generating hydrologic dynamics is developed (Figure 4). The basic dynamic hypothesis shows that the feedback structure of the basic state variables is related to the hydrologic flow processes as well as exogenous variables. There are five fundamental state variables controlling the hydrologic dynamics: snow storage, canopy storage, surface soil storage, lower soil storage and groundwater storage. The strength of each hydrologic flow process is represented by a rate variable. Feedback loops are formed by linking state and rate variables to control the behavior of hydrologic system. When rainfall, or snowmelt water enters into the system, feedback loops will regulate all hydrologic flow processes.

Snow storage is regulated by the snowfall and the snowmelt that both depend on an external factor - temperature. Two processes control the canopy storage: water interception and evaporation. Water interception rate is dependent on the interception capacity and existing amount of water in the canopy, while evaporation dependents on the external weather conditions. There is also one negative feedback loop related to water interception:

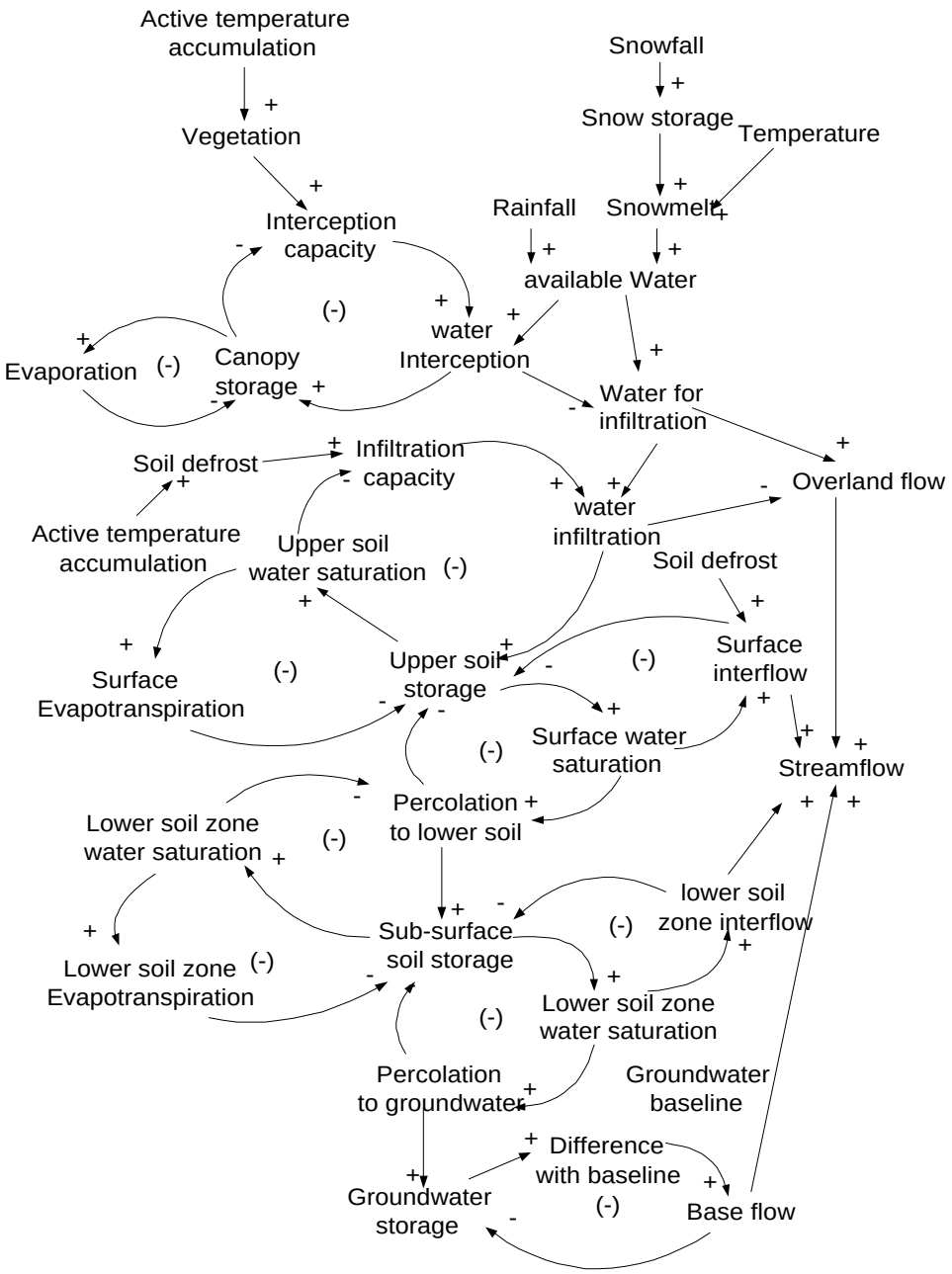

Figure 4. Basic dynamic hypothesis of watershed dynamics

(1) Water interception +> Canopy storage ->Interception capacity +> water interception.

The signs in the above loop (+ and -) represent the causal relationships between linked variables. ‘Plus’ sign means that the first variable positively affects the next variable, while ‘minus’ sign means that the first variable negatively influences the next one. Loop

(1) shows that the water interception by canopy increases the amount of water in the canopy storage, which reduces the interception capacity, and finally limits water interception rate. Interception capacity depends on the vegetation size which is subjected to active temperature accumulation during snowmelt period.

There are four processes that control surface soil storage: water infiltration, evapotranspiration, percolation and interflow. Following negative feedback loops can be traced:

(2) Water infiltration +> Surface soil storage +> Surface soil water saturation -> Infiltration capacity +> Water infiltration.
(3) Surface soil storage +> Surface soil water saturation +> Evapotranspiration -> Surface soil storage.
(4) Surface soil storage +> Surface soil water saturation +> Percolation to lower soil -> Surface soil storage.
(5) Lower soil storage +> Lower soil water saturation -> Percolation to lower soil +> Lower soil storage.
(6) Surface soil storage +> Surface soil water saturation +> Surface soil interflow -> Surface soil storage.

There are four processes that regulate the lower soil storage: percolation from surface soil storage, evapotranspiration, percolation into groundwater and interflow. Except for percolation from surface to subsurface layer, other negative loops are identified that control subsurface soil storage:

(7) Lower soil storage +> Lower soil water saturation +> Evapotranspiration -> Lower soil storage.
(8) Lower soil storage +> Lower soil water saturation +> Lower soil interflow -> Lower soil storage.
(9) Lower soil storage +> Lower soil water saturation +> Percolation to groundwater -> Lower soil storage.

Loops (7) to (9) show that evapotranspiration, interflow and percolation processes are determined by lower soil water saturation. Base flow from groundwater storage is determined by:

(10) Groundwater storage +> Difference from groundwater baseline +> Base flow -> Groundwater storage.

This loop states that the groundwater storage is assumed to behave as a shallow reservoir, and the base flow depends on the difference between the current groundwater level and its baseline value.

The stated dynamic hypothesis shows that both, rainfall and snowmelt are external water sources. They are directly affecting the soil water balance and the amount of water in the

groundwater storage. Internal hydrologic processes and negative feedback structures among soil layers and groundwater reservoir provide internal storage buffers and adjustment mechanisms that attempt to reduce or delay the impact of external disturbance on the streamflow and return the system back to the equilibrium state. Flooding will occur when external water exceeds internal storage buffers and its adjusting capacity.

Mathematical model formulation

The model integrates the whole watershed into a single hydrologic system and simulates vertical water balance. Temperature and precipitation are considered as external inputs that generate the streamflow as the output. Six sectors are used in the model development: snow storage, canopy storage, surface soil storage, subsurface soil storage, groundwater storage and streamflow recession sector. Presentation of the mathematical formulation of the model, that is based on the vertical water balance, follows.

Snow storage sector

Precipitation falling as a snowfall is accumulated in the snow storage. A critical temperature is used to determine whether the measured or forecasted precipitation is rainfall or snowfall (Martinec et al, 1983). Snowmelt rate is calculated by the degree-day factor (Martinec, 1960, 1970, 1975; Anderson, 1973; Singh and Kumar, 1996). Using simple water balance equation, the snow storage change rate in a time interval dt is mathematically expressed as:

$$\frac{dSS}{dt} = SF * swec - SM \tag{1}$$

$$SF = \begin{cases} P & \text{if} \quad T < ct \\ 0 & \text{if} \quad T > ct \end{cases} \tag{2}$$

$$SM = \begin{cases} \min(a * T, SS) & \text{if} \quad SS > 0 \\ 0 & \text{if} \quad SS < 0 \end{cases} \tag{3}$$

Where: SS is snow storage (cm); SF is snowfall (cm/day); swec is the snow-water equivalent coefficient (cm snow/cm precipitation); SM is the snowmelt rate (cm/day); P is precipitation (cm/day); T is daily mean temperature (°C); ct is the critical temperature that determines whether precipitation is snowfall or rainfall (°C); and α is the degree-day factor for snowmelt (cm/°C/day).

Canopy storage sector

Canopy can intercept water from snowmelt and rainfall. Water loss from the canopy storage is due to the evaporation. Water balance equation for canopy storage is written as:

$$\frac{dCS}{dt} = CI - EP \tag{4}$$

Where: CS represents canopy storage (cm); CI stands for canopy interception rate (cm/day); and EP is evaporation (cm/day).

Canopy interception rate is dependent on the canopy interception capacity, the existing amount of water in the canopy storage, and the availability of water from snowmelt and rainfall. Actual interception rate is the lesser one from available water for interception and available interception capacity, and is written as:

$$CI = \min(ASR, (CIC - CS)) \tag{5}$$

$$ASR = SM / swec + RF \tag{6}$$

$$RF = \begin{cases} P & \text{if} \quad T > ct \\ 0 & \text{if} \quad T < ct \end{cases} \tag{7}$$

Where: ASR is water available for interception from snow and rainfall (cm/day); CIC represents canopy interception capacity (cm/day); and RF stands for rainfall (cm/day).

Canopy interception capacity varies with the seasonal vegetation growth. In the winter, the canopy interception capacity is very small since leaves are fallen down and grasses are waded. As normal biological growth pattern, canopy growth follows an S-curve pattern, i.e. when temperature reaches active temperature, plants start to grow, and growth increases as temperature increases until it reaches its maximum. In order to represent this process, active temperature accumulation is taken as an index to estimate canopy interception capacity:

$$CIC = CIC_{max} * (CIC_c + T_{CIC}) \tag{8}$$

$$T_{CIC} = \begin{cases} (TA_c / TA_{c\,max})^{tc} & \text{if} \quad TA_c < TA_{c\,max} \\ 1 & \text{if} \quad TA_c > TA_{c\,max} \end{cases} \tag{9}$$

$$TA_c = \sum T \quad \text{if} \quad T > 0 \tag{10}$$

Where: CIC_{max} is the maximum CIC (cm/day); CIC_c is the minimum coefficient of CIC during the winter (dimensionless); T_{CIC} is the influence of active temperature accumulation on the canopy size (dimensionless); TA_C is the active temperature

accumulation after snowmelt starts (°C); tc is an exponential parameter for the influence of active temperature accumulation on canopy growth, and TA_{cmax} is the maximum TA_C point at which the canopy storage reaches its maximum.

Evaporation potential of the canopy storage is dependent on the weather conditions. The model assumes that evaporation is related to the air temperature and than the evaporation rate can be expressed as:

$$EP = \min(epc * T, CS) \tag{11}$$

Where: epc stands for evaporation coefficient (cm/°C/day).

Surface soil storage
The change of water in surface soil storage is expressed by:

$$\frac{dSW}{dt} = I - SWEP - SWIF - SWP \tag{12}$$

Where: SW is the surface soil water storage (cm); I is the infiltration rate (cm/day); SMEP is the surface soil evapotranspiration (cm/day); SMIF is the surface soil interflow (cm/day); and SMP is the percolation rate (cm/day) from surface to subsurface soil storage.

Infiltration rate depends on the availability of water after canopy interception (W_a) and soil infiltration limit (I_l):

$$I = \min(W_a, I_l) \tag{13}$$

Water availability for infiltration depends on the total water availability after canopy interception. It can be expressed as:

$$W_a = \begin{cases} ASR - CI & \text{if} \quad ASR > CI \\ 0 & \text{if} \quad ASR \le CI \end{cases} \tag{14}$$

The infiltration rate is a function of soil properties and water saturation. A limit of the infiltration rate at which moisture can enter this storage is taken as assumed in the HYSIM (Manley, 1978). Temperature is the critical factor that affects soil state during

the snowmelt active period. It also determines water availability for interflow and percolation. Process of soil and water defrosting depends on the active temperature and its duration. Defrosting process can be expressed as an exponential function so that the infiltration limit can be written as:

$$I_l = (I_c / S_{ms}^{\ g}) * T_I \tag{15}$$

Where: I_c is an infiltration coefficient (cm/day); S_{ms} is the moisture saturation in surface soil layer (dimensionless); γ is an exponential parameter expressing the impact of water saturation on infiltration; T_I is the effect of temperature on the physical state of soil. In HYSIM, S_{es} is defined as:

$$S_{ms} = (M_s - S_{rs})/(1.0 - S_{rs}) \tag{16}$$

Where: M_s is the surface soil moisture saturation (cm/cm); and S_{rs} is the minimum surface soil moisture saturation that can be attained. M_s can be defined as:

$$M_s = SW / SWN \tag{17}$$

Where: SWN is the nominal surface soil storage (cm).

The effect of temperature on infiltration is a complex phenomenon. It depends on the temperature fluctuation and the length of time of temperature above and below the active temperature. This phenomenon results in soil defrosting and/or refreezing. It is assumed that the soil defrosts exponentially with active temperature accumulation. However, soil will be refrozen again after a given number of days with the below-active temperature. The impact of active temperature accumulation will be lost, and the process of active temperature accumulation will start again from zero. Hence, T_I can be written as:

$$T_I = \begin{cases} (TA_I / TA_{Imax})^{ti} & \text{if} \quad TA_I < TA_{Imax} \\ 1 & \text{if} \quad TA_I > TA_{Imax} \end{cases} \tag{18}$$

$$TA_I = \begin{cases} \sum T & \text{if} \quad T > 0 \\ 0 & \text{if} \quad N_{TBA} > N_n \end{cases} \tag{19}$$

$$N_{TBA} = \begin{cases} \sum N_{dTBA} & \text{if} \quad T < 0 \\ 0 & \text{if} \quad T > 0 \end{cases} \tag{20}$$

$$N_{dTBA} = \begin{cases} 1 & \text{if} \quad T < 0 \\ 0 & \text{if} \quad T > 0 \end{cases} \tag{21}$$

Where: TA_I is the active temperature accumulation (°C); TA_{Imax} is the maximum TA_I point at which the surface soil is fully defrosted (°C); ti is an exponential parameter for the influence of active temperature accumulation on soil defrosting process (dimensionless); N_{TBA} is the number of days with temperature below active point (day); N_n is the maximum N_{TBA} after which the active temperature accumulation will be lost and surface soil will refreeze again; N_{dTBA} is a logical variable that identifies the day with the temperature above or below the active temperature.

Water in excess of infiltration limit will route as overland flow (OF) that equals to:

$$OF = W_a - I \tag{22}$$

Evapotranspiration from the surface soil is determined by water saturation (Bicknell et al., 1997) and climatic conditions (Manley, 1982). Since moisture movement and biological activities are significantly dependent on the temperature, evapotranspiration can be defined as a function of water saturation, availability and temperature:

$$SWEP = SWEPc * T * S_{ms}{}^{l} * T_I \tag{23}$$

Where: SWEPc is an evapotranspiration coefficient (cm/°C/day); λ is an exponent parameter (>1) that describes the impact of water saturation on evapotranspiration and interflow.

Surface soil interflow is also a very complex process dependent on the properties of soil, water saturation (Manley, 1982) and water availability. It can be expressed as:

$$SWIF = SWIFc * S_{ms}{}^{l} * T_I \tag{24}$$

Where: SWIFc is an interflow coefficient (cm/day).

Percolation from the surface to the subsurface storage depends on the water saturation in both layers and only occurs when the difference of water saturation between the surface and the subsurface soil storage is greater than 0.01 (Bicknell et al., 1997). When this happens, the percolation from the surface soil is calculated by the empirical expression:

$$SWP = \begin{cases} SWP_c * (S_{ms} - S_{mss})^3 * T_I & \text{if} \quad S_{ms} - S_{mss} > 0.01 \\ 0 & \text{if} \quad S_{ms} - S_{mss} \le 0.01 \end{cases} \tag{25}$$

Where: SWPc is a percolation coefficient of the surface soil layer (cm/day); and S_{mss} is the effective saturation into the subsurface soil layer (dimensionless).

Subsurface soil storage

The source of moisture for the subsurface soil storage comes from the surface soil percolation. Similar to the surface stirage, losses of moisture from this storage are due to evapotranspiration, interflow and percolation into the groundwater storage. Moisture dynamics of the subsurface soil storage can be expressed as:

$$\frac{dSSM}{dt} = SWP - SSMEP - SSMIF - SSMP \tag{26}$$

Where: SSM represents the subsurface soil moisture (cm); SSMEP, SSMIF and SSMP stand for moisture loss rate by evapotranspiration from, interflow to, and percolation from subsurface soil storage (cm/day), respectively.

Evapotranspiration from the lower soil depends on the vegetation cover, water saturation of the subsurface soil and the climatic conditions. Similar equation to the one used for the canopy interception capacity is developed expressing vegetation as a function of active temperature accumulation. In this case too, the temperature is used as representative of climatic conditions. Hence, the evapotranspiration can be written as:

$$SSMEP = SSMEPc * T * S_{mss}^{\ l} * T_{CIC} \tag{27}$$

Where: SSMEPc is an evapotranspiration coefficient for the subsurface soil layer (cm/°C/day); and S_{mss} is defined as:

$$S_{mss} = (M_{mss} - S_{rl})/(1.0 - S_{rl}) \tag{28}$$

Where: M_{mss} is the subsurface soil moisture saturation (cm/cm); S_{rl} is the minimum lower soil moisture saturation that can be attained. M_{mss} is defined as:

$$M_{mss} = SSM / SSMN \tag{29}$$

Where: SSMN is the nominal subsurface soil storage (cm).

Interflow and percolation rates in the lower soil storage are affected by the soil moisture saturation and expressed as (Manley, 1982):

$$SSMIF = SSMIFc * S_{smm}{}^{l} \tag{30}$$

$$SSMP = SSMPc * S_{smm}{}^{l} \tag{31}$$

Where: SSMIFc is the subsurface soil interflow coefficient (cm/day); and SSMPc is a percolation coefficient (cm/day).

Groundwater storage
Water enters the groundwater storage through percolation from the subsurface soil storage and leaves the groundwater storage as the baseflow directly into the stream. Differential equation for the change in the groundwater storage is:

$$\frac{dGWS}{dt} = SSMP - BF \tag{32}$$

Where: GWS is the groundwater storage (cm); and BF stands for the baseflow (cm/day).

The groundwater storage is described as a linear shallow reservoir. It is assumed that there exists a baseline groundwater level. The baseflow rate is dependent on the difference between the amount of water in the groundwater storage and the baseline groundwater level:

$$BF = (GWS - BFL) / BF_c \tag{33}$$

Where: BFL is the baseline groundwater level (cm); and BF_c is the baseflow coefficient (per day).

Runoff recession

Total water available (TWA) for routing as runoff comes from the overland flow, the interflow from surface and lower soil storage as well as the baseflow from the groundwater storage. Mathematically it is expressed as:

$$TWA = OF + SSIF + LSIF + BF \tag{34}$$

Streamflow responds to the availability of internal and/or external water with the time delay. An average travel time is used in the model and represented using a third-order exponential smooth function (HPS, 1997). This function is obtained by setting up a cascade of three first-order exponential smoothes, each with an average time of time/3. Hence, the stream flow (Q) can be calculated as:

$$Q = SMTH3(TWA * Area, AT, Q_i) * 10000 / 86400 \tag{35}$$

Where: Area is catchment area (km^2); 10000/86400 units conversion factor from cm km^2/day to m^3/s; AT represents the average time (day); and Q_i stands for the initial streamflow (cm km^2/day). If Q_i is not specified available, smooth function assumes the value to be the initial value of the input.

Model implementation

The model was developed and implemented using STELLA II development tool (High Performance System Inc., 1997). This modeling tool provides a user-friendly graphic interface. Under STELLA environment, the modeler can use available building blocks to define the objects and the functional relationships. The basic graphical building blocks are stocks, flows, converters and connectors. Stocks represent storage accumulations that vary with flows. Flows may carry water in or out of the storage. Flows are defined and regulated by converters. Converters are used to store algebraic relationships, define external input into the model and hold values for constants. Connectors are connecting model elements (stocks, flows and converters) and indicate the cause-effect relationships. The model is represented by differential and difference equations that can be solved with Euler's or Runge-Kutta's numerical methods.

3.3 Application of the hydrologic model

The developed system dynamics model has been applied for simulation of runoff in two river basins in Southern Manitoba, Canada: the Assiniboine River basin and the Red River basin.

Calibration and verification of the model

Flood flow records in both basins were divided for the purpose of model calibration and verification. Calibration of parameters includes determining model parameters and initial values of state variables. Calibration of parameters for the present study was done by the trial and error method. Physically based parameters can be determined from the knowledge of the catchment characteristics. Most hydrologic parameters can be obtained from the literature and field observations. Climate variables are retrieved from the field observations. Those variables, which could not be derived from the literature and field observations, were calibrated through repeated simulation until a fair match is obtained between calculated and observed flows. Statistical analysis was conducted for assessing the goodness of fit and guiding the calibration process (Aitken, 1973).

Initial values of all state variables used in the model are chosen from experience as well as from the precipitation record during the previous fall and winter. Streamflow record was obtained from the Environment Canada Hydrologic Database (HYDAT) and USGS real streamflow record database, while climatic data were retrieved from the Environment Canada Climate Station Database and the American National Weather Service. In the Assiniboine River basin, floods of 1995 and 1979 were selected for calibration and verification, respectively. Flows were measured at the entrance into the Shellmouth Reservoir. In the Red River basin, floods of 1996 and 1997 were selected. Since the Red River flows south to north with a geographically wide span in which there exist a great gradient in temperature and precipitation, it was necessary to divide the basin into several sub-catchment areas. Three sub-catchments were identified: Grand Forks with 77,959 km^2, Emerson with 24,087 km^2 and Ste. Agathe with 12,954 km^2. For each sub-catchment, above presented differential and difference equations are used to calculate streamflow. Following equations are used to route water from Grand Forks, Emerson and Ste. Agathe:

$$Q_{GF} = SMTH3(TWA_{GF} * Area_{GF}, AT_{GF}, Q_{GFi}) * 10000/86400 \quad (36)$$

$$Q_{EM} = SMTH3(TWA_{EM} * Area_{EM}, AT_{EM}, Q_{EMi}) * 10000/86400 + SMTH3(TWA_{GF} * Area_{GF}, AT_{GF} + AT_{GF-EM}, Q_{GFi}) * 10000/86400 \quad (37)$$

$$Q_{SG} = SMTH3(TWA_{SG} * Area_{SG}, AT_{SG}, Q_{SGi}) * 10000/86400 + SMTH3(TWA_{EM} * Area_{EM}, AT_{EM} + AT_{EM-SG}, Q_{EMi}) * 10000/86400 + SMTH3(TWA_{GF} * Area_{GF}, AT_{GF} + AT_{GF-EM} + AT_{EM-SG}, Q_{GFi}) * 10000/86400 \quad (38)$$

Where: SF_{GF}, SF_{EM} and SF_{SG} represent simulated streamflow (m^3/s) at Grand Forks, Emerson and Ste. Agathe' SMTH3 is the 3rd order smooth function; TWA_{GF}, TWA_{EM} and TWA_{SG} stand for the total water available for routing as runoff (cm/day) at Grand Forks, Emerson and Ste. Agathe; 10000/86400 converts units from cm km^2/day to m^3/s; AT_{GF}, AT_{EM} and AT_{SG} represent average travel time (day) at Grand Forks, Emerson and Ste. Agathe sub-catchments; AT_{GF-EM} and AT_{EM-SG} are the average travel time (day) from

Grand Folks to Emerson and Emerson to Ste. Agate; and SF_{GFi} SF_{EMi} and SF_{SGi} stand for initial streamflow (cm km^2/day) at Grand Folks, Emerson and Ste. Agate. Observed streamflow at Grand Forks, Emerson and Ste. Agathe were used in model calibration.

Model results

After calibration of all parameters, the model is fed with temperature and precipitation as well as initial values of the state variables. The main parameters used in the model are shown in Table 2. For the Assinibione River basin, data for the 1995 flood year is used for calibration, and 1979 for verification. For the Red River basin, 1996 flood year is 1996 is used for calibration and 1997 for verification.

Table 2. Calibrated values of the main model parameters

Catchment	α (cm/°C/d)	SSMN (cm)	LSSN (cm)	TA_{Imax} (°C)	TA_{Cmax} (°C)	tc (no unit)	ti (no unit)	CIC_{max} (cm)
Assiniboine River	0.4	2.5	4.0	45	800	2.8	4	0.5
Red River	0.4	2.5	4.2	45	800	2.8	4	0.5

Results - Assiniboine River

A visual examination of simulated versus measured streamflow from calibration and verification years in Assiniboine River is shown in Figures 5 and 6. Results indicate that simulated streamflow patterns are quite similar to those observed by measurements. In the case of calibration flood year (Figure 5), streamflow is smaller during the winter season due to the frozen surface soil. Active temperature starts in early March and that results in snowmelt and increased streamflow. A small flow peak appeared during this snowmelt active period. From the late March to early April, negative temperature lasted for about two weeks, which lead to freezing of surface soil again, and streamflow receded to normal low level due to the absence of snowmelt. In the middle of April, temperature rose to active point and snowmelt starts again. As temperature increased, more water was produced from snowmelt, and streamflow rapidly increases. In the meantime, active temperature gradually defrosts the surface soil, which increased infiltration rate and available surface soil storage capacity. More water infiltrated into the surface soil increased water saturation of the surface storage, which, in turn, limited further infiltration. Although infiltration rate increased with the rise of the temperature, streamflow continues to increase due to the time delay affecting the snowmelt. Before the surface soil was fully defrosted, streamflow reached a peak with a rainfall in late April. Fully defrosted surface soil infiltrated most of the snowmelt water and reduced the streamflow. Lasting high active temperature gradually depleted accumulated snow pack before the middle of May, and streamflow returned to the normal level. After the snowmelt period, both the groundwater and the soil storage became again the main contributors of the streamflow, and fluctuations in streamflow are strongly dependent on the rainfall magnitude.

The moisture dynamics of the surface and the sub-surface soil layers and their response to precipitation are showed in Figure 7. In the winter, moisture content in the surface soil kept stable because surface soil was frozen, and losses were negligent. As temperature

reached active point in early March, the surface soil started to thaw, and snowmelt water was infiltrated into the soil to increase the moisture content. Moisture in the surface soil rapidly increased and kept at a high level after snowmelt started. More moisture in the surface soil resulted in an increase in lower soil storage moisture content with a time delay due to percolation into the lower soil storage. More lower soil moisture also increased water saturation, which reduced percolation rate. After surface soil defrosted, moisture levels in the surface and the subsurface soil storage kept at the high level because more water from the snowmelt entered into the surface storage, and the high water saturation in lower soil layer reduced percolation. After snowmelt period, moisture in the surface storage was reduced and strong fluctuations caused by variations in the rainfall magnitude started. After October, the temperature reached zero level, and snowfall started accumulating as the snow pack. The moisture level in the surface storage kept stable. Moisture amount accumulated in the surface storage in the fall is an important factor for the generation of the next year flood. Figure 7 also indicates that the surface soil storage is a fast responding component of the rainfall during the active temperature period, while lower soil storage is a slow responding component exhibiting a smooth change.

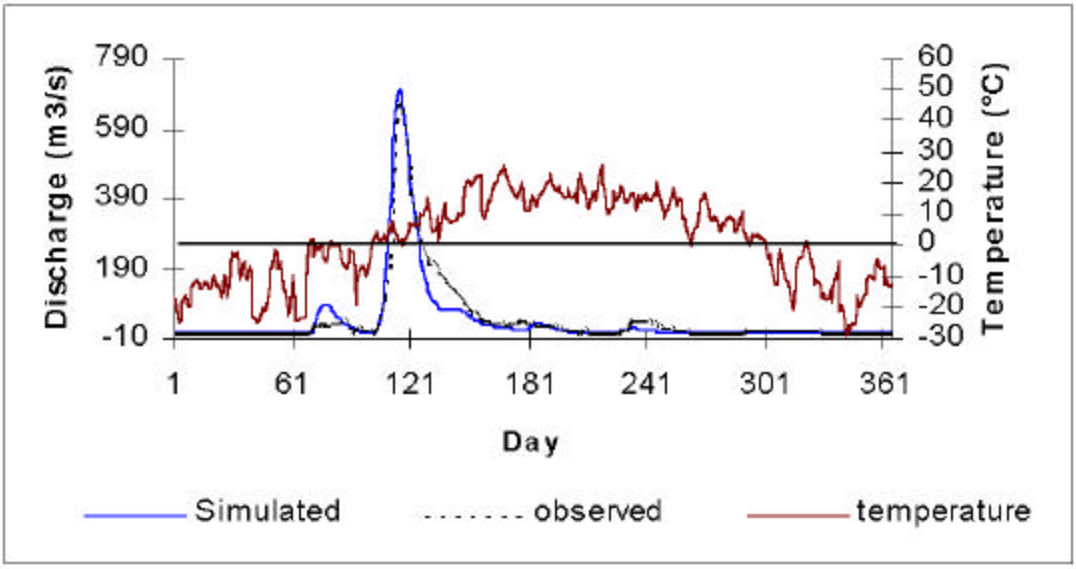

Figure 5. Simulated and measured streamflow in the Assiniboine River basin for 1995 (calibration)

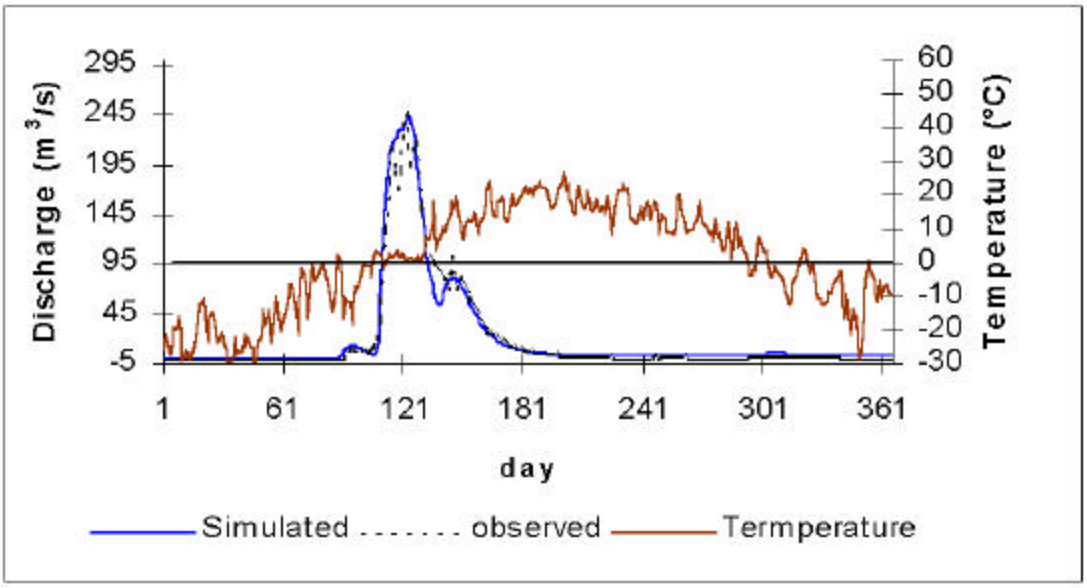

Figure 6. Simulated and measured streamflow in the Assiniboine River basin for 1979 (verification)

The verification results for 1979 flood year also reproduced reasonably well the flood starting time, and peak (Figure 6). Simulated flow was underestimated at the beginning of April due to the temperature being below active point. During the peak period, the fluctuations in measured flow were observed, while simulated flow was smooth with one peak. The influence of active temperature and its duration on both, the surface-soil defrosting and the snowmelt may be responsible for this difference. The model uses daily mean temperature to calculate the snowmelt rate. In the real situation, temperature varies during the day. Duration of negative and active temperature also significantly affect the surface soil state and the infiltration rate. The model does not capture daily variations of temperature and their implications on the streamflow. However, the main purpose of the model is to assess the long-term behavior and trends in the streamflow, not diurnal changes. In middle of May, the daily mean temperature rapidly reached to about 20°C, which produced more snowmelt water resulting in an overestimation of flow in this period.

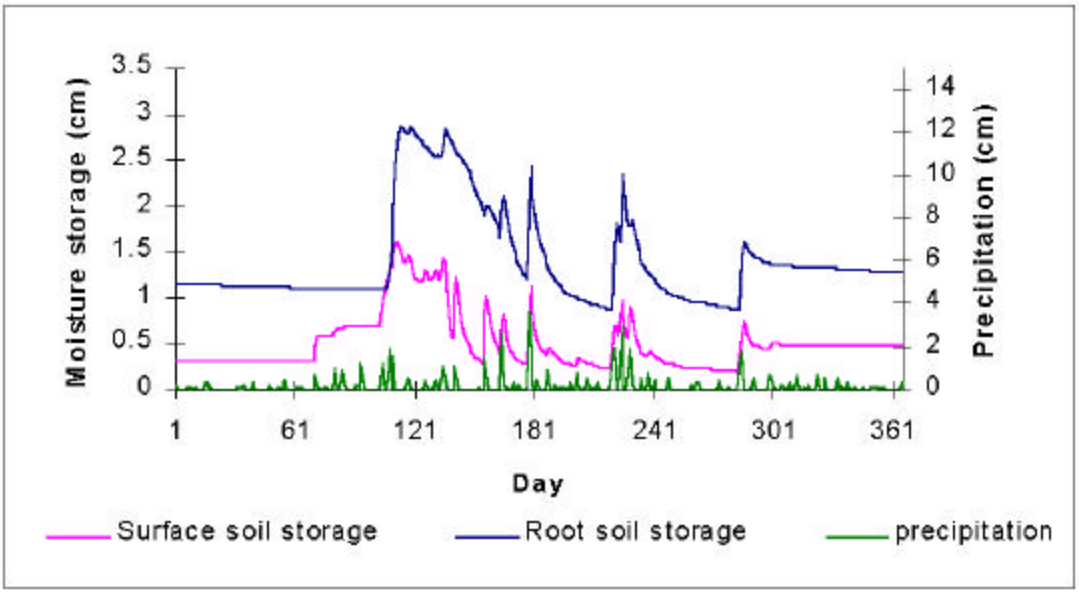

Figure 7. Moisture dynamics in the surface and the subsurface soil storage versus precipitation in the Assiniboine River basin in 1995

Results - Red River

Since the catchment area of the Red River basin is large, a division into three sub-catchments is implemented and routing is performed using local inflow and time delay between sub-catchments. Since the Red River flows north, melting of snow in its southern reaches starts earlier than in the lower reaches. As a result, flood starting time and flood peak time in the lower reaches occurs later than that in the southern reaches. Calibration and verification results of the hydrologic model implementation in the Red River basin show that this pattern was well reproduced and that the model captured the most important dynamics of flow occurring in the basin. In the calibration year (1996), simulated streamflow matched observed flood pattern well during the snowmelt active period at Grand Forks. Flooding from snowmelt started and reached peak in the middle of April, and lasted about 30 days (Figure 8a). In the late May, heavy rainfall resulted in the second peak. Flood pattern at Emerson and Ste. Agathe is to the great extent determined by the pattern in the southern reaches with a time delay. Adding snowmelt water in lower reaches, flow peaks at Emerson and Ste. Agathe were higher than that at Grand Forks and flood duration at Emerson and Ste. Agathe was much longer than that at Grand Forks. This pattern in flood starting time and time of peak occurrence as well as duration was reproduced by the model at Emerson and Ste. Agathe (Figures 8b and 8c). However, the magnitude of the peak at Emerson was overestimated. At Ste. Agathe, a second peak

generated in late May was overestimated by the model. This peak was mainly generated by local heavy rainfall in the lower reaches.

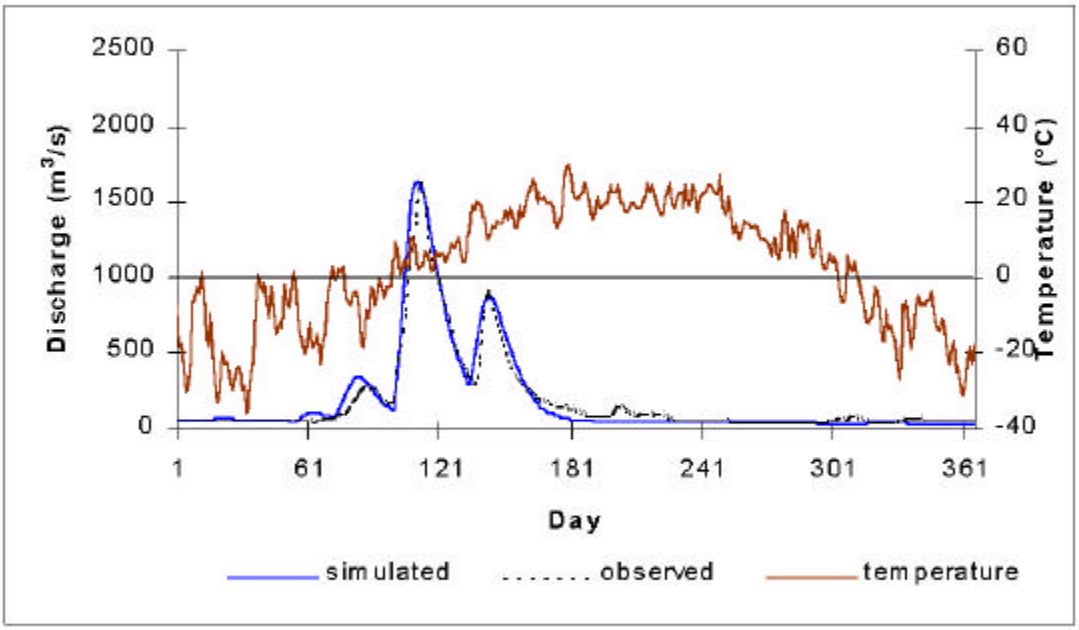

Figure 8a. Results of the model calibration (1996) at Grand Forks

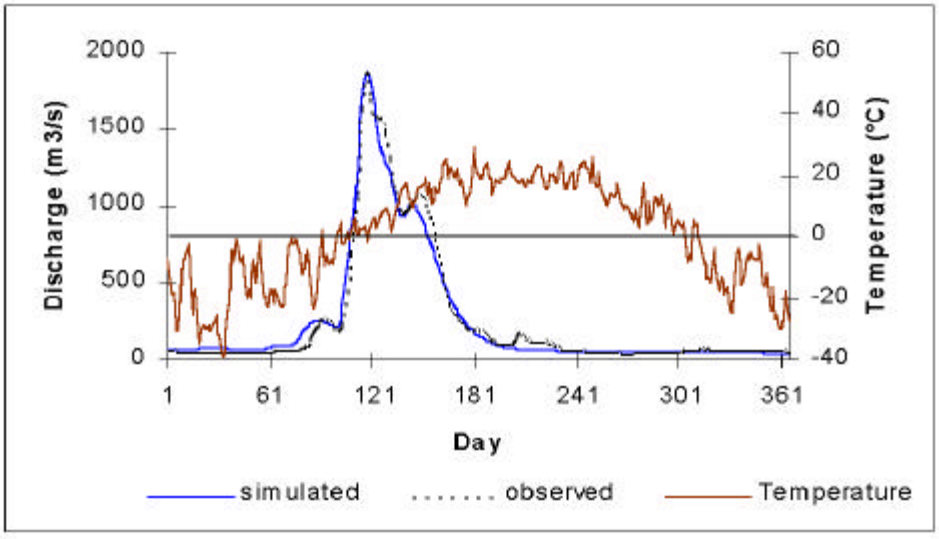

Figure 8b. Results of the model calibration (1996) at Emerson

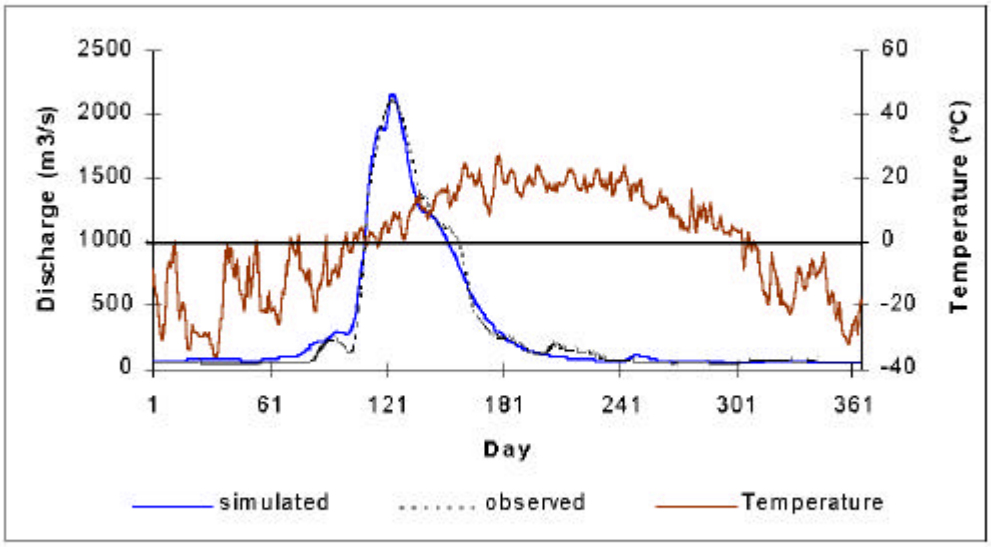

Figure 8c. Results of the model calibration (1996) at Ste. Agathe

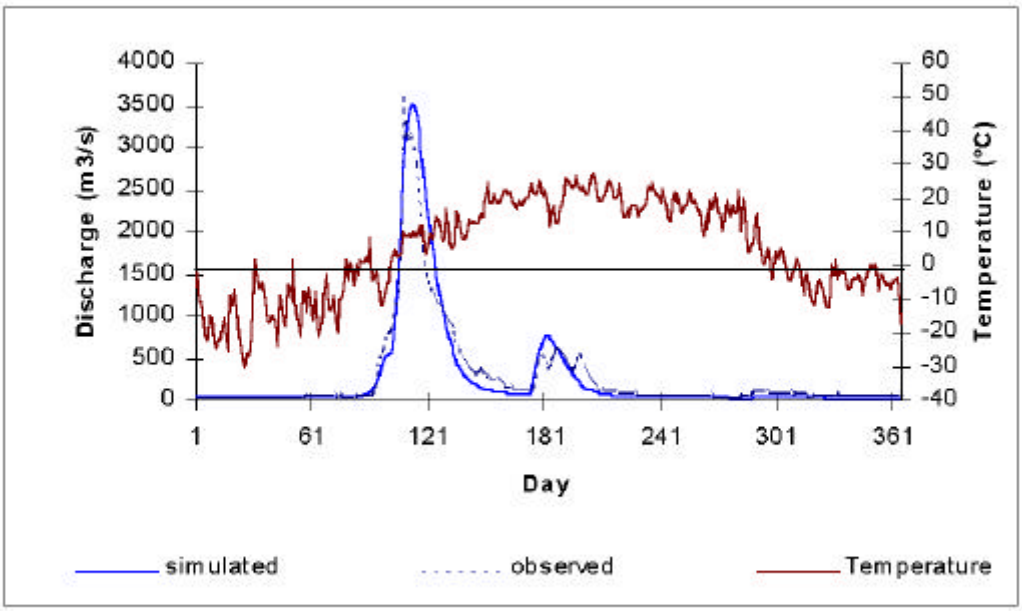

Figure 9a. Results of the model verification (1997) at Grand Forks

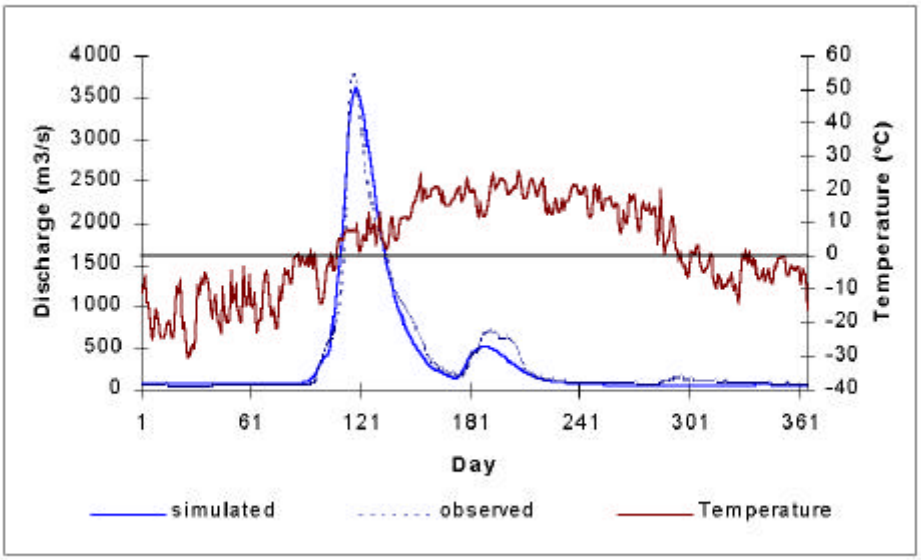

Figure 9b. Results of the model verification (1997) at Emerson

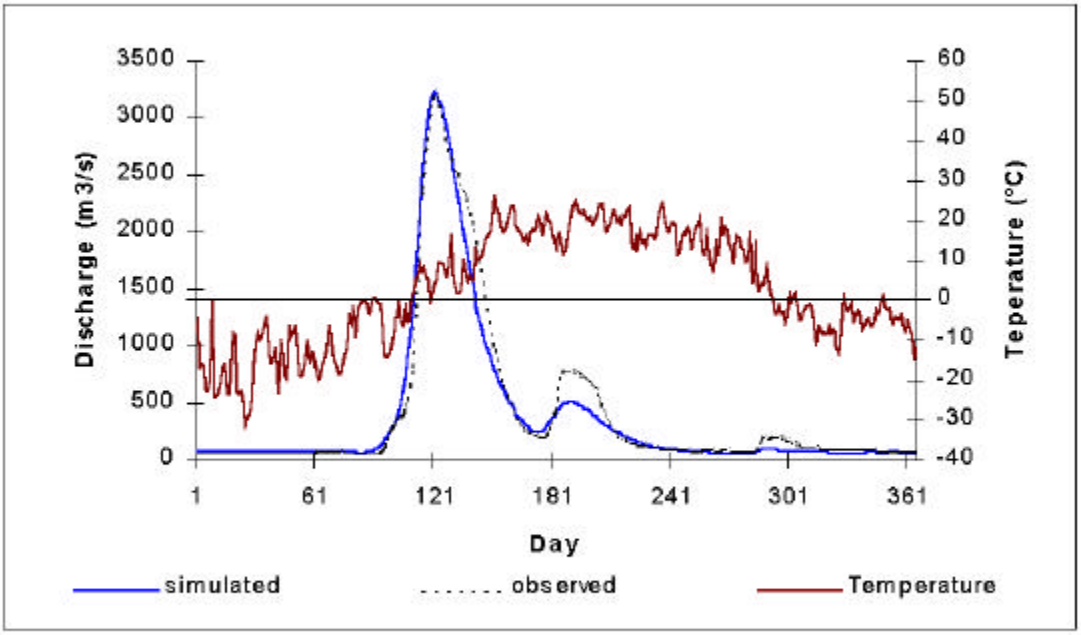

Figure 9c. Results of the model verification (1997) at Ste. Agathe

Figures 9a, b and c compare simulated and measured discharge for the verification run (1997 'flood of the century'). At Grand Forks, predicted flood duration matched the observed one, but the peak magnitude is smaller than observed and timing of peak is delayed. At Emerson and Ste. Agathe locations, the peak magnitude and time matched measured very well. After snowmelt active period, there was a heavy rainfall in early July, which produced another streamflow peak. After July, streamflow kept at the normal level.

Statistical evaluation of model results

The reproduction of historical records is the most important test of model performance. The goodness of fit of model results can be assessed graphically and statistically comparing simulated and observed values over time. In order to measure the goodness-of-fit between simulated and observed data, three statistical measures are employed in this study: coefficient of efficiency (R_E^2), coefficient of determination (R_D^2) or the square of the correlation coefficient, and the residual mass curve coefficient (R_R^2). They are calculated as:

$$R_E^2 = 1 - \left[\sum_{t=1}^{n} (Q_{St} - Q_{Mt})^2 / \sum_{t=1}^{n} (Q_{Mt} - \overline{Q}_M)^2 \right] \tag{39}$$

$$R_D^2 = \left[\frac{\frac{1}{n}\left[\sum_{t=1}^{n} (Q_{St} - \overline{Q}_S)(Q_{Mt} - \overline{Q}_M) \right]}{S_{Q_S} S_{Q_M}} \right]^2 \tag{40}$$

$$R_R^2 = 1 - \left[\sum_{t=1}^{n} (D_{Mt} - D_{St})^2 / \sum_{t=1}^{n} (D_{Mt} - \overline{D}_M)^2 \right] \tag{41}$$

Where: n is the length of time; t is the time; Q_{St} and Q_{Mt} are simulated and observed streamflow values at time t; $\overline{Q}_S$ and $\overline{Q}_M$ are the mean values, S_{Q_S} and S_{Q_M} are standard deviations; D_{Mt} is the departure from the mean for the measured residual mass curve; D_{St} is the departure from the mean for the simulated residual mass curve; and $\overline{D}_M$ is the mean of the departures from the mean for the measured residual mass curve.

R_E^2 is a measure of the overall performance of the model, while R_D^2 and R_R^2 provide information concerning the systematic error in the model (Aitken, 1973; Putty and Prasad, 2000). Higher values of R_E^2, R_D^2, and R_R^2 indicate better fit of calculate data to observed values. The statistical measures of the model performance are summarized in Table 3. The model-simulated mean and standard deviation are close to measured ones

and the R_E^2 is high (0.89 to 0.99). Therefore, the overall model performance is good. The magnitude of R_D^2 and R_R^2 reveals that the error is unsystematic and random.

Table 3. Statistical measures of the hydrologic model performance

Catchment	**Year**	**Mean**		**Standard Deviation**		**(R_E^2)**	**(R_D^2)**	**(R_R^2)**
		Measured	Simulated	Measured	Simulated			
Assiniboine River	1995	43.69	39.02	102.20	108.35	0.9378	0.9430	0.9350
	1979	19.89	20.65	47.62	50.17	0.9733	0.9766	0.9723
Red River Grand Forks	1996	187.36	187.95	281.75	318.60	0.9552	0.9755	0.9550
	1997	291.09	276.51	540.60	634.33	0.8836	0.9282	0.8841
Red River Emerson	1996	257.25	254.24	411.07	405.40	0.9851	0.9847	0.9846
	1997	371.83	351.04	670.65	705.42	0.9710	0.9758	0.9718
Red River Ste. Agathe	1996	310.32	310.28	515.49	502.20	0.9896	0.9881	0.9877
	1997	413.19	383.91	717.76	701.73	0.9710	0.9701	0.9701

In summary, calibration and verification of the model for the Assiniboine and the Red River shows that simulated streamflow stays within the bounds of measurement error, and fit the measured data quite well. The model successfully captures the most important watershed dynamics.

4. Model for the flood protection system performance assessment

Flood protection system for the City of Winnipeg is fairly complex. It includes the Red River Floodway, the Portage Diversion (on the Assiniboine River), the Shellmouth Dam and Reservoir on the Assiniboine River), and the primary diking systems and related flood protection infrastructure within the City. The performance of this complex system is dependent on the:

a. Flow from the upper Assiniboine river into the Shellmouth Reservoir;
b. Outflow from the Shellmouth Reservoir;
c. Local inflow along the Assiniboine River between the Shellmouth Reservoir and Portage diversion;
d. Operation of Portage diversion;
e. Red River flow upstream from the floodway;
f. Floodway operation; and
g. Total Red River flow in Winnipeg downstream from the Assiniboine River.

The hydrologic model presented in the previous section of the Report can predict the river flow at Shellmouth Reservoir on the Assiniboine River and at Emerson and Ste. Agathe on the Red River. Outflow from the Shellmouth Reservoir depends on the Shellmouth Reservoir operation rules. Portage diversion and the floodway are also controlled by the operating rules. Local inflow along the Assiniboine River and the Red River are estimated using the available data (Ahmad and Simonovic, 2000). A regional System Dynamics simulation model (DYHAM) is developed to allow for investigation of system behavior in response to different climate change scenarios. Three statistical indices: system reliability, vulnerability and resiliency, are employed to assess the performance of the flood protection system under different climatic conditions. DYHAM model contains two major sectors: (a) Shellmouth Reservoir operations sector; and (b) Red River Flood protection system indices sector. Both sectors are integrated within the model for seamless simulation of the flood protection system performance.

4.1 Modeling of Shellmouth reservoir operation

Effective operation and management of the Shellmouth reservoir provides water for the needs of agriculture, industry and ecological systems. System analysis has been found to play an important rule in reservoir operation and management, and system analysis techniques have been widely applied for reservoir operation and management in last three decades. Simulation has been used as an essential tool for developing a quantitative basis for reservoir management decisions Simonovic (1992). A majority of the management models focusing on reservoir storage and operation policies has been built. As an alternative promising tool, system dynamics simulation is gaining popularity in water resources modeling and management. Examples include global river basin planning (Palmer (1994; Palmer et al. (1993, 1995), drought studies (Keyes and Palmer, 1993; Fletcher, 1998) and long-term water resources planning and policy analysis (Simonovic et al., 1997, Simonovic and Fahmy, 1999). More recent study of the reservoir operation for flood management using system dynamics approach was conducted by Ahmad and

Simonovic (2000). This study applied system dynamics to analyze internal system structure of the reservoir management decisions that related the water inflow to the reservoir storage, water outflow control and reservoir operating rules, and extent of flooding upstream and downstream from the dam. Potential to reduce floods and damages through modification of spillway and alterations of operation rules were presented. Our study is using the modified Shellmouth reservoir management model developed by Ahmad and Simonovic (2000).

Simulation of reservoir performance (calculation of reservoir storage and release) depends on the reservoir inflow, flooding potential upstream and downstream from the dam, and demands for water from the reservoir for different uses. Figure 10 shows a feedback causal loop diagram that describes reservoir dynamics. Control variable for reservoir operation is the water release rate, which is determined from the demand structure, desired reservoir level, and upstream and downstream flooding conditions. There are three negative feedback loops that control the release:

(1) Release -> Reservoir storage +>Storage difference +> Release;
(2) Release -> Reservoir storage +>Reservoir level +> Reservoir area +> Upstream flooding +> Release;
(3) Release +> River flow +>Downstream flooding -> Release.

Loop (1) controls reservoir storage (to follow operating rule), while loops (2) and (3) comprehensively consider the upstream and the downstream flooding conditions with the objective of minimizing the total flooded area.

Water losses from the Shellmouth Reservoir include evaporation and seepage. The losses are dependent on the reservoir storage and surface area. A negative feedback loop that control the losses can be resented in the following form:

(4) Reservoir loss -> Reservoir storage +> Reservoir surface area +> Reservoir loss.

Based on the mass balance equation, the reservoir storage can be calculated using:

$$\frac{dRS}{dt} = INFLOW - RELEASE - LOSS \qquad (42)$$

Where: RS represents the reservoir storage (acre feet); INFLOW stands for inflow entering into the reservoir; RELEASE denotes water discharge through the conduit and the spillway; and LOSS denotes the total losses through seepage and evaporation.

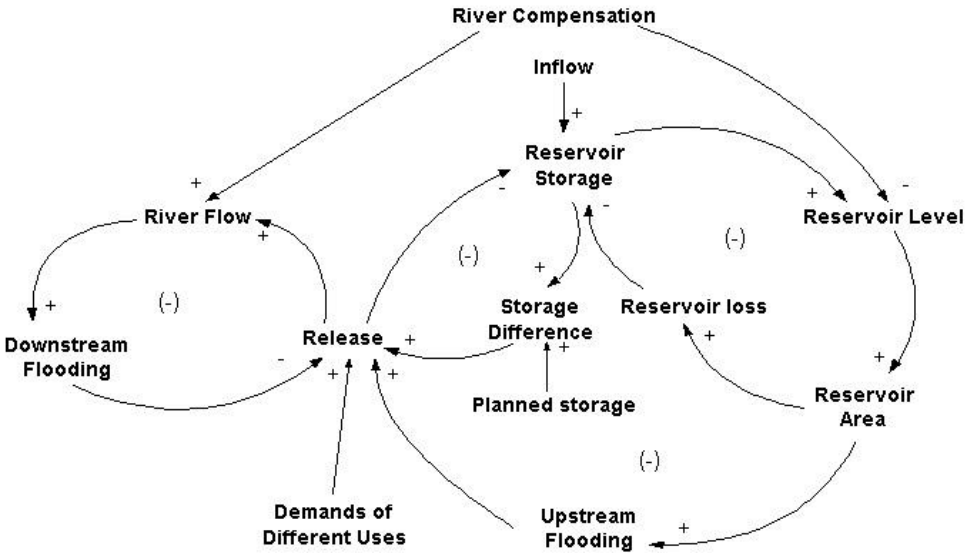

Figure 10. A feedback causal diagram of Shellmouth reservoir operation

INFLOIW will in our model will be either measured historical flow or predicted flow by the hydrologic model corresponding to different climate change scenarios.

RELEASE consists of conduit outflow and spill of water. Conduit outflow depends on the minimum water demand (50 acre-feet/day), planned reservoir storage, outflow capacity under selected conduit operation, and flooding conditions. Reservoir operating rule curve and conduit rating curve are plotted in Figures 11 and 12.

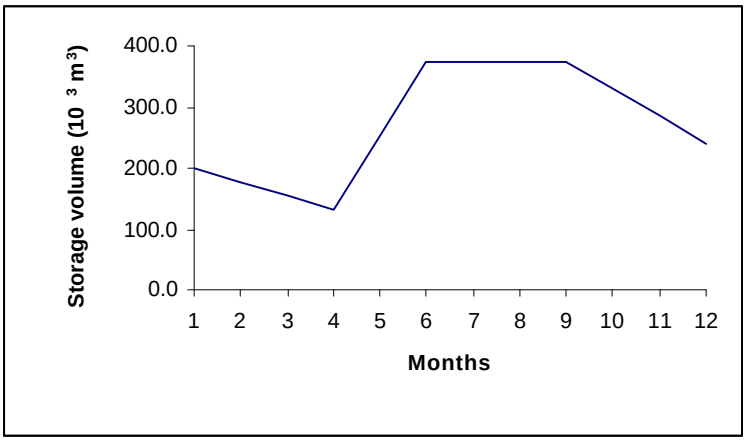

Figure 11. Shellmouth Reservoir rule curve

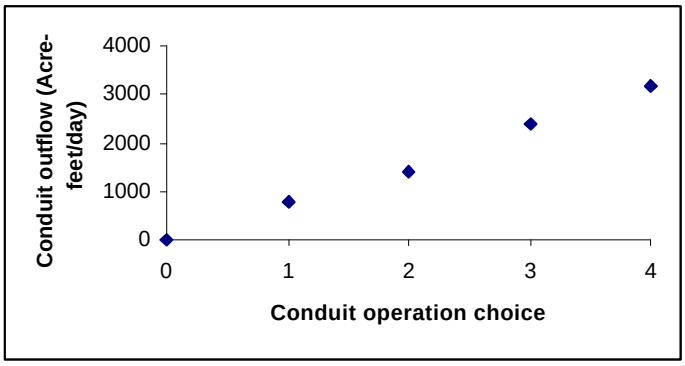

Figure 12. Shellmouth Reservoir conduit rating curve

Reservoir seepage and evaporation losses are assumed to be proportional to reservoir storage as shown in Figure 13.

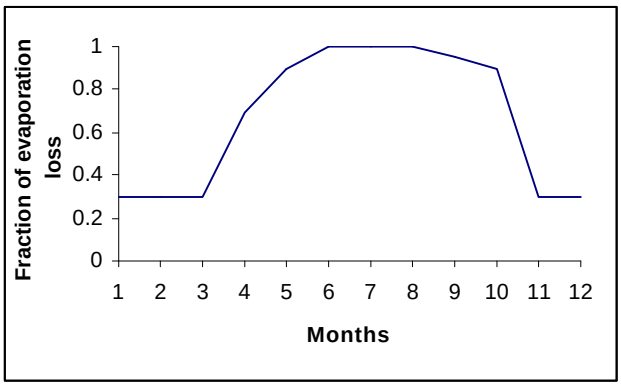

Figure 13. Shellmouth Reservoir losses

Upstream flooding

Upstream flooding is triggered by a combination of streamflow and the current reservoir level. It is represented in the model using the flooded area and the duration of flooding conditions measured in days. Each of them is expressed as a function of reservoir inflow and reservoir level. The number of days is also calculated when upstream is flooded.

Downstream flooding

Downstream flooding is triggered by the reservoir operation and the local inflow. Individual flooded area and duration of flooding at selected locations between the dam and the final disposal points of the river is calculated from the reservoir outflow and the local inflow. Downstream flooded area is divided into five sub-areas (Ahmad and Simonovic, 2000). Rating curves are provided for each of them by the Manitoba Conservation (Ahmad and Simonovic, 2000). Total downstream flooded area is also calculated.

4.2 Red River flood protection system indices

The main objective of this study is to investigate the ability of the existing Red River flood protection flood protection system to operate satisfactorily under different scenarios of future climate change. Risk-based criteria for evaluating the performance of water resources systems have been used in the past by a number of researchers. Hashimoto (1982) formulated three criteria for evaluating the possible performance of water resource systems, including reliability, resiliency and vulnerability. After Hashimoto et al. (1982), Moy et al. (1986), Burn et al, (1991) and Simonovic et al. (1992), reliability is defined as the likelihood of system failure, vulnerability is used to describe the severity of the failure, and resiliency measures how quickly the system recovers from the failure state. These three criteria were adapted and modified in this study for the assessment of performance of the Red River flood protection system.

Reliability
The reliability is defined as the probability of system being in a satisfactory state. It can be expressed as a ratio of the number of non-failure time intervals to the total number of time intervals in the period under consideration, i.e.:

$$a = \frac{1}{NS}\sum_{t=1}^{NS} z_t \tag{43}$$

with

$$z_t = 1 \quad \forall x_t \in S \tag{44}$$

$$z_t = 0 \quad \forall x_t \in F \tag{45}$$

Where: α is the reliability; z_t is the state of the flood control system in the time interval t; S is the satisfactory state; F is the failure state; NS is the duration of the operating period.

Failure states in this study are considered to be time intervals during which flow exceeds the channel capacity at different control locations along the river. In the case of Shellmouth Reservoir the failure state is determined on the basis of reservoir water level and its relationship to the rule curve. In this study, the yearly reliability and the total reliability (calculated over the operating horizon) are considered.

Vulnerability
Vulnerability measures the severity of failure. In this study, it is simply defined as the maximum difference between the maximum and calculated value of a certain variable (river flow or reservoir water elevation). It is calculated on the yearly basis as:

$$b_y = \begin{cases} 0 & \text{if} \quad V_t \le V_f \\ \text{Max}[V_t - V_f] & \text{else} \end{cases} \tag{46}$$

Where: β_y is the notation for vulnerability; V_t is reference level of river flow or reservoir water elevation at the time t; V_f is the calculated value of river flow or reservoir water elevation. If it is used as the long-term indicator, vulnerability is defined as the mean normalized value of yearly vulnerability:

$$b_m = \frac{\sum_{f=1}^{NF} b_y}{NF} \tag{47}$$

$$b_n = \frac{\sum_{f=1}^{NF} b_y}{V_f * NF} \tag{48}$$

Where: β_m is the mean vulnerability; f is the counter of failure states; NF is the total number of failure states during the operating period; and β_n is the normalized mean vulnerability.

Resiliency

Resiliency describes system's ability to bounce back from the failure state. It is evaluated in this study on a yearly basis. An original formulation for measuring resiliency of water resources systems was developed by Simonovic et al. (1992):

$$g = \frac{1}{\left(\frac{MD}{NS}\right) * FN} \tag{49}$$

Where: γ is the resiliency indicator; MD is the maximum number of consecutive time intervals of failure state in a year; NS is the number of days in a year; FN is the number of failure state time internals in a year.

4.3 Development of the regional dynamic hydroclimatologic assessment model and its application

Description of regional dynamic hydroclimatologic assessment mode DYHAMl
Regional dynamic hydroclimatologic assessment model integrates three modules: (a) climate change scenario generator that is based on different general circulation models; (b) hydrologic model; and (c) flood protection system performance assessment model. Figure 14 presents a schematic diagram of the DYHAM model.

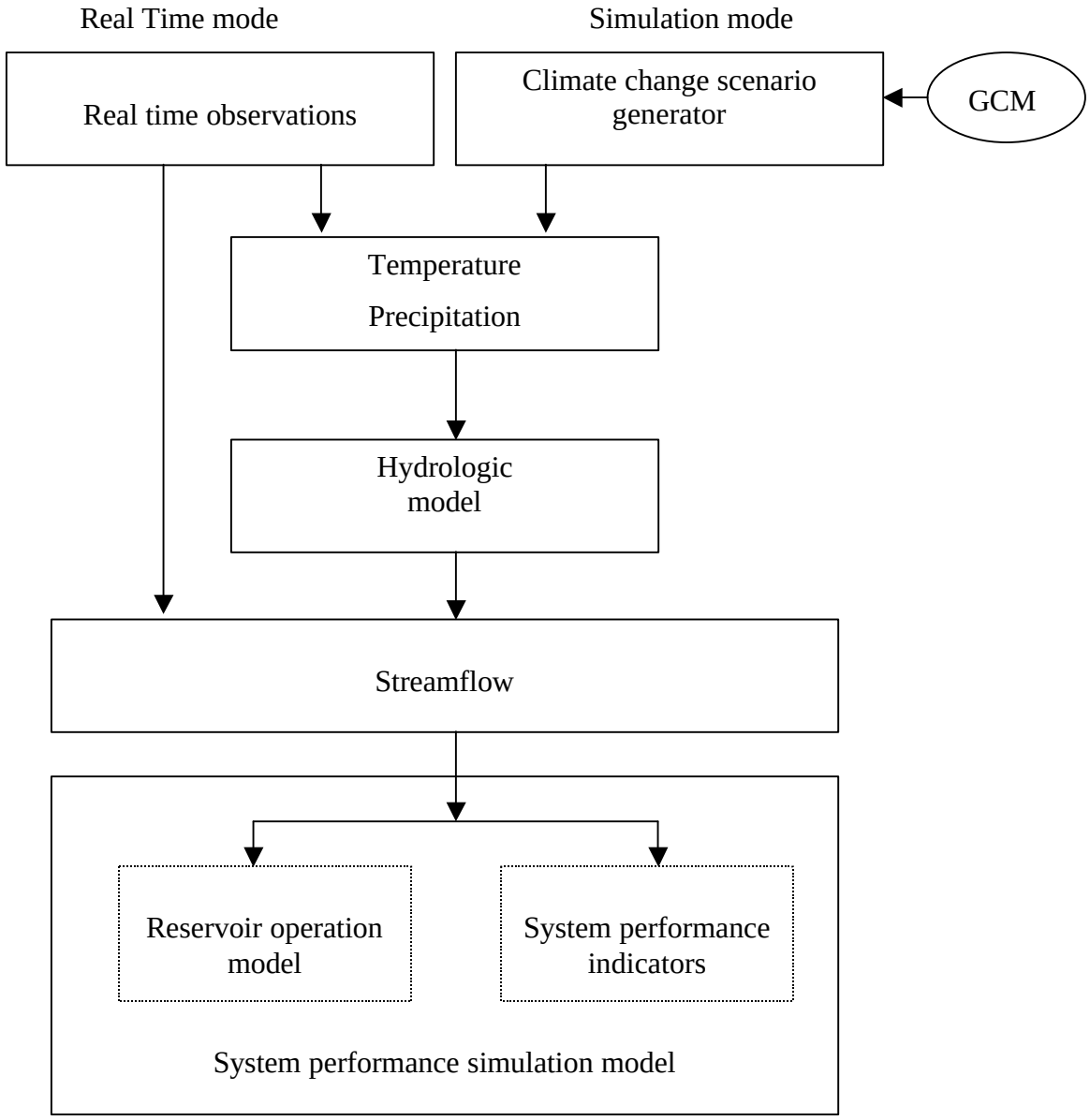

Figure 14. Schematic diagram of DYHAM model

GCM module is based on the fundamental conservation laws of mass, momentum and energy which describe the apportioning and transport of heat and moisture by the atmosphere and ocean (Cubasch and Cess, 1990). It provides information to the climate change scenario generator in the form of daily temperature and precipitation. The output of scenario generator represents the input into the system dynamics hydrologic model. Hydrologic model bridges the gap between global climate change information and regional data needed for assessment of the performance of flood protection system. Hydrologic model simulates streamflow and flood patterns generated by snowmelt under different temperature regimes. Streamflow generated by the hydrologic model is used as input into the system dynamics assessment model that includes two important sectors: (a) reservoir operation model; and (b) flood protection system simulation. DYHAM is fully implemented in STELLA II programming environment using system dynamics modeling approach.

DYHAM model can be used in real time and simulation mode. Real time mode uses observed temperature and precipitation data as inputs into the hydrologic model for streamflow simulation, or directly employs observed streamflow as input into the assessment process. Therefore, three components of DYHAM can be separately applied for different purposes. Flexibility of the STELLA programming environment allows for easy use of the model in different modes.

5. Application of DYHAM in the Red River basin

5.1 Description of the study area

The proposed regional dynamic hydroclimatologic assessment model has been applied for simulating streamflow and assessing the impact of climate variability and change on performance of complex flood protection system in the Red River basin. The main purpose of this system is protection of the City of Winnipeg, a largest population location in the Red River basin with a population of about 670,000.

There are two main rivers flowing through the City: Assiniboine River and Red River. Assiniboine River originates in the middle northwest Saskatchewan and drains the area from eastern part of Saskatchewan to the western part of Manitoba. Its major tributaries include Qu'Appelle River and Souris River. The Assiniboine River flows from Northwest to Southeast and enters into the Red River at Winnipeg in Manitoba. Assiniboine River and its tributaries drainage basin is 110,450 km^2 large. The Red River originates in Minnesota and flows north to its outlet at Lake Winnipeg in Manitoba, passing through the flat and fertile valley of the former glacial Lake Agassiz. With the exclusion of the Assiniboine River and its tributaries, the Red River basin covers 116,550 km^2 of which 103,600 km^2 in the United States.

The flooding in the Assiniboine and Red River, mainly caused by snowmelt and heavy rain in the spring, has resulted in extensive damage to residential, agricultural, and industrial properties. Prior to 1997, the flood protection system had performed well to protect Winnipeg and other cities between the Shellmouth dam and Winnipeg along the Assiniboine River from the flooding. Even in 1997 when the flood protection system was stretched to its limits, Winnipeg suffered comparatively much less damage due to extensive flood control infrastructure that has been in place since early 1970s.

This study attempts to predict the discharge patterns and assess the performance of the existing complex flood protection system along the Red and the Assiniboine River under different climate change and variability scenarios. Study area and towns considered in this study are shown in Figure 15.

5.2 Description of the flood protection system

General design criteria used in the design and construction of the Winnipeg flood protection system was to provide protection for the 1:160 year flood with a capacity of 4,786 m^3/sec (169,000 cfs) at Redwood Bridge downstream from where the Assiniboine and the Red River merge. The major components of the Winnipeg flood protection system are the Red River Floodway, the Portage Diversion, the Shellmouth Dam and the diking system and related infrastructure within the City. The location of these facilities is shown in Figure 15. Capacity of the existing flood protection structures has been evaluated by many engineering studies (IJC, 1999; 2000; KGS Group, 1999; 2000).

The Red River Floodway is the most important flood protection structure providing extensive protection for the City of Winnipeg. The floodway construction started in 1962 and was completed in 1968. It consists of four main components, i.e. the floodway channel, the inlet control structure, the dikes and the outlet structure. Designed capacity of the floodway is 1,700 m^3/sec (60,000 cfs) with a high reliable capacity of 2,070 m^3/sec (73,000 cfs) and a low reliability capacity of 2,520 m^3/sec (89,000 cfm) (KGS Group, 1999). Current floodway operating rule initiates floodway operation when the flow within Winnipeg exceeds 1700 m^3/sec.

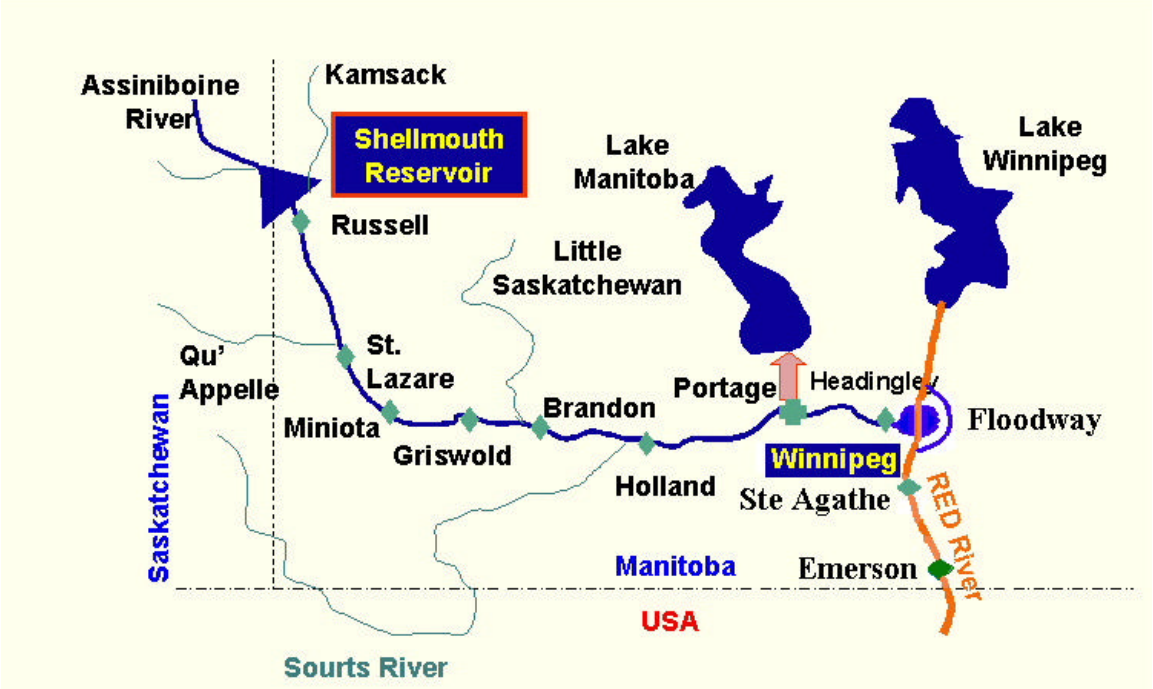

Figure15. Case study area and location of major flood control structures (After Ahmad and Simonovic, 2000)

The Portage Diversion, an 18-mile long channel designed to carry up to 708 m^3/sec (25000 cfs) of flood flow from the Assiniboine River into the Lake Manitoba, is located at a point just upstream of Portage la Prairie. The Portage Diversion provides flood protection for the City of Winnipeg and Portage la Prairie, and the area between the cities. Construction of Portage Diversion started in 1965 and was completed in 1970. Its major elements include the dam in the Assiniboine River, the concrete spillway control structure, the diversion structure that controls water entering the Portage Diversion, the diversion channel itself, two gradient control structures and the outlet structure where the diverted flow passes into the Lake Manitoba.

Shellmouth Dam, approximately 1,319 m long and 19.8 m high, is located about 48 miles northwest of Russell, Manitoba. Construction of the dam started in 1964 and was completed in 1972. Shellmouth dam contains a gated concrete horseshoe-shaped conduit with a maximum discharge capacity of 198.2 m^3/s on the east abutment and a concrete

chute spillway on the west abutment control. Flood flows in excess of the conduit capacity are either stored in the reservoir or passed over the ungated concrete chute spillway. The reservoir created by the Shellmouth Dam is about 56 km long, 1.28 km in average width. The reservoir covers about 61 km^2 surface area and is capable of storing 390,000 acre-feet of water when it is full. The elevation of the top of the dam is 435 m above mean sea level with a dead storage elevation level of 417 m. The spillway elevation is at 429 m which is 6 m lower than the top of the dam. The reservoir has a $12.3x10^6$ m^3 storage volume of the inactive pool below the conduit invert elevation. The difference between volume of reservoir at active storage ($370x10^6$ m^3) and crest level of natural spillway ($477x10^6$ m^3) is the flood storage capacity of the reservoir, i.e. $107x10^6$ m^3 (Ahmad and Simonovic, 2000). Current operating rule specifies that the reservoir storage should reach the seasonal goals all year around (Figure 11), with maximum reservoir outflow being limited to 42.5 m^3/s to prevent flooding downstream. Also, the outflow must be greater than 0.71 m^3/s to avoid damage to fish and aquatic life in the river system. Original designed capacity of Shellmouth Dam is 198 m^3/s. The protection offered by the reservoir benefit entire reach of Assiniboine River between the Shellmouth Dam and its confluence with the Red River at Winnipeg by both flood reduction and low flow augmentation (IJC, 1999).

The diking system within the City of Winnipeg was built in 1950 and encloses the Red, Assiniboine and Seine Rivers. The dikes are mostly built to the designated Flood Protection Level (FPL) or higher. The FPL is designed as the profile along the Red and Assiniboine Rivers that corresponds to the design flood, plus 2 ft of freeboard (IJC, 1999). Designed capacity of river channel is about 2,180 m^3/sec (77000 cfs), with a high reliable capacity of 2,010 m^3/sec (71000 cfs), and low reliable capacity of 2,633 m^3/sec (93000 cfs) (IJC, 1999).

Total capacity of the overall flood protection system is shown in Table 4. The designed capacity of flood protection works was to provide protection for the 1:160 year flood of 4,786 m^3/sec (169000 cfs) at merging point of Red and Assiniboine Rivers. Total capacity with high reliability is about 4,986 m^3/sec, and with low reliability about 6,059 m^3/sec.

Table 4. Capacity of the Red River flood protection system (modified after IJC, 1999, 2000)

Component	**Design capacity**		**1997**		**High reliable capacity**		**Low reliable capacity**	
	m^3/sec	cfs	m^3/sec	cfs	m^3/sec	cfs	m^3/sec	cfs
Shellmouth Dam	198	7,000	113	4,000	198	7,000	198	7,000
Portage Division	708	25,000	337	11,900	708	25,000	708	25,000
Red River Floodway	1,700	60,000	1,900	67,100	2,070	73,000	2,520	89,000
Diking System	2,180	77,000	2,260	80,000	2,010	71,000	2,633	93,000
Total	4,786	169,000	4,610	163,000	4,986	176,000	6,059	214,000

5.3 Results of the DYHAM model application

Temperature and precipitation data for selected climate variability and change scenarios have been processed by the hydrologic model to provide streamflow value at different locations in the Assiniboine and the Red River basin. Streamflow scenarios are used as input into the assessment model to evaluate the performance of the flood protection system. The results of DYHAM applications are presented below.

GCM simulation of temperature
Temperature pattern, together with precipitation, generated by three different GCM models is affecting streamflow generation and at the end flood protection system performance. GCM generated temperature data are shown in Figures 16 and 17. Comparison of the average monthly temperature calculated from 100 years of simulated data for two scenarios of HADCM3 (control and S1) are clearly showing higher temperature at each location in the case study area for S1 scenario (Figure 16).

Comparison of different GCM models is illustrated in Figure 17. Average monthly temperature calculated from 100 years of simulated data from HADCM3 and ECHAM4 S1 scenarios are showing that the ECHAM4 model predicts higher temperature increase than the HADCM3 model throughout the case study area. These model differences must be taken into consideration in the discussion of the final performance assessment results.

GCM simulation of precipitation
Three GCM models used in this study provide data with different spatial resolution (see Section 2 of this report). Therefore, three different data comparison experiments are presented:

(i) Comparison of annual precipitations from Control run and Scenario 1 (S1) of HADCM3;
(ii) Comparison of annual precipitation from Scenario 1 (S1) of ECHAM4 and HADCM3; and
(iii) Comparison of annual precipitation from Scenario 2 (S2) of CGCM1 and Scenario 1 (S1) of ECHAM4.

First experiment is designed to illustrate the difference between control and one of the climate change scenarios (S1). In the second experiment the impact of model choice is illustrated through the comparison between HADCM3 and ECHAM4 simulations of scenario 1. Third experiment provides some additional insight in the difference that may occur due to the choice of GCM and different scenario of climate development. Since this comparison is based on the two different climate change scenarios results should be taken with caution.

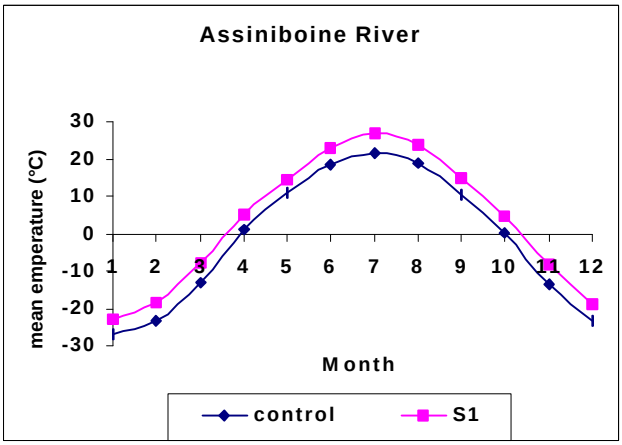

(a)

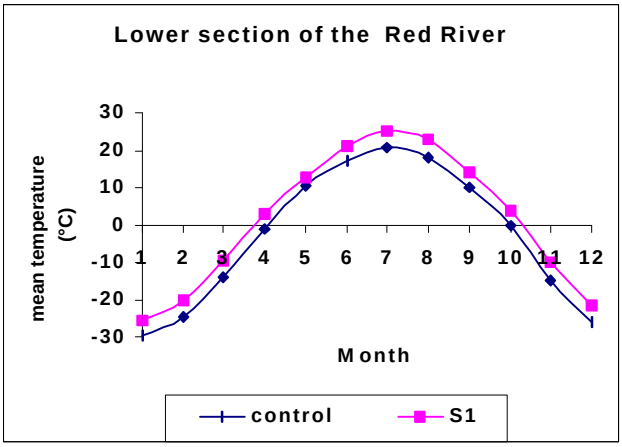

(b)

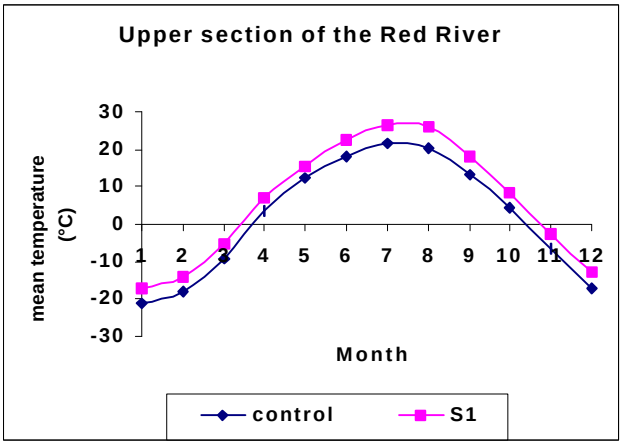

(c)

Figure 16. Mean monthly temperature simulated using HADCM3 model

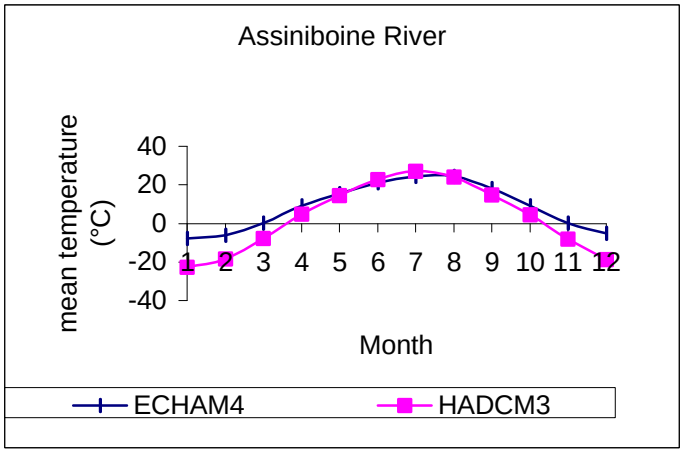

(a)

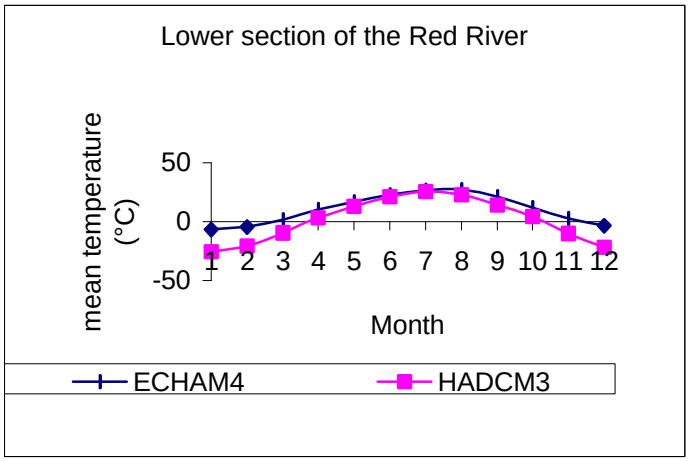

(b)

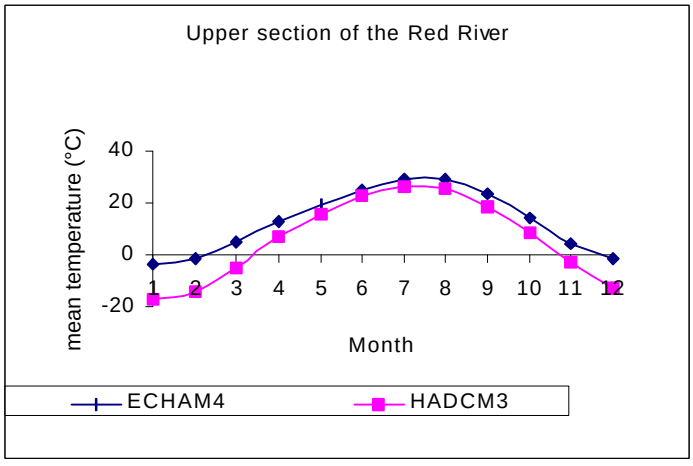

(c)

Figure 17. Average monthly temperature generated by ECHAM4 and HADCM3 models for scenario S1

The generated annual precipitation is shown in Figures 18, 19 and 20. The results indicate that precipitation generated by S1 of HADCM3 exceeds in most years precipitation generated by the control scenario of the same model. In the Assiniboine River basin, the average annual precipitation over the 100-year simulation horizon from the HADCM3 control run and S1 run is 19.35% and 28.57% higher than the historical average (450 mm), respectively (Table 5). Scenario S1 produces 11.43% higher average annual precipitation than the control run (Table 5). In the Red River basin, generated annual precipitation in different sections of the basin from the HADCM3 control and S1 simulation is higher than that from historical data (basin average is 500 mm). In the Red River basin scenario S1 produced higher average annual precipitation than the control run in all sections (Table 5).

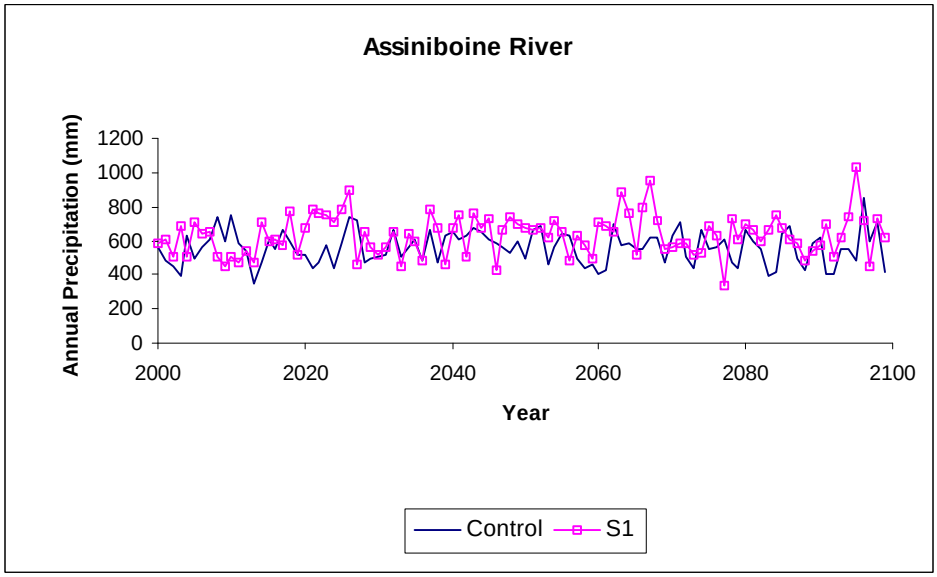

(a)

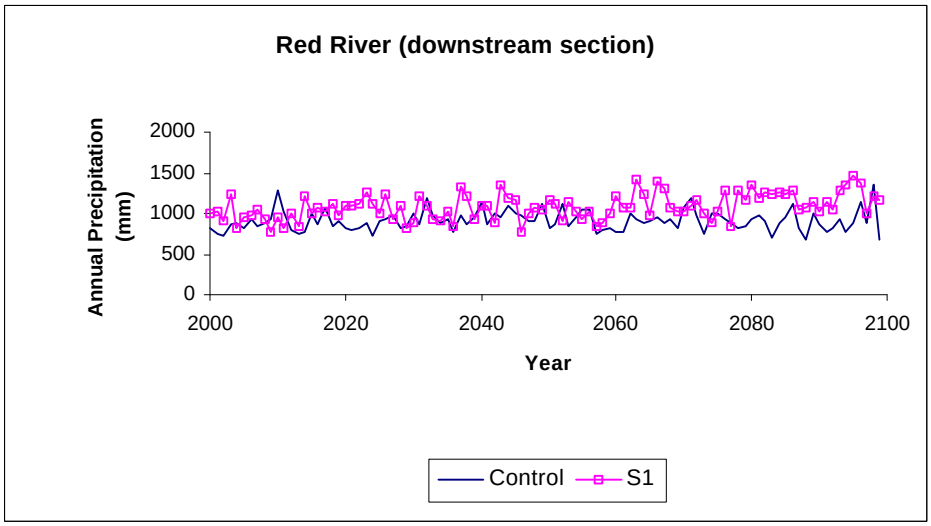

(b)

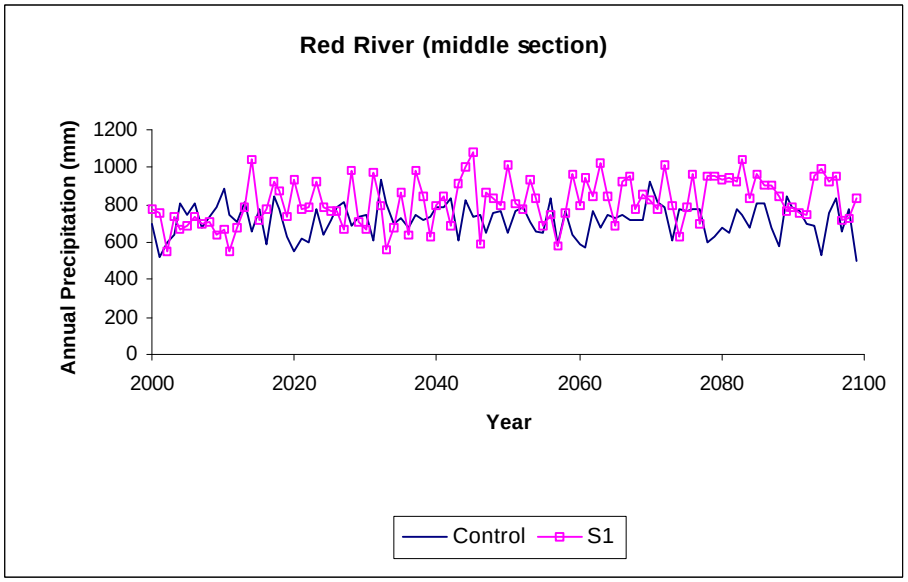

(c)

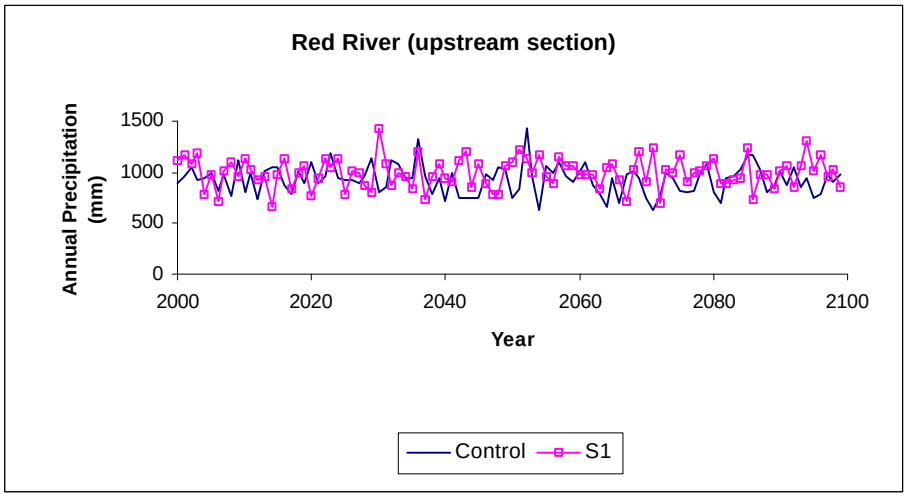

(d)

Figure18. Comparison of annual precipitation generated by HADCM3

Table 5. Comparison of average annual precipitation (mm) generated by HADCM3

	Assiniboine River		**Downstream section of the Red River**		**Middle reach of the Red River**		**Upstream section of the Red River**	
	Control	S1	Control	S1	Control	S1	Control	S1
Max	851.1	1036.4	1341.0	1469.6	935.2	1084.3	1425.7	1427.4
Min	347.4	336.1	671.9	765.9	497.8	551.3	624.9	661.2
Mean	558.0	630.2	908.1	1080.9	720.9	815.7	927.3	994.6

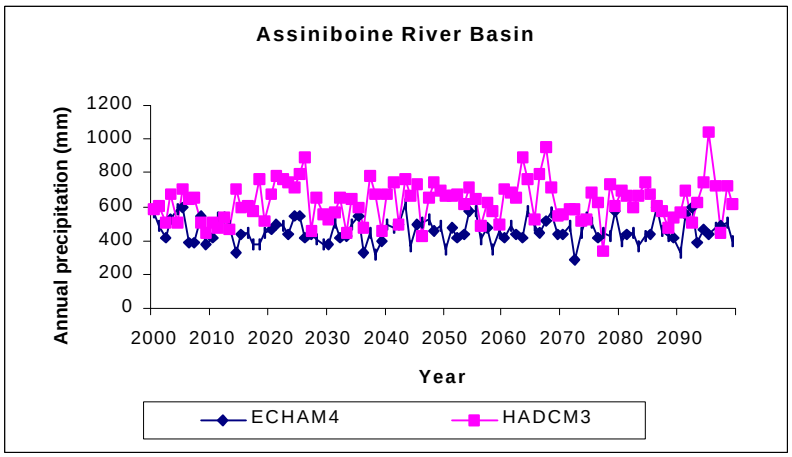

(a)

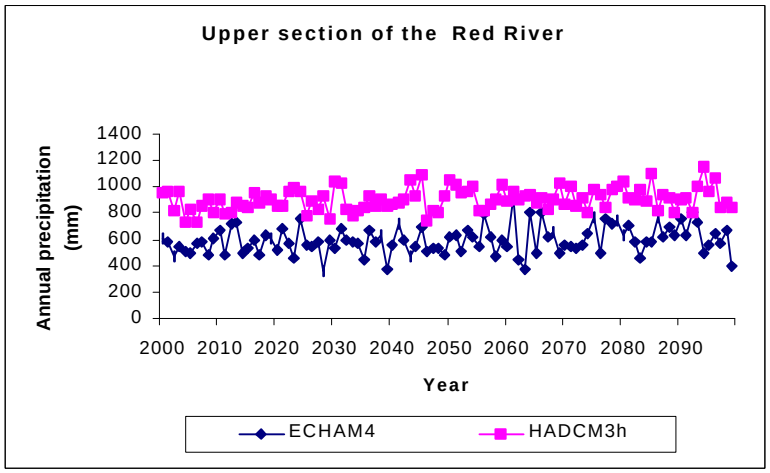

(b)

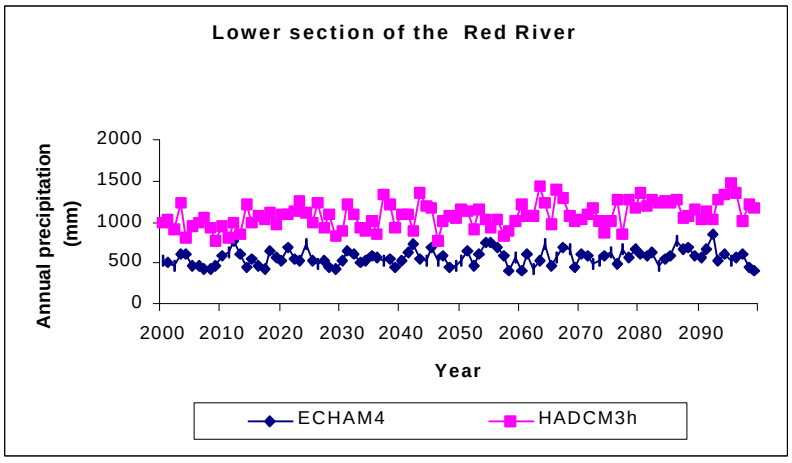

(c)

Figure 19. Comparison of annual precipitation generated by HADCM3 and ECHAM4 models for Scenario 1

Annual precipitation generated by ECHAM4 and CGCM1 models is presented in Figure 20 and Table 6. It is important to note that they are generated from different scenarios since daily data was not available for scenario 1 of CGCM1. Comparison of three scenarios (control run, S1 and S2) from three different models shows that HADCM3 S1 predicted the highest annual precipitations, while ECHAM4 S1 generated the lowest. When compared with the historical data, ECHAM4 generated average annual precipitation of 459 mm (minimum 283 mm and maximum 619 mm) in the Assiniboine River basin, 564.1 mm in the downstream sub basin of the Red River and 594.1 mm in the upstream sub basin of the Red River. These figures are closest to the historical average of 450 mm in the Assiniboine River basin, and 550 mm in the Red River basin. HADCM3 and CGCM1 predicted higher average annual precipitation than the historical data in both river basins (Tables 5 and 6). The results also indicate that the downstream section of the Red River might receive more precipitation than the upstream section (Tables 6) under the climate change scenarios.

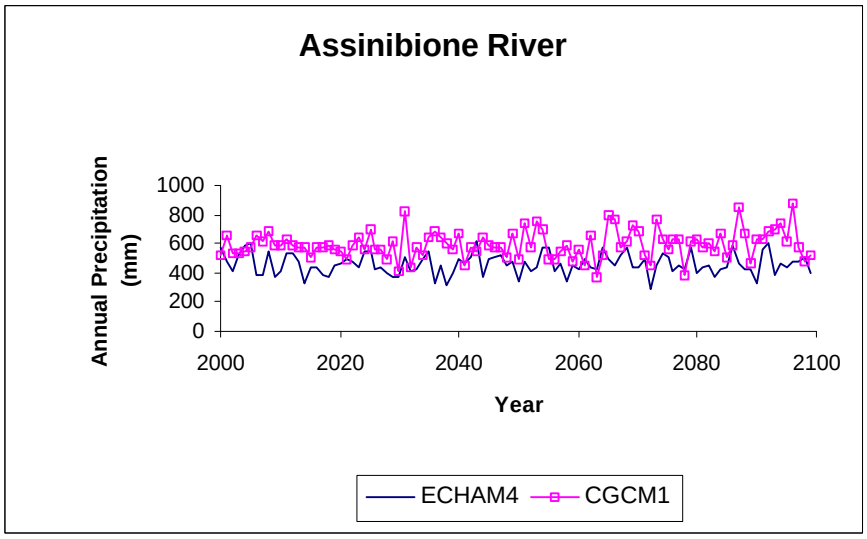

(a)

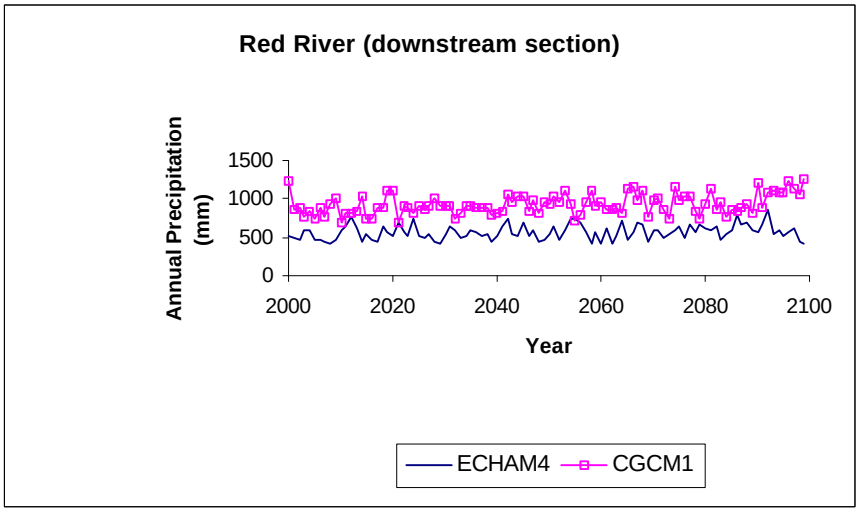

(b)

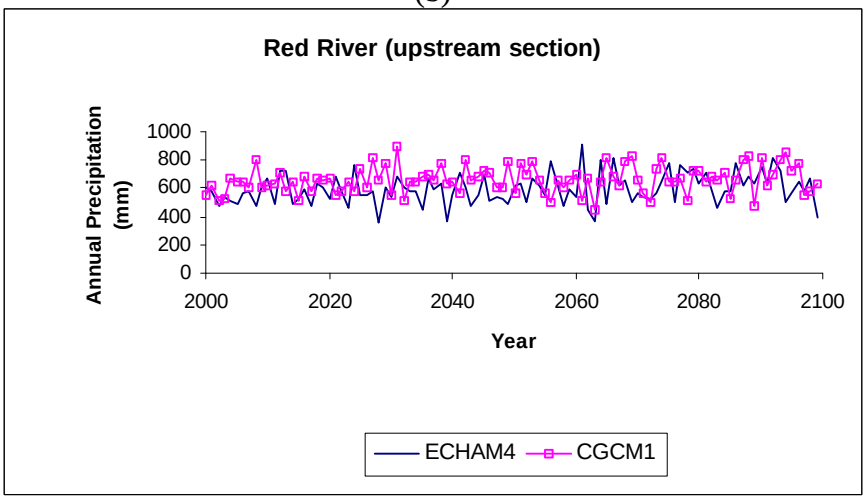

(c)

Figure20. Comparison of annual precipitation generated by CGCM1 for scenario S2 and ECHAM4 for scenario S1

Table 6. Comparison of annual precipitation (mm) generated by ECHAM4 and CGCM1

	Assiniboine River		**Downstream section Red River**		**Upstream section Red River**	
	ECHAM4 (S1)	CGCM1 (S2)	ECHAM4 (S1)	CGCM1 (S2)	ECHAM4 (S1)	CGCM1 (S2)
Max	617.9	878.7	856.9	1255.7	911.2	888.5
Min	283.6	375.9	407.5	678.7	361.3	448.7
Mean	459.6	594.9	564.1	927.4	594.1	660.2

Hydrologic model simulation of streamflow

Hydrologic model simulations are performed to generate streamflow in the basin using the temperature and precipitation data generated by GCM models. Model calibration and verification are presented in the Section 3.2 of this report. Simulated streamflow at Shellmouth dam location in the Assiniboine River basin, and at Ste. Agathe and Floodway entrance in the Red River basin are shown in Figures 21-32. Careful analysis of simulation results shows that different GCM scenarios resulted in different streamflow patterns.

First analysis of generated streamflow data involves comparison with historical floods. In the Assiniboine River basin, simulation of HADCM3 control scenario from 2000 to 2100 results in only one flood greater than that of 1995. Scenario S2 of the CGCM1 generated three floods larger than that of 1995. Scenario S1 of HADCM3 and S1 of ECHAM4 did not generate floods greater than flood of 1995. In the Red River basin over the period from 2000 - 2100, only scenario S1 of HADCM3 generated one flood greater than that of 1997. All other scenarios did not result in floods exceeding that of 1997.

Second analysis is performed to compare the streamflow data generated for different climate change scenarios. Choice of GCM impacts the analysis of climate change impacts. Figures 33 and 34 presents the average annual streamflow at Shellmouth dam location in the Assiniboine River basin and at Ste. Agathe and Floodway entrance in the Red River basin. It is important to repeat that comparison of same scenarios generated by different models was not possible as explained earlier.

In the Assiniboine River basin, the average annual streamflow at the Shellmouth dam generated by HADCM3 control run and scenario S1 do not show significant difference. However, the average (over 100 years) annual streamflow generated by the scenario S1 is lower than the streamflow generated by control run (Table 7). Further comparison between different models shows that the difference in generated streamflow (average value over 100 years) can be as high as 30 – 31% (see Table 8).

Among scenarios of three GCM models, scenario S2 of CGCM1 resulted in the highest annual streamflow and scenario S1 of ECHAM4 in the lowest (Figures 33 and 34 and Tables 7 and 8). The average annual streamflow over 100 years also shows the same tendency. The scenario S2 of CGCM1 produces higher flow the scenario S1 of HADCM3 that produces higher flow than the control run of HADCM3 that produces higher flow than the scenario S1 of ECHAM4 (Tables 7and 8).

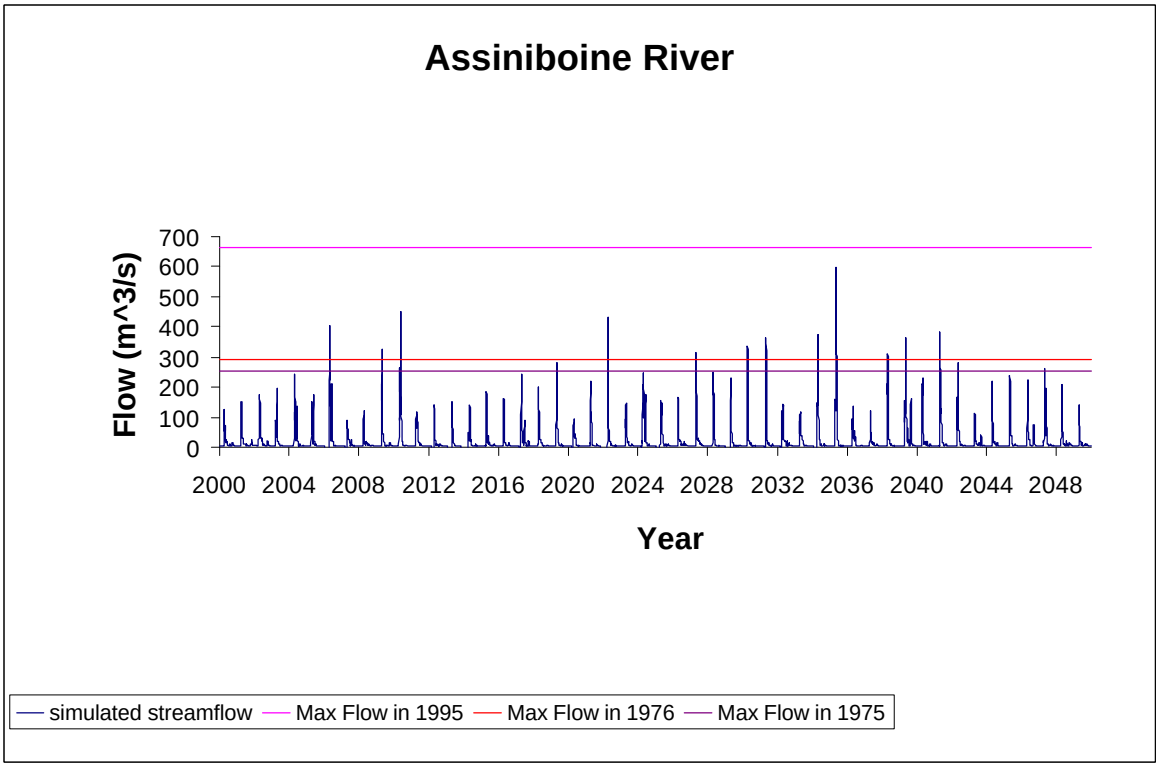

(a)

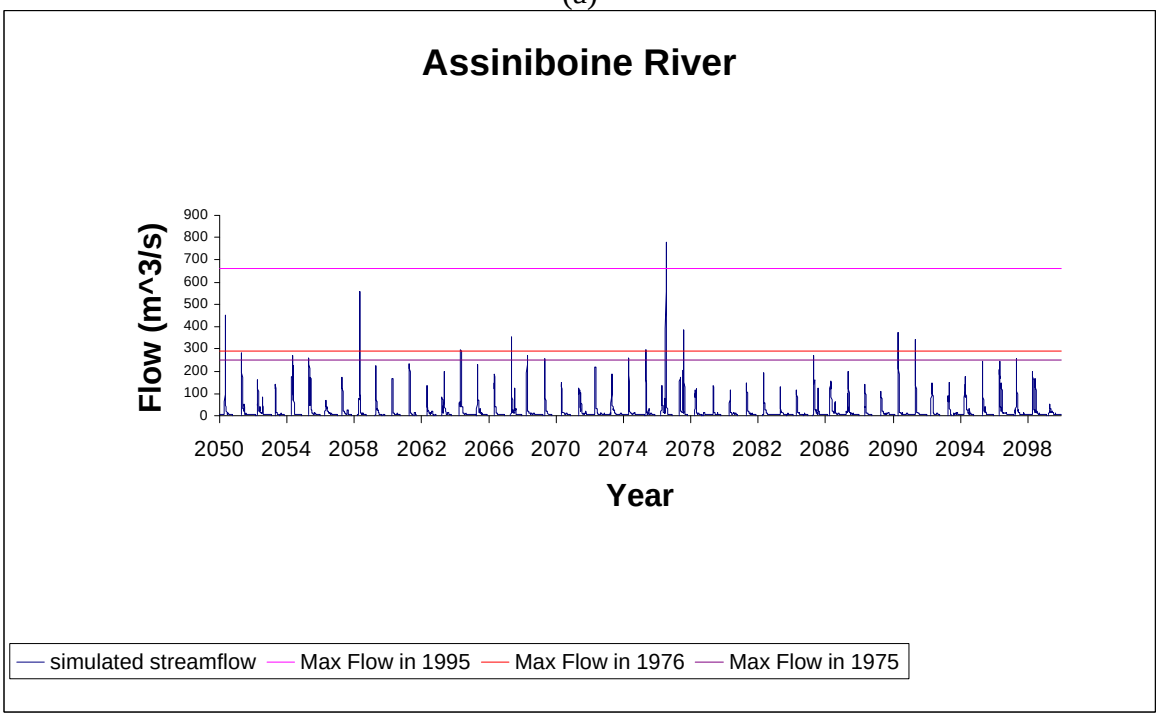

(b)

Figure 21. Comparison of the historical data with the simulated streamflow for the control scenario of HADCM3 – Assiniboine River

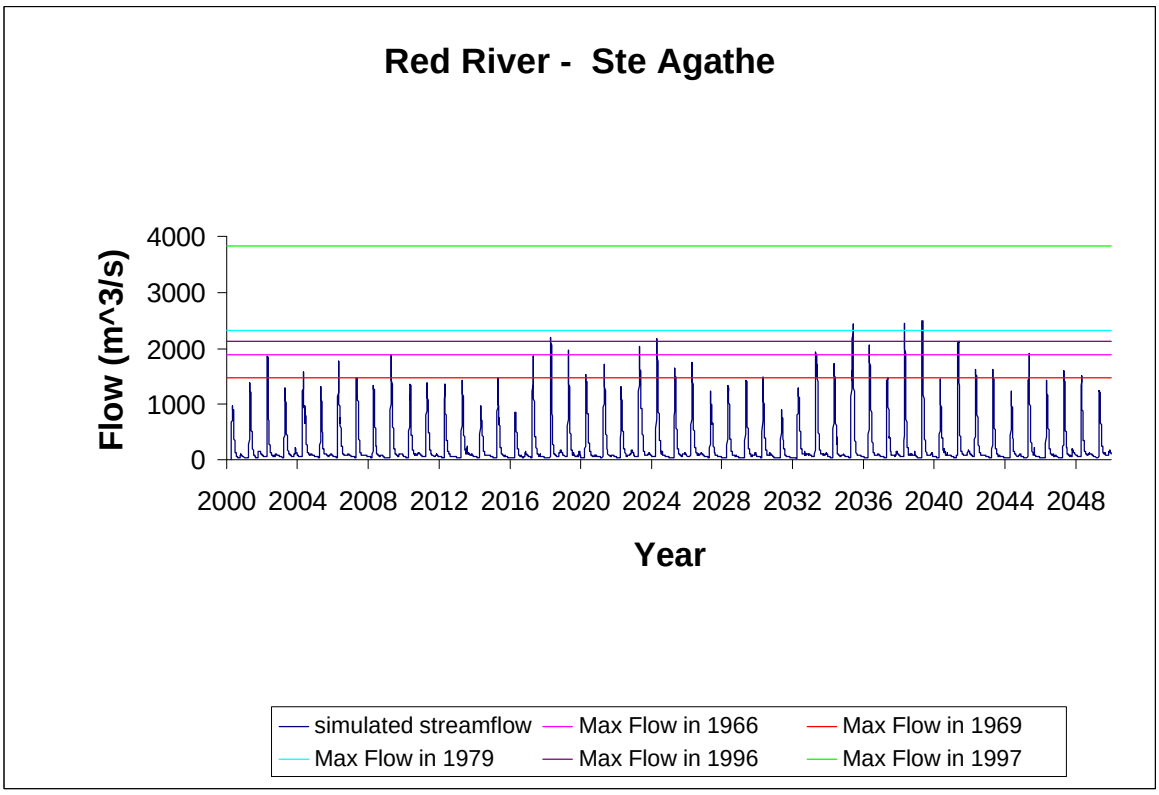

(a)

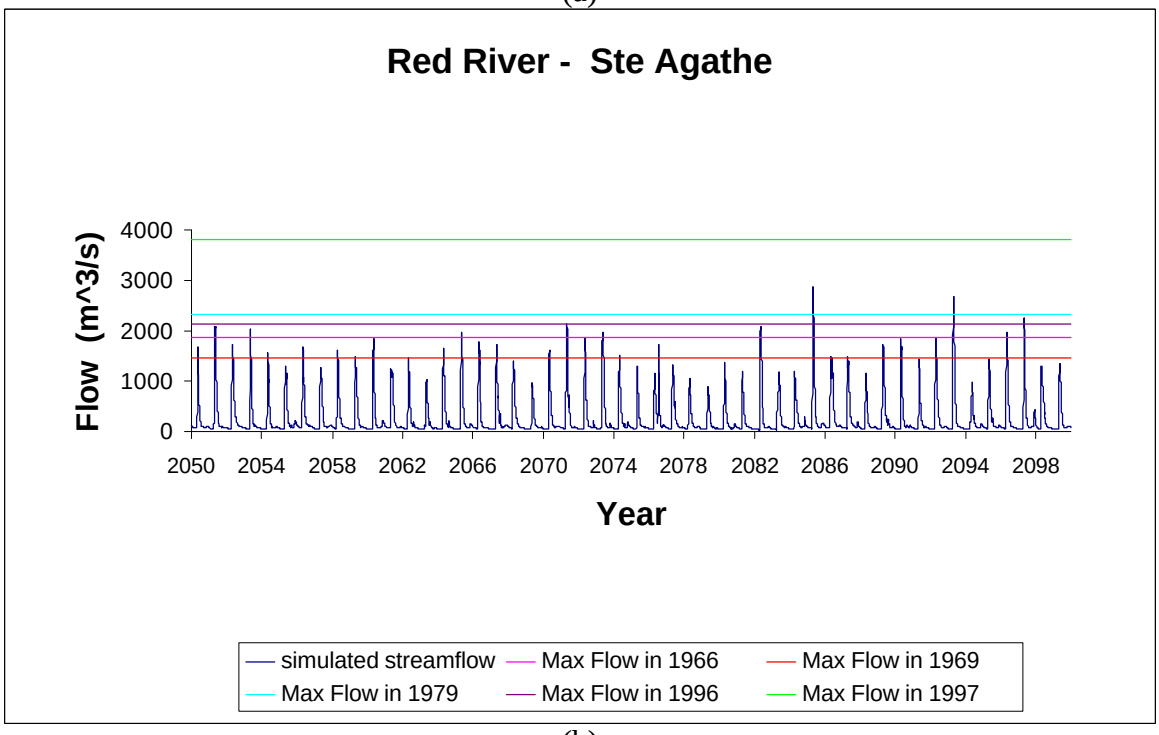

(b)

Figure 22. Comparison of the historical data with the simulated streamflow for the control scenario of HADCM3 – Red River at Ste Agathe

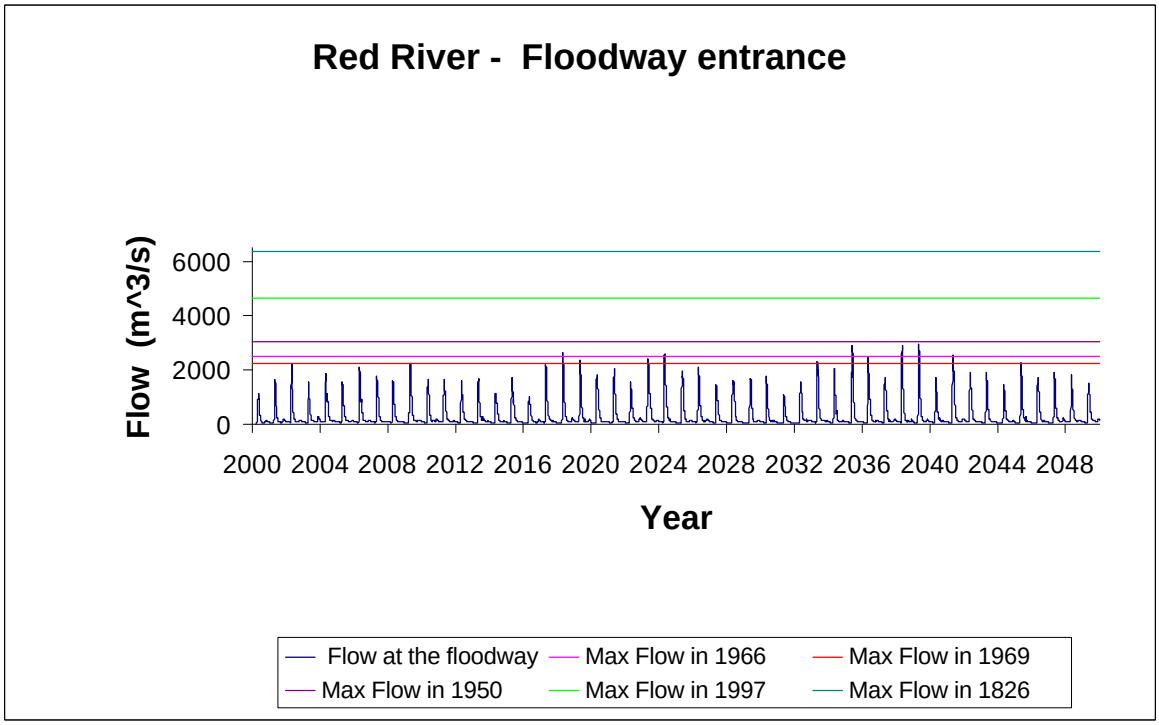

(a)

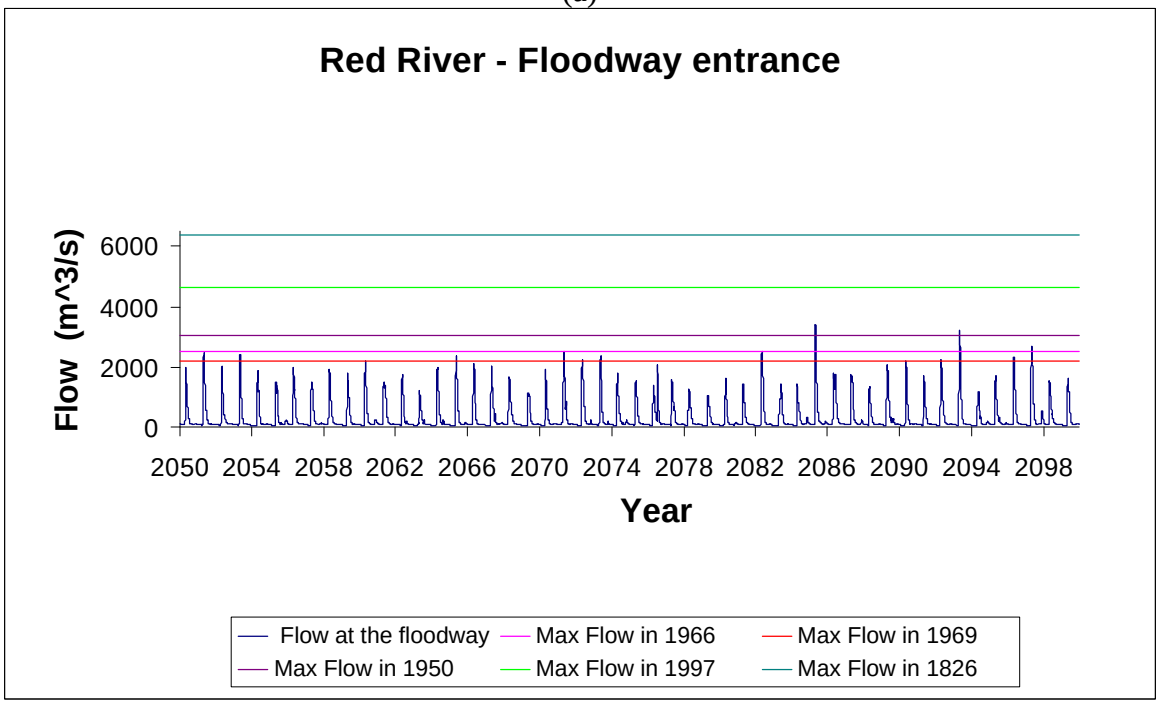

(b)

Figure 23. Comparison of the historical data with the simulated streamflow for the control scenario of HADCM3 – Red River at Floodway entrance

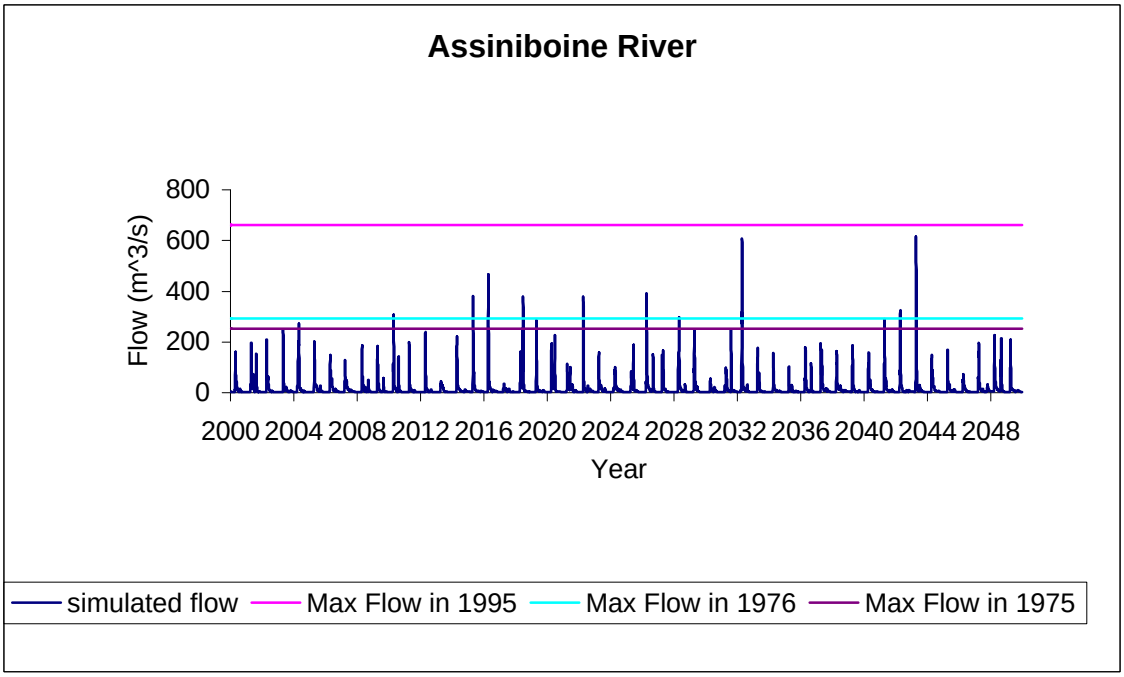

(a)

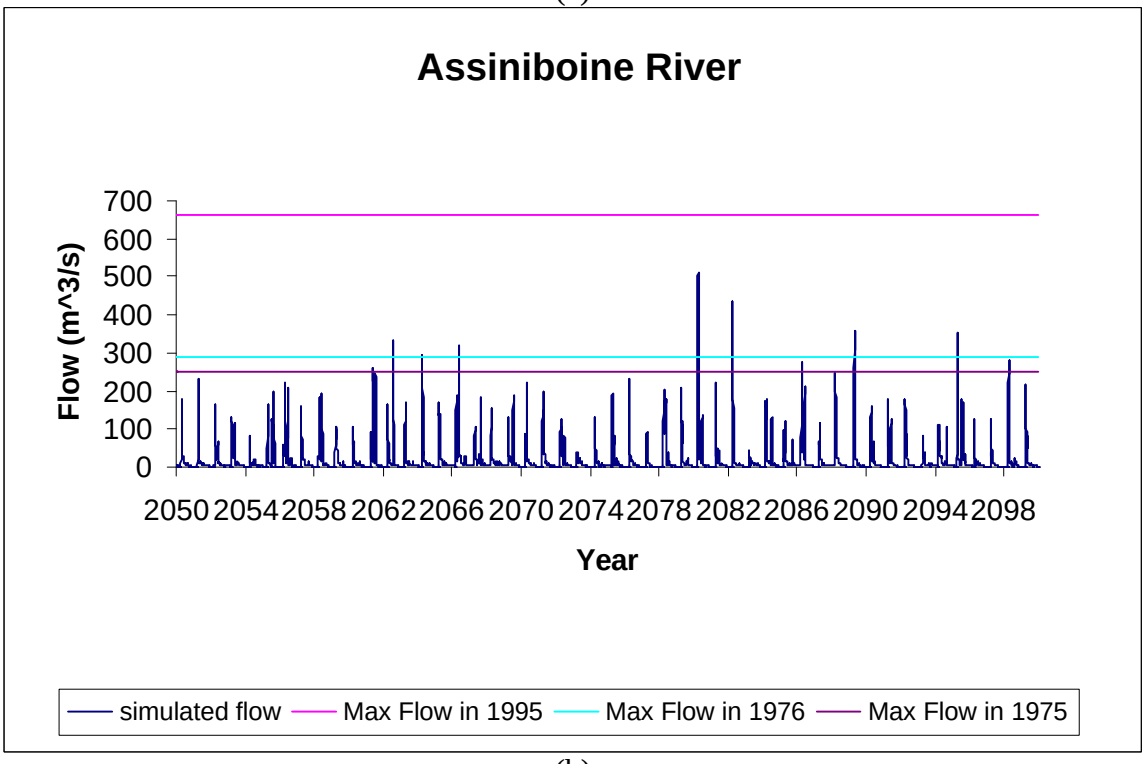

(b)

Figure 24. Comparison of the historical data with the simulated streamflow for the scenario 1 of HADCM3 – Assiniboine River

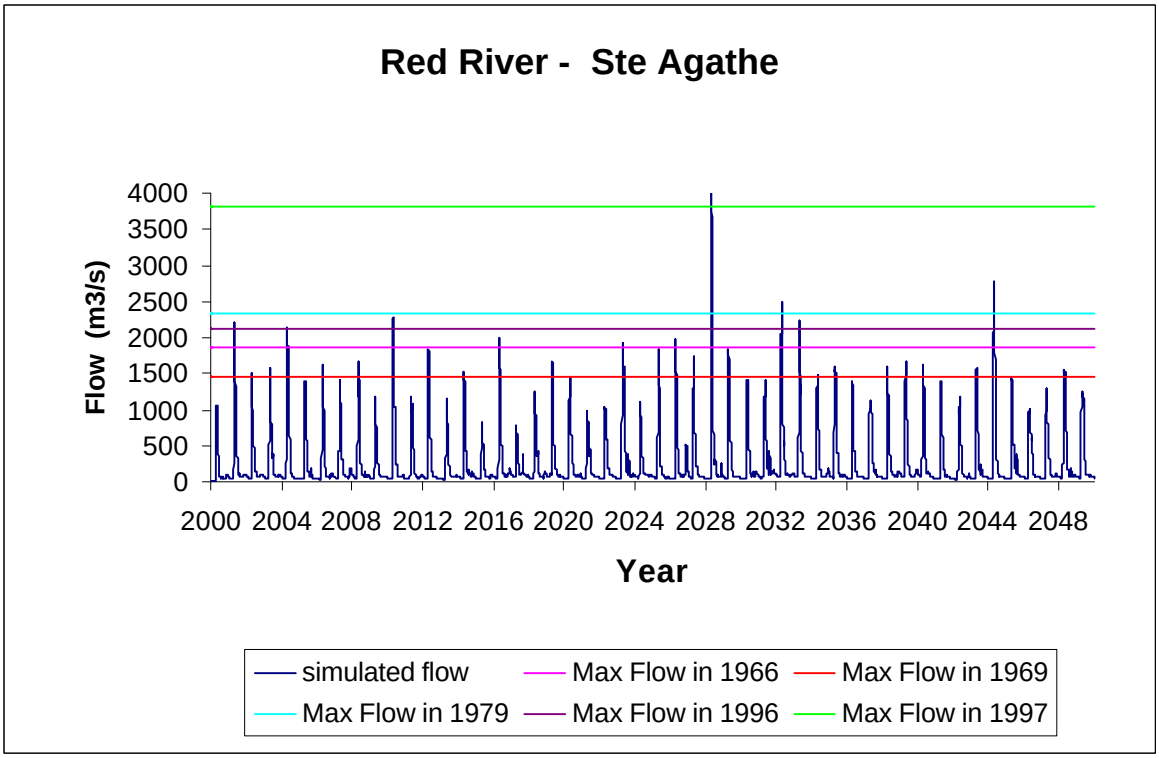

(a)

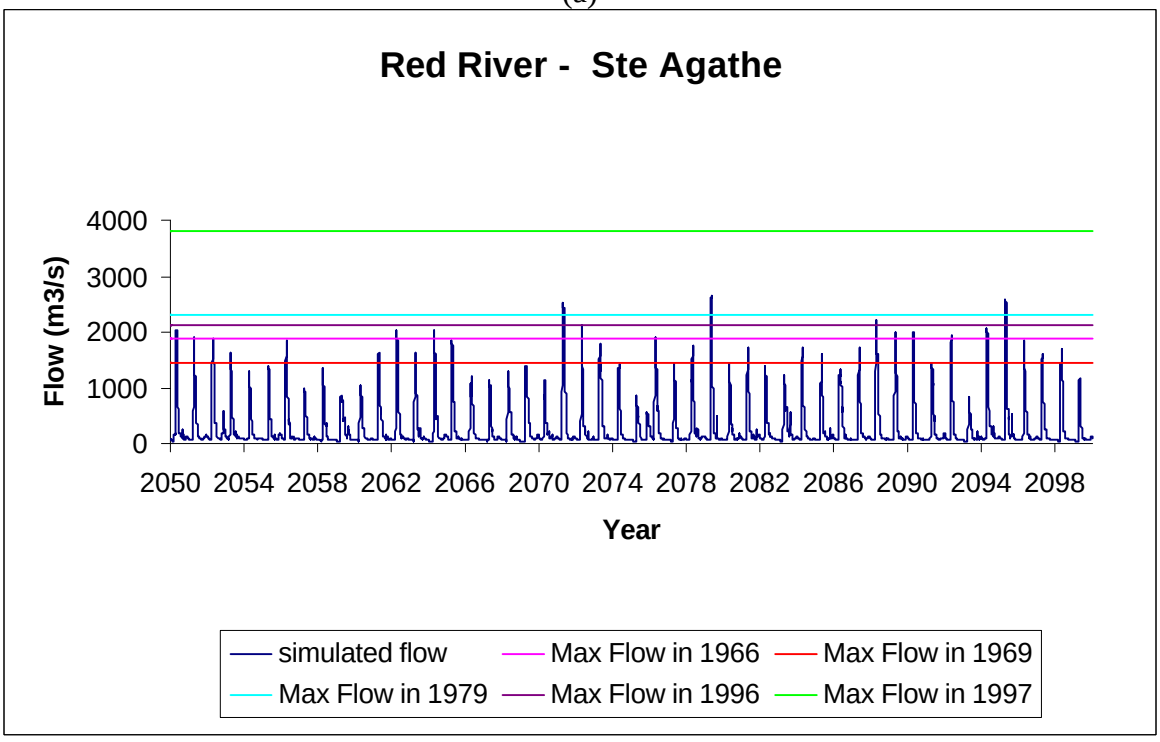

(b)

Figure 25. Comparison of the historical data with the simulated streamflow for the scenario 1 of HADCM3 – Red River at Ste Agathe

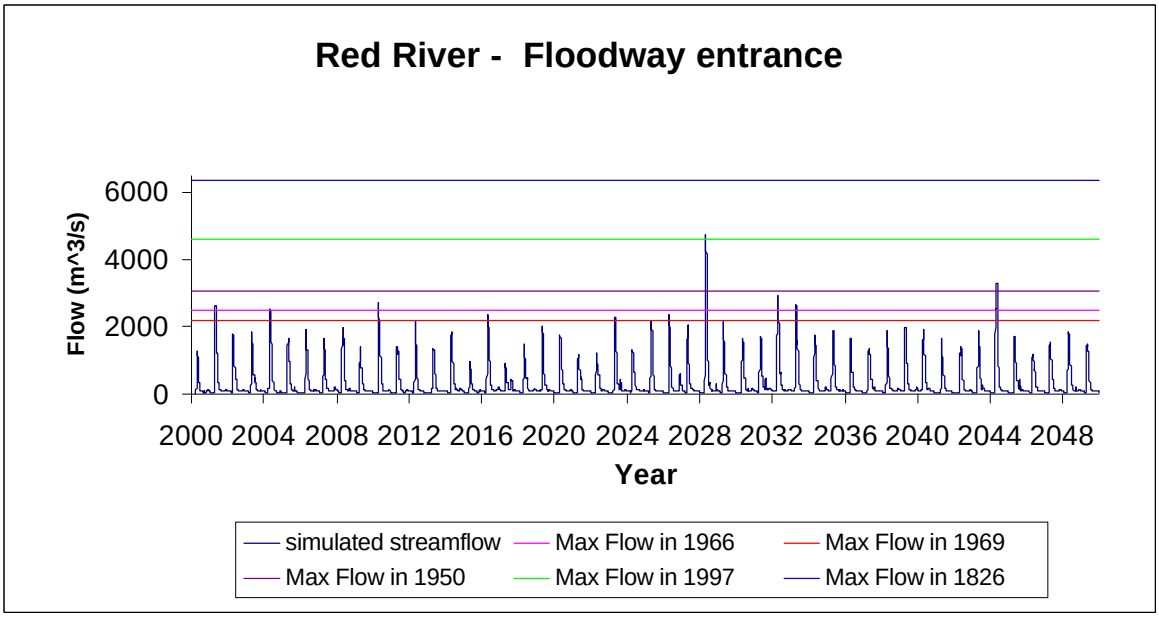

(a)

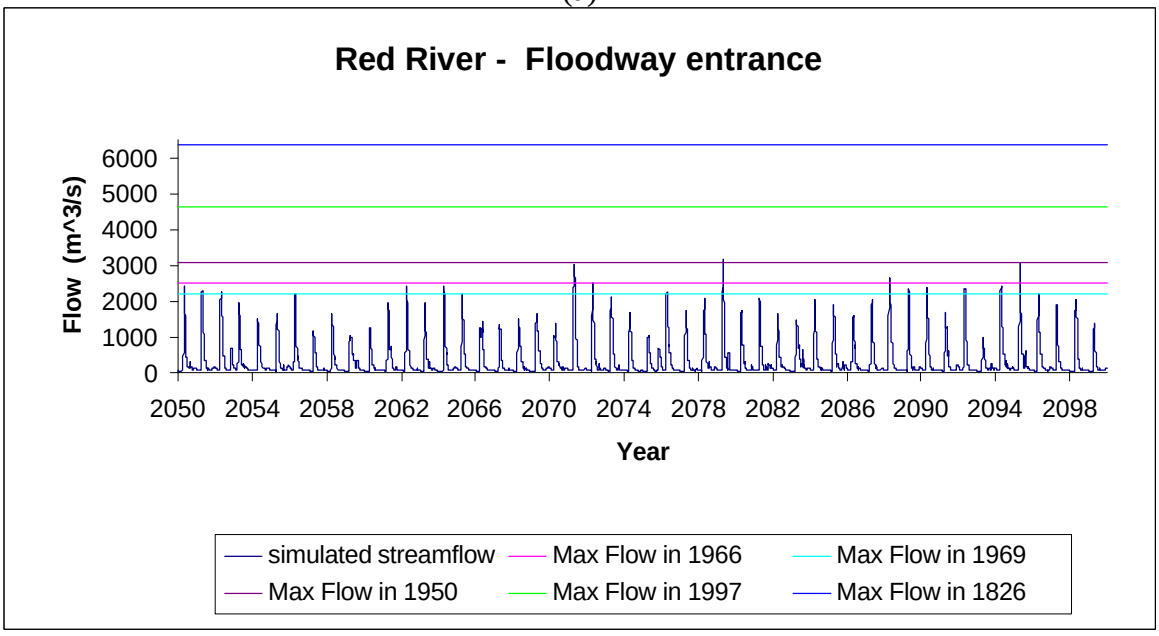

(b)

Figure 26. Comparison of the historical data with the simulated streamflow for the scenario 1 of HADCM3 – Red River at Floodway entrance

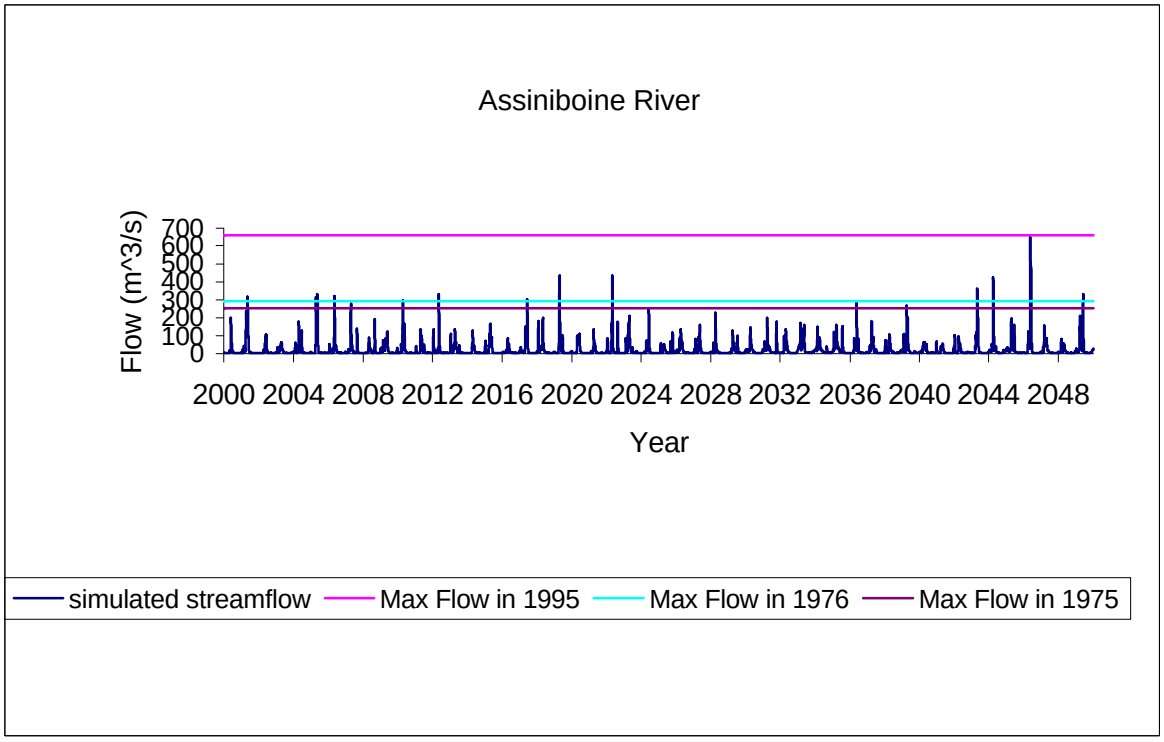

(a)

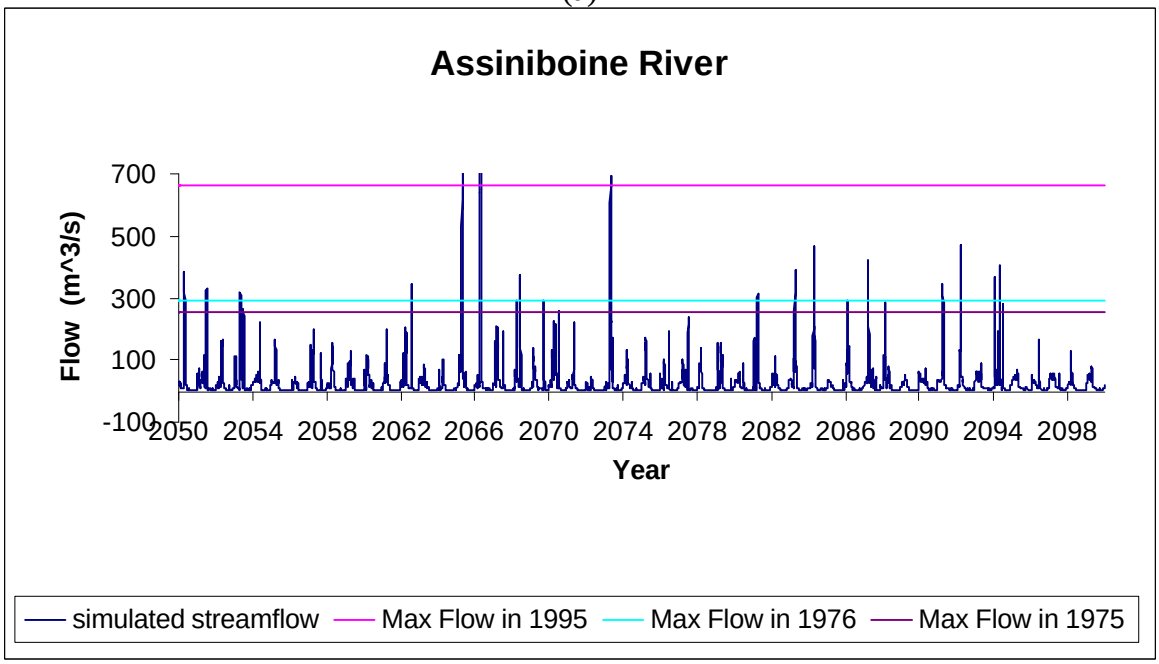

(b)

Figure 27. Comparison of the historical data with the simulated streamflow for the scenario 2 of CGCM1 – Assiniboine River

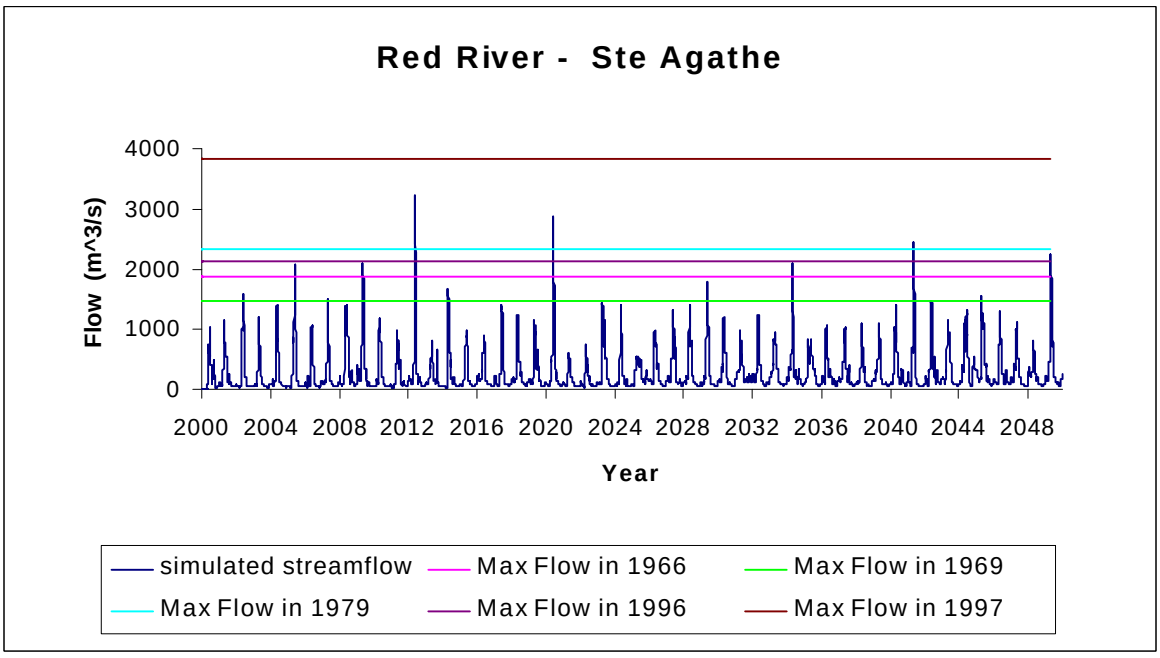

(a)

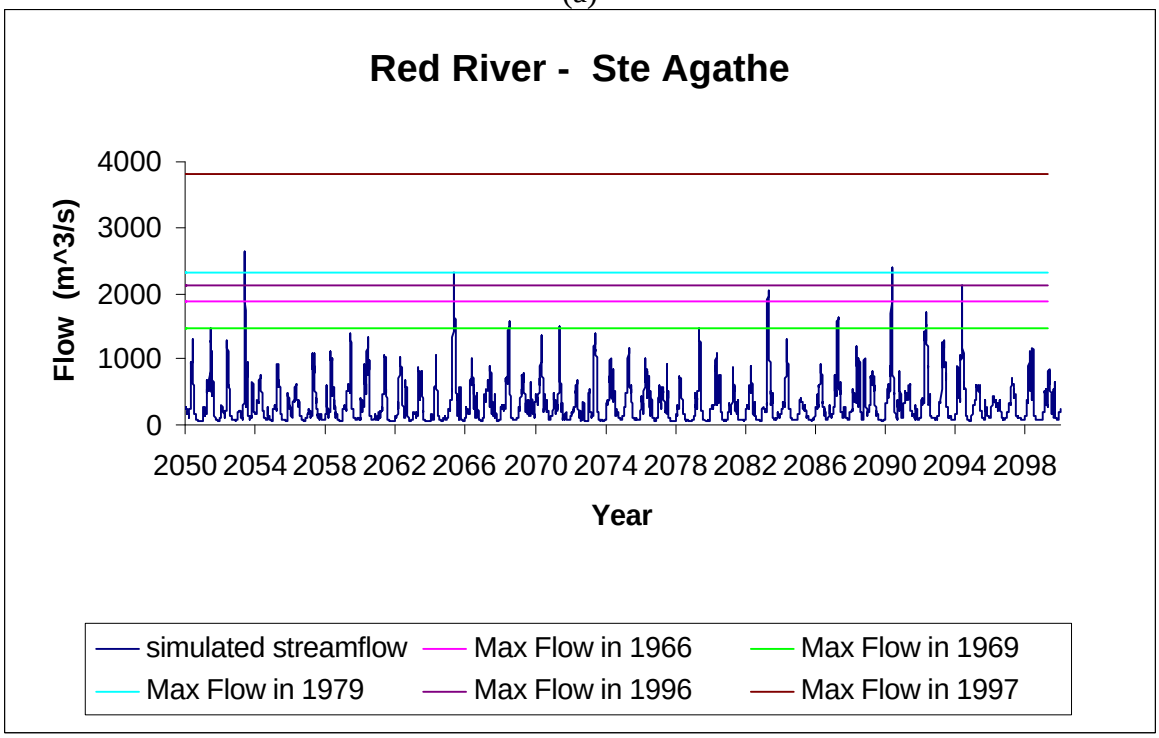

(b)

Figure 28. Comparison of the historical data with the simulated streamflow for the scenario 2 of CGCM1 – Red River at Ste Agathe

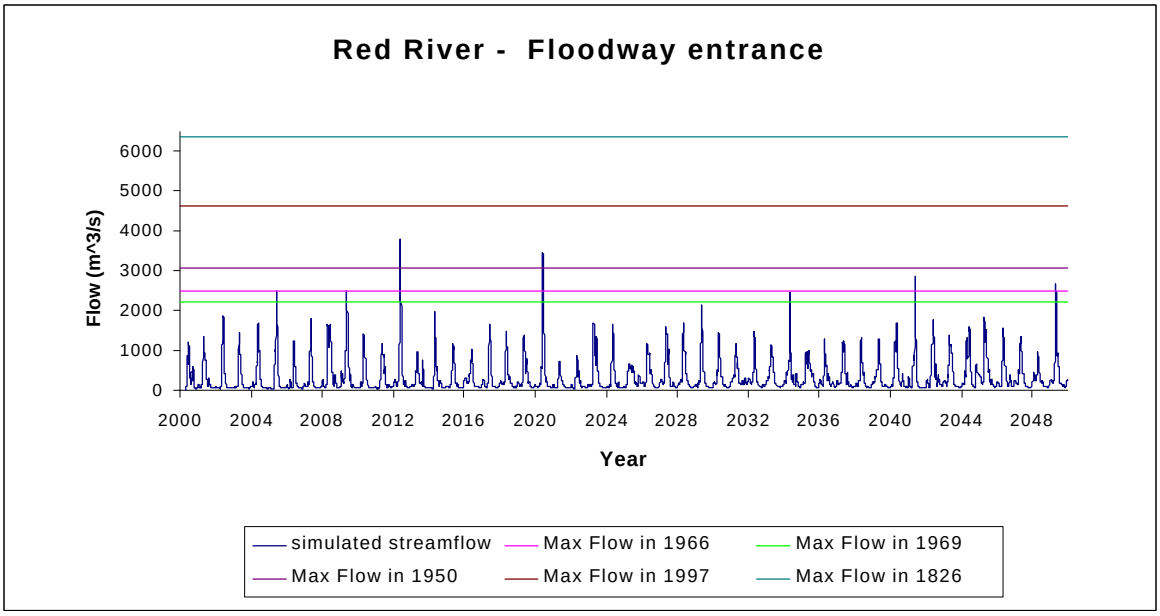

(a)

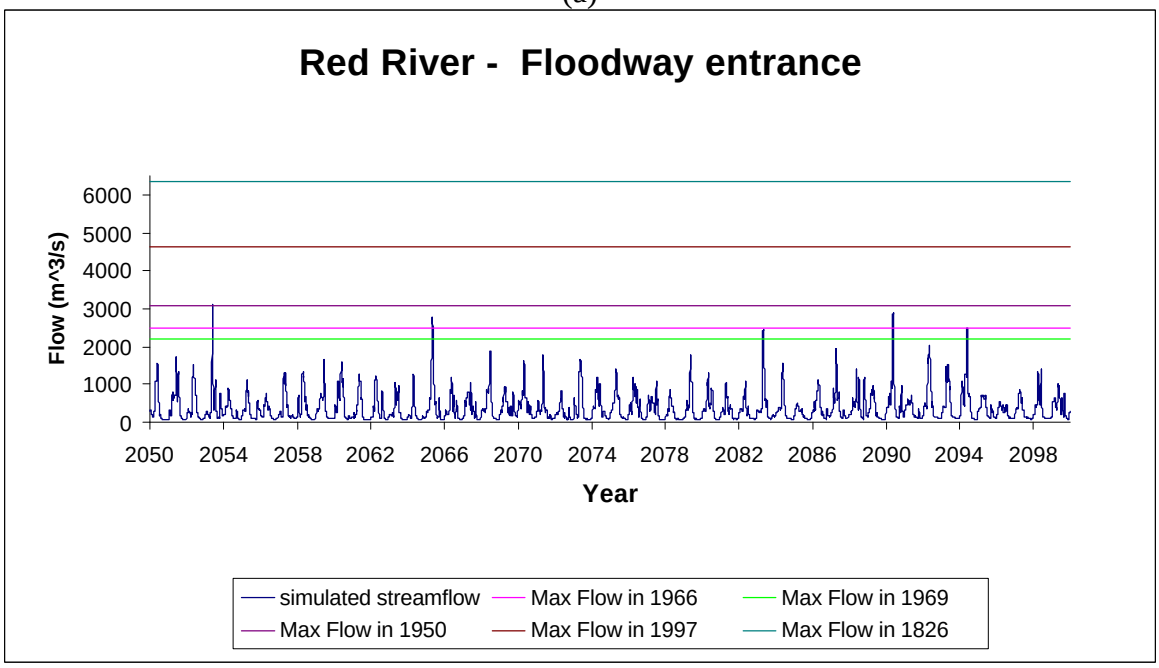

(b)

Figure 29. Comparison of the historical data with the simulated streamflow for the scenario 2 of CGCM1 – Red River at Floodway entrance

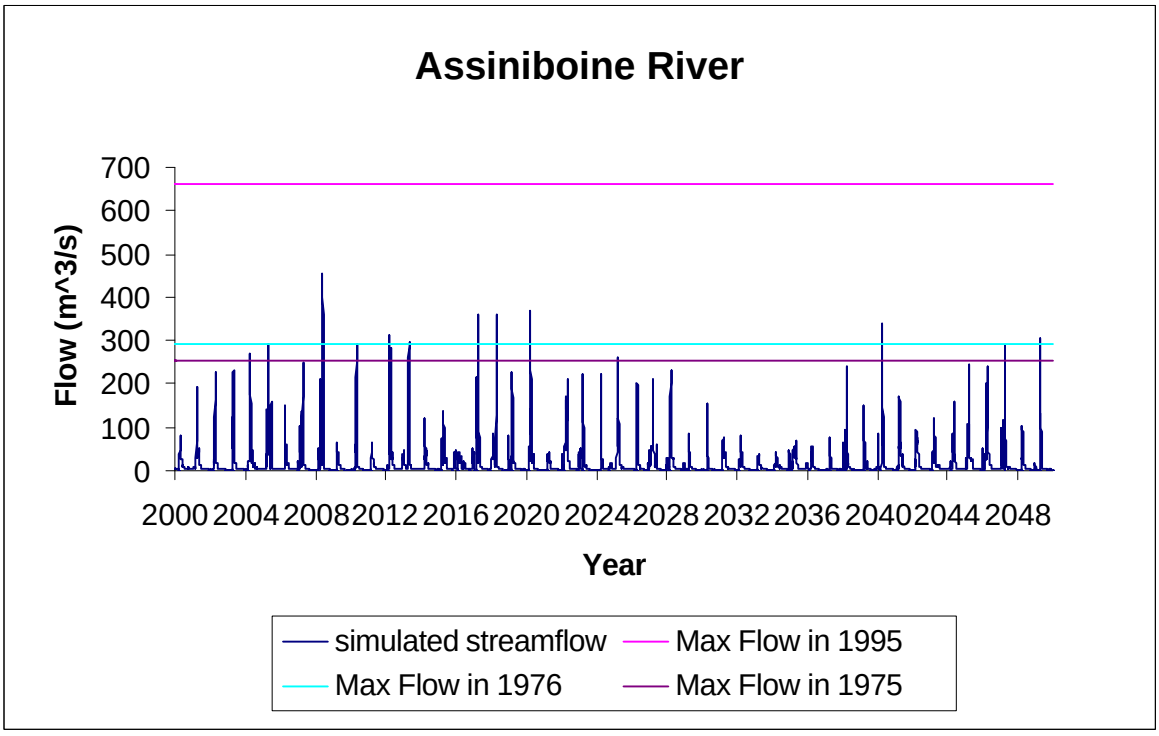

(a)

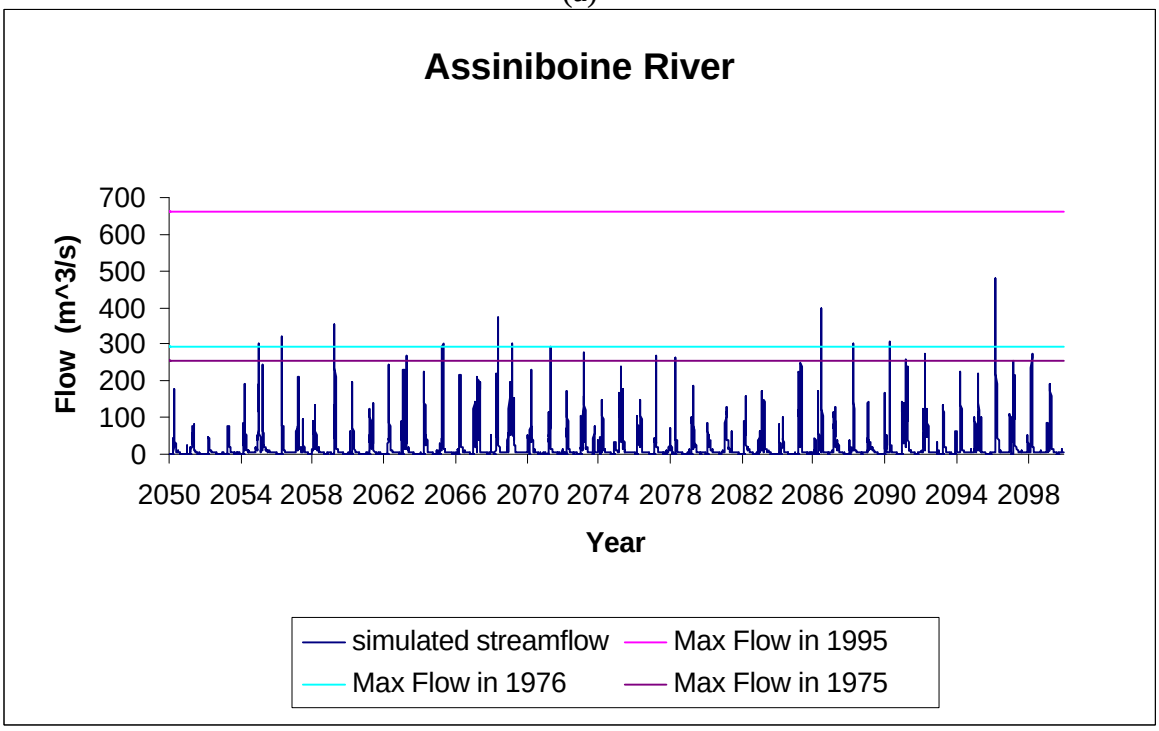

(b)

Figure 30. Comparison of the historical data with the simulated streamflow for the scenario 1 of ECHAM4 – Assiniboine River

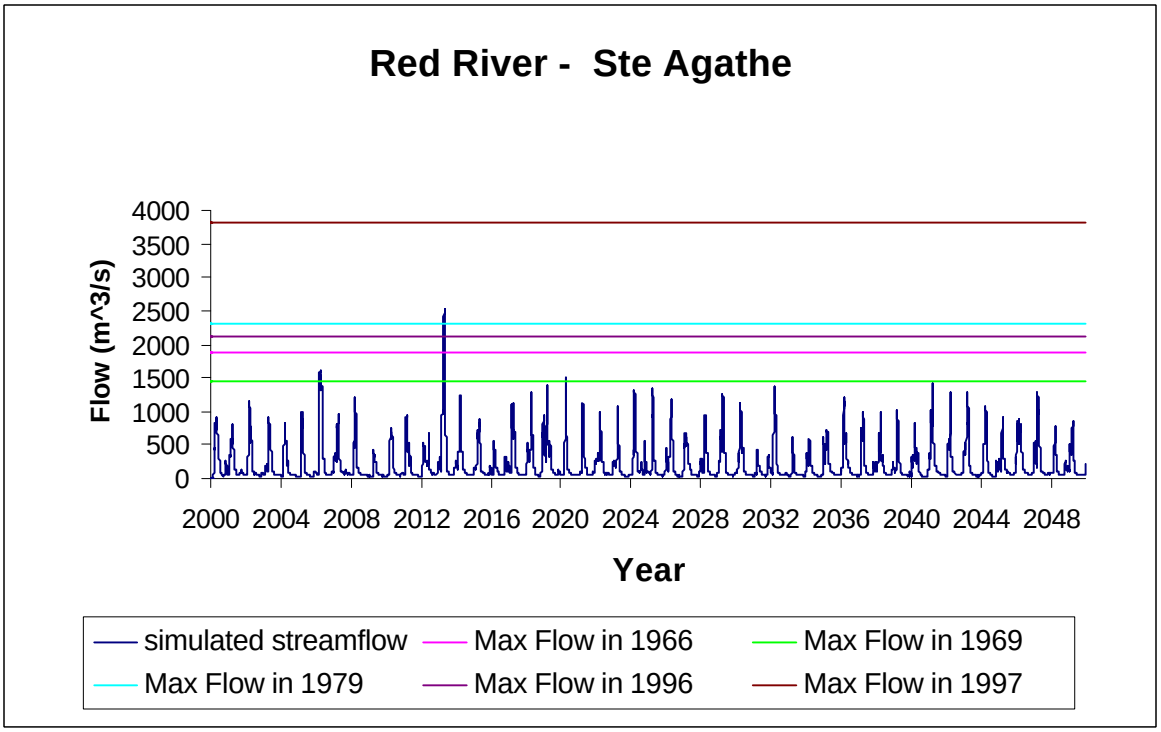

(a)

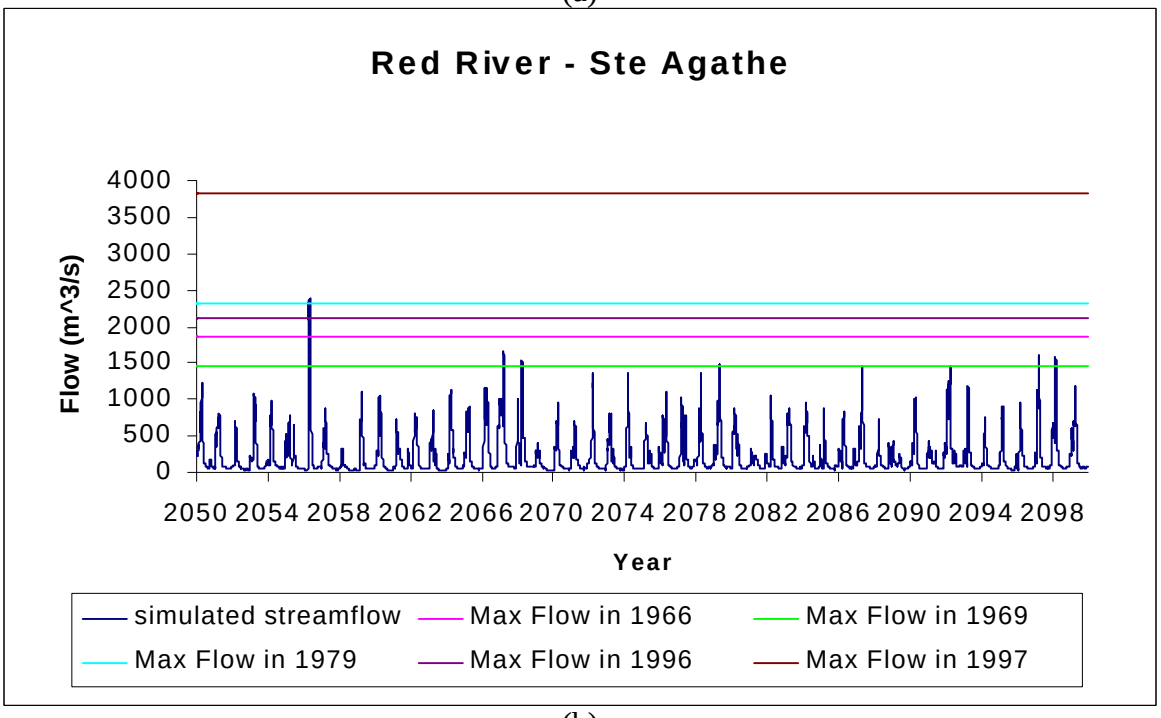

(b)

Figure 31. Comparison of the historical data with the simulated streamflow for the scenario 1 of ECHAM4 – Red River at Ste Agathe

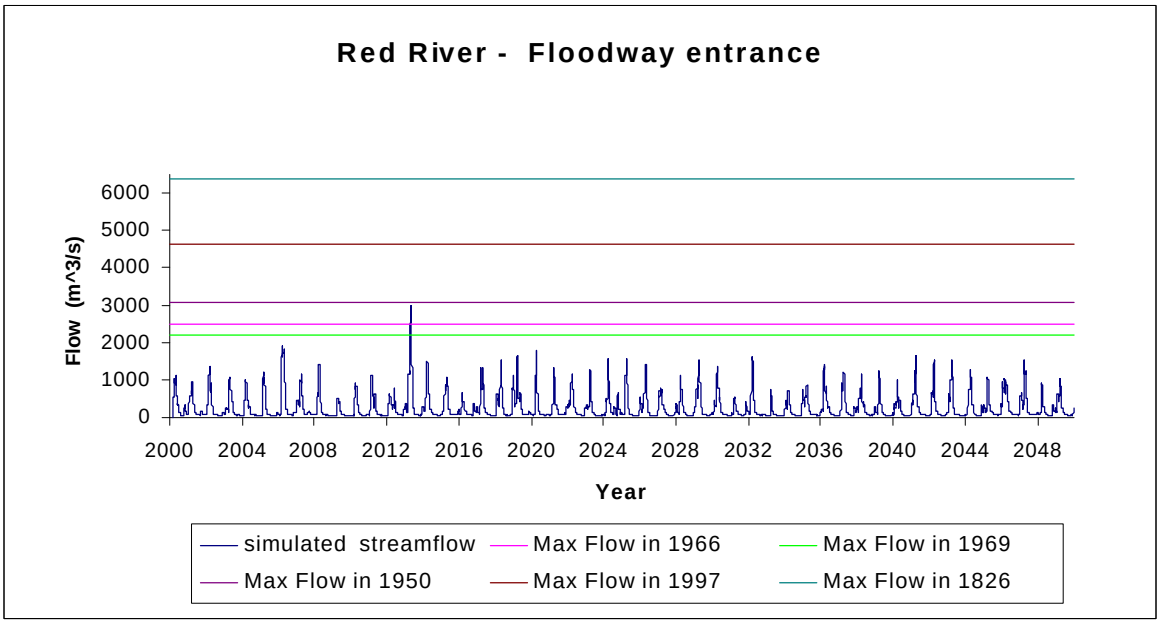

(a)

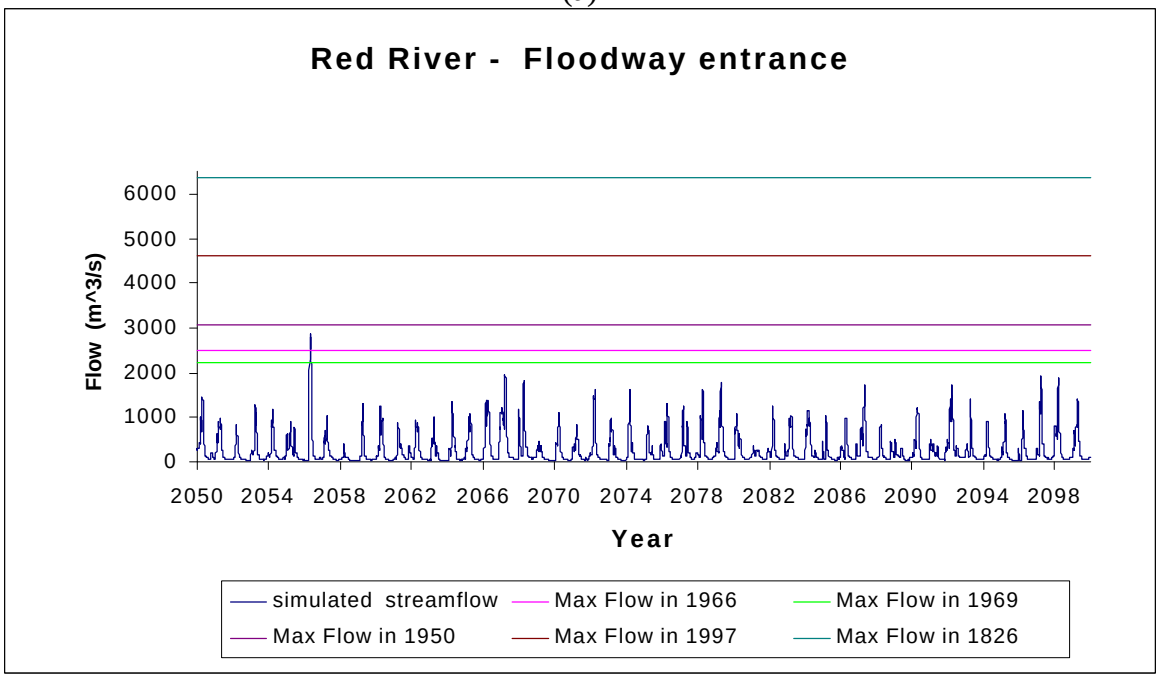

(b)

Figure 32. Comparison of the historical data with the simulated streamflow for the scenario 1 of ECHAM4 – Red River at Floodway entrance

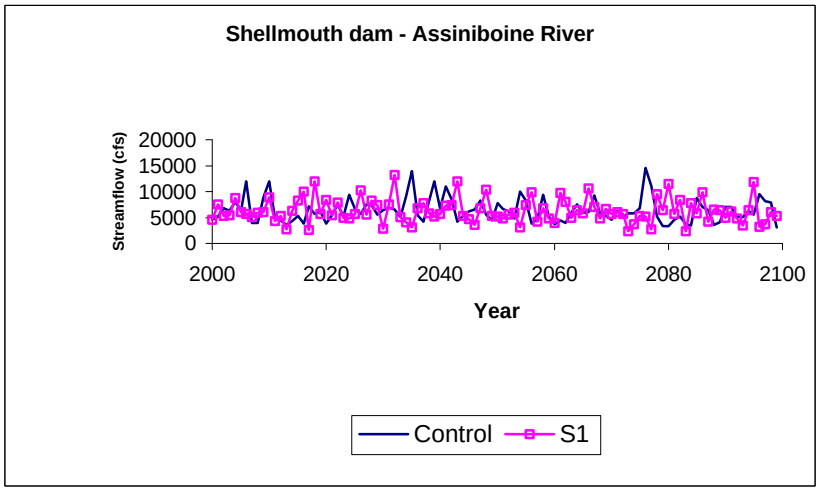

(a)

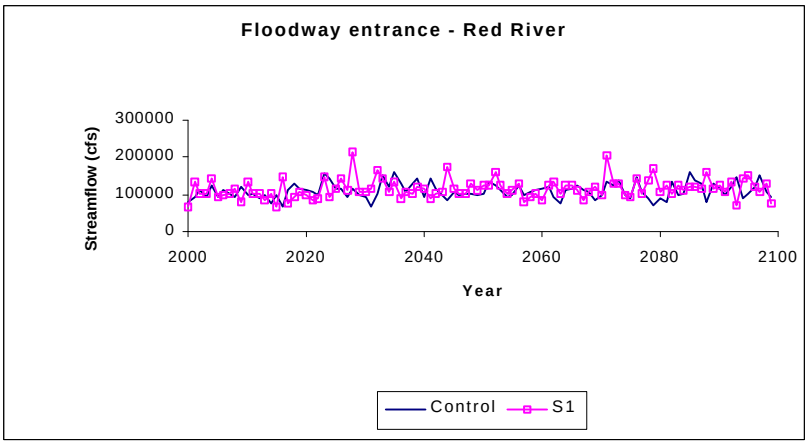

(b)

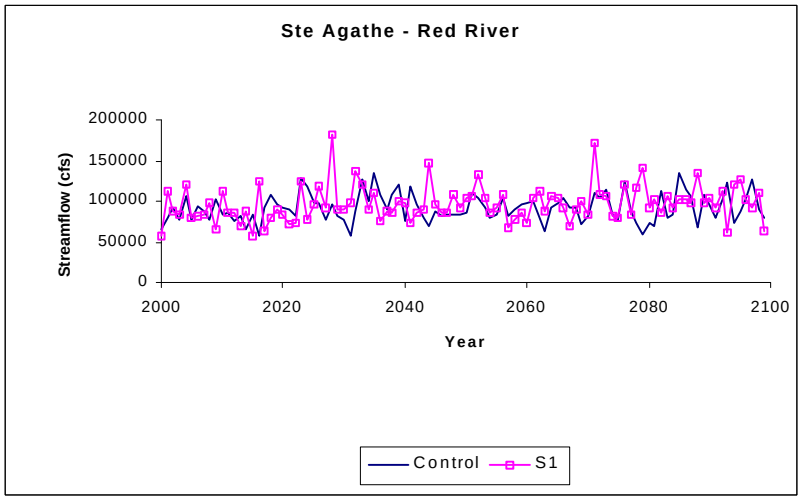

(c)

Figure 33. Comparison of streamflow generated using HADCM3 model

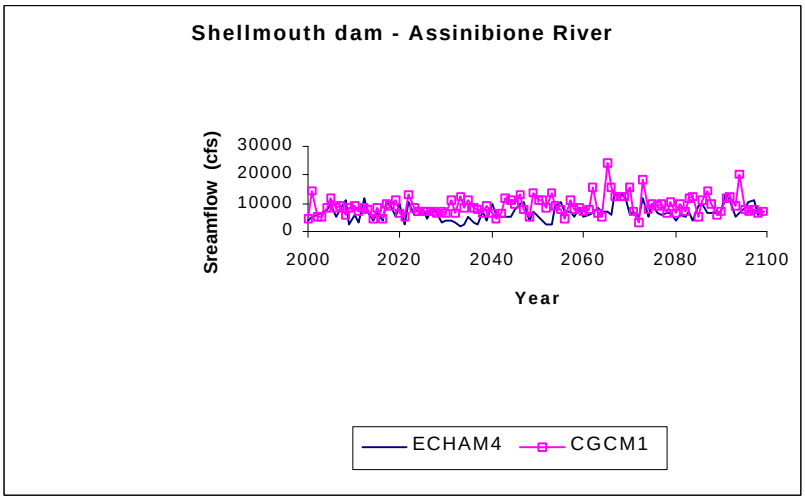

(a)

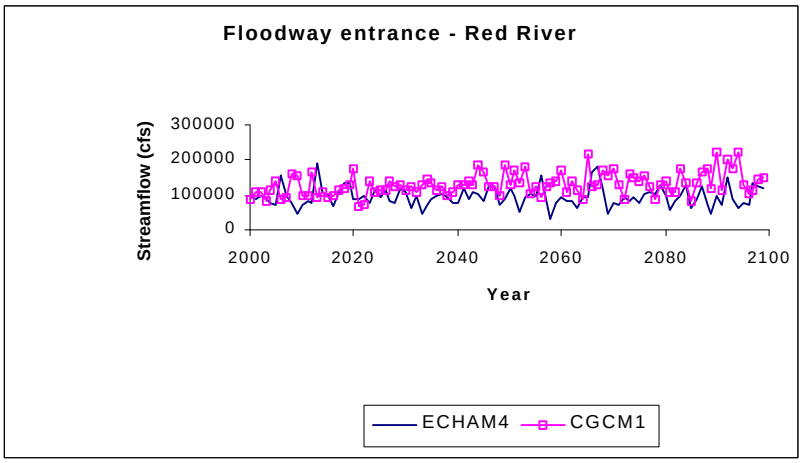

(b)

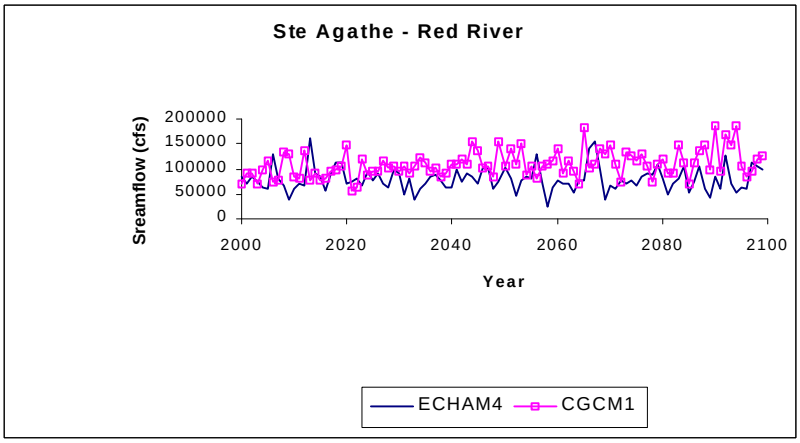

(c)

Figure 34. Comparison of annual streamflow generated using ECHAM4 and CGCM1 models

Table 7. Comparison of streamflow (cfs) generated using HADCM3 model

	Shellmouth		Ste. Agathe		Floodway entrance	
	Control	S1	Control	S1	Control	S1
Max	14594.3	13158.1	134739.5	180947.0	161659.7	217091.5
Min	3102.9	2380.8	57118.8	56274.55	68452.2	67502.8
Mean	6410.8	6279.5	91580.9	96674.48	109894.5	116005.8

Table 8. Comparison of streamflow (cfs) generated using ECHAM4 and CGCM1 models

	Shellmouth		Ste. Agathe		Floodway entrance	
	ECHAM4 (S1)	CGCM1 (S2)	ECHAM4 (S1)	CGCM1 (S2)	ECHAM4 (S1)	CGCM1 (S2)
Max	13714.4	24085.7	160600.7	186893.5	192618.2	224411.8
Min	2082.8	3024.1	25773.0	57149.2	30977.1	68628.2
Mean	6729.2	9165.9	79112.0	108854.3	94933.1	130620.3

Analysis of flood patterns

The most important impact of climatic change on hydrologic processes within a watershed should be demonstrated through the change of flood patterns: flood starting time, flood peak value and flood peak timing. Following section of the report focuses on the analyses of flood patterns under different climate change scenarios. Shellmouth dam on the Assiniboine River and Ste. Agathe on the Red River were selected as locations for analyses of flood patterns. Starting and peak time at other locations can be estimated using mean travel time between different locations.

Flood starting time

The temperature and the river flow identify flood starting time. In this research, the point in time, when the temperature reaches above 0°C and after that the streamflow continuously increases, is identified as the flood starting time. Probability distributions of flood starting time obtained using different scenarios of three GCM models are shown in Figure 35. In the case of HADCM3, floods at the Shellmouth dam and at the Ste. Agathe generated for the scenario S1 start earlier than floods generated using the control run scenario. More than 90% of flood starting times at both locations for the scenario S1 are between early March and early April, while those from the control run scenario are between late March and late April. The higher temperatures that may be the consequence of climatic change result in an earlier flood starting time in both river basins.

Comparison of flood starting times obtained from the scenario S1 of ECHAM4 model and the scenario S2 of CGCM1 model shows the same pattern, i.e. floods generated by these two scenarios will start earlier than floods generated by the control run of HADCM3 in both river basins (Figure 35). More than 90% of floods from those two models started between middle of February and late March. The impact of climate change on the flood starting time at Ste. Agathe may be more significant due to the Red River flow direction from south to north.

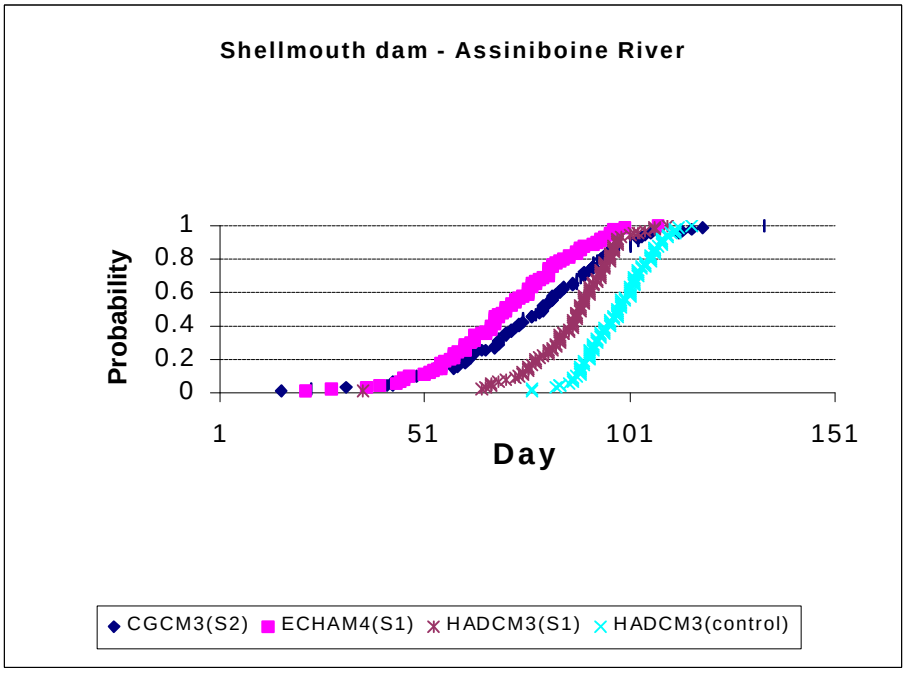

(a)

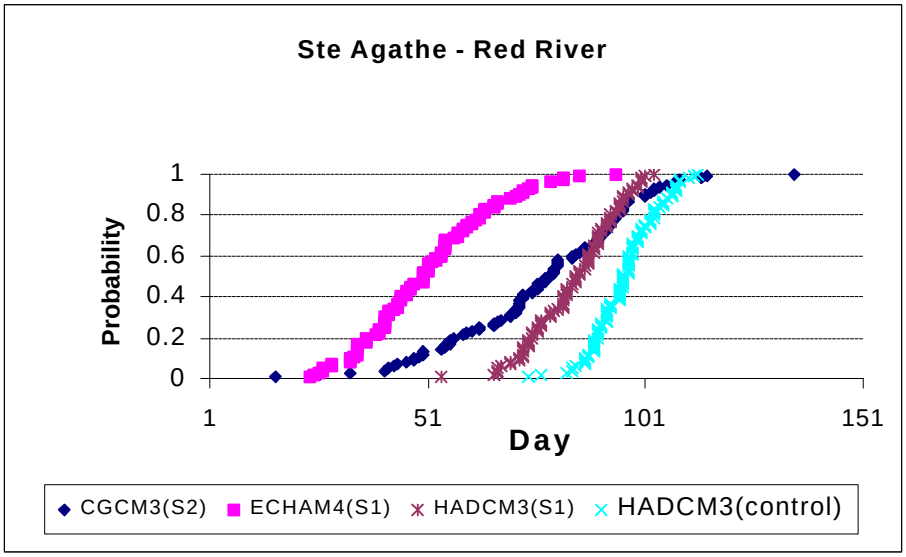

(b)

Figure 35 Comparison of flood starting time generated by different scenarios

Flood peak flow and timing

The timing of flood peak and the flood peak magnitude assessed impact of climatic change on the flood peak. Figures 36 and 37 show the impact of climate variability and change on flood peak time and magnitude at the Shellmouth dam in the Assiniboine River basin and at the Ste. Agathe in the Red River basin.

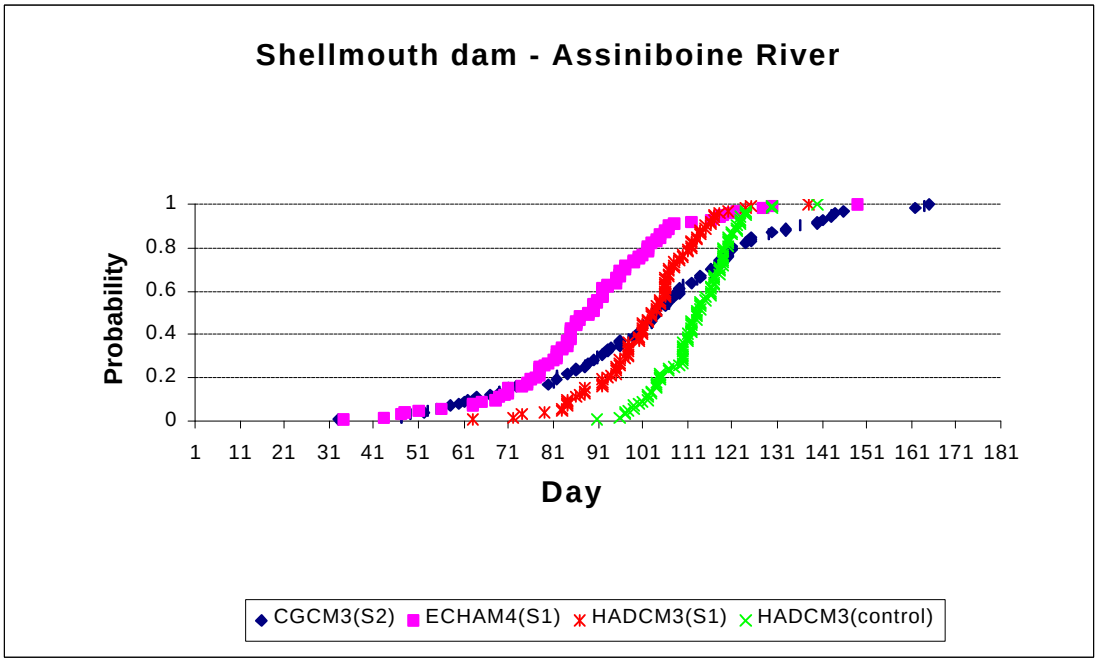

(a)

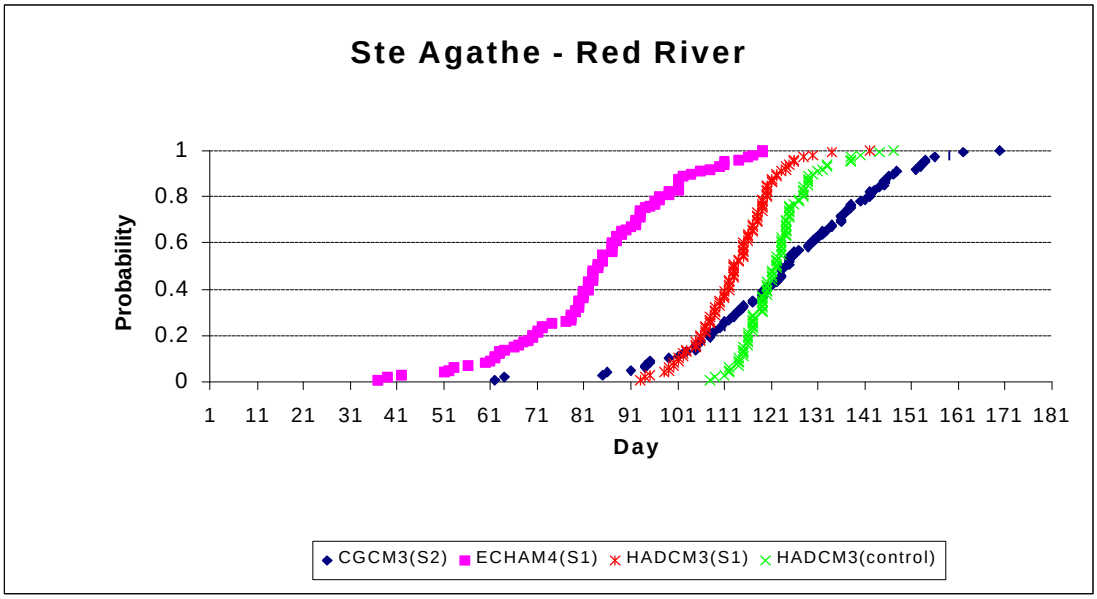

(b)

Figure 36 Comparison of flood peak time generated by selected scenarios

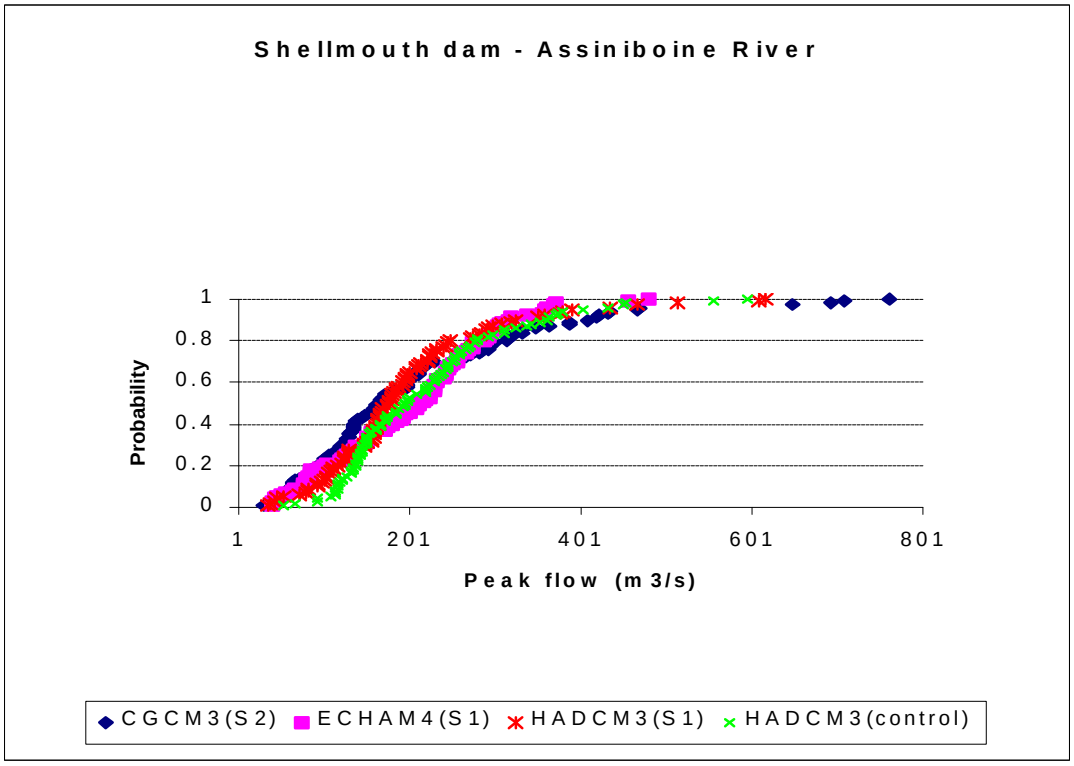

(a)

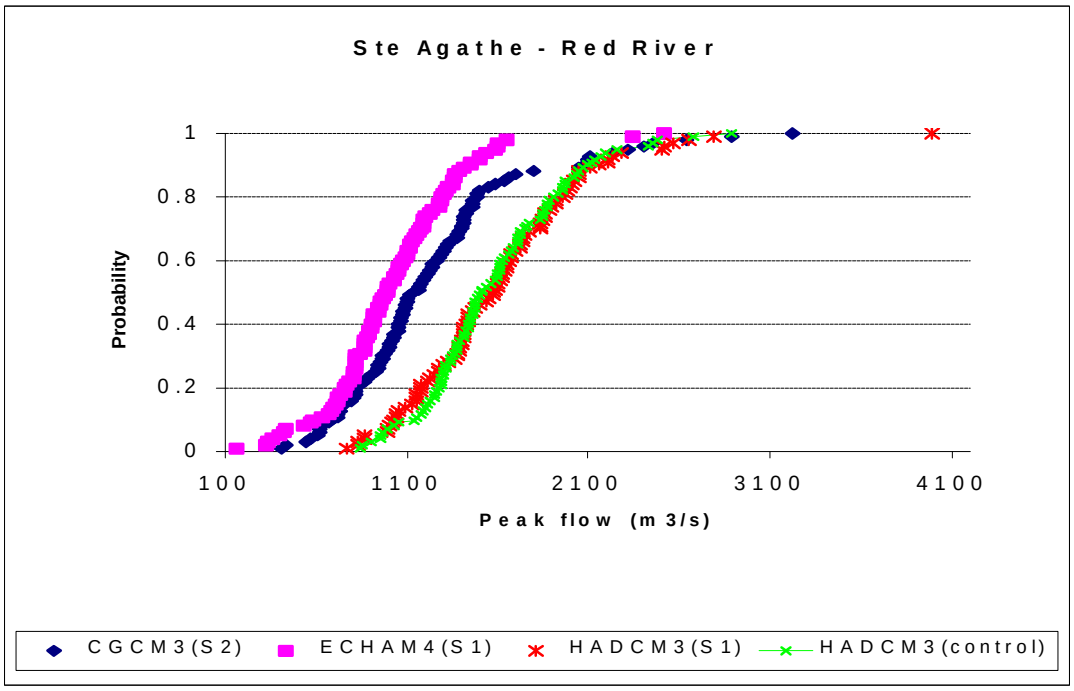

(b)

Figure 37. Comparison of flood peak flow generated by selected scenarios

At the Ste. Agathe, more than 90% of predicted floods from the scenario S1 of HADCM3 occurred from early April to early May, while that from the control run of HADCM3 occurred from middle April to middle May (Figure 36b). The result demonstrates that the climate change might shift the flood peak time to occur earlier. The same trend was observed at the Shellmouth dam (Figure 36a). When comparing different scenarios from the three models it is possible to observe that the timing of flood peak from the scenario S1 of ECHAM4 model and the scenario S2 of CGCM1 covers wider range than that from the scenario S1 and the control run of HADCM3 (Figure 36).

The distribution of flood peak magnitude at the Shellmouth dam did not show significant difference for different scenarios (Figure 37). For all scenarios of the three models, more than 90% of flood peak values are less than 400 m^3/s. Scenario S2 of CGCM1 generated three times floods greater than 600 m^3/s. Scenario S1 of ECHAM4 model and control run of HADCM3 model did not generate floods greater than 600 m^3/s. At the Ste. Agathe, the distribution of flood peak values from the scenario S1 and the control run of HADCM3 followed almost the same pattern. Scenario S1 generated one flood greater than the flood of 1997.

When comparing all four scenarios of the three models, 98% of flood peak values generated by the scenario S1 of ECHAM4 model were smaller than 2,000 m^3/s, while the scenarios S1 and control run of HADCM3 generated about 85% of flood peak values larger than 2,000 m^3/s (Figure 37). CGCM1 model produced 90% of flood peak values larger than 2,000 m^3/s.

5.4 Flood protection system performance assessment

The assessment of the performance of the complex flood protection system for the City of Winnipeg is based on the flood flow, the capacity of each flood control facility and the failure flow at each location within the system. The reliability, vulnerability and resiliency are calculated at the selected locations within the system under different climate variability and change scenarios generated using the three GCM models.

Reliability

Total system reliability at the selected locations in the study area are presented in Tables 9 and 10. In the Assiniboine River basin, the total reliability at selected locations generated using scenario S1 of HADCM3 model ranges from 0.9847 at the Shellmouth Reservoir to 0.9988 at Portage. Meanwhile, the control scenario of HADCM3 produced a greater range of yearly reliability at the selected locations. Of the four scenarios from the three GCM models, the scenario S2 of CGCM1 and the scenario S1 of ECHAM4 model result in lower total reliability and wider range of yearly reliability when compared to both scenarios of HADCM3 model. Scenario S2 of CGCM1 generated the lowest total reliability of 0.9599 at the Shellmouth Reservoir and 0.9951 at Portage. Scenario S2 of CGCM1 generated the minimum yearly reliability of 0.7014 at the Shellmouth Reservoir. The results along the Assiniboine River also show that higher total and yearly reliabilities are reached at the locations downstream from the reservoir. This indicates that the Shellmouth reservoir plays an important role in reducing downstream floods.

In the Red River basin, four scenarios of the three GCM models generated a different trend from the one observed in the Assiniboine River basin. Control and S1 scenarios of HADCM3 generated lower reliability at the Ste. Agathe than the scenario S2 of CGCM1 and the scenario S1 of ECHAM4 model. Scenario S1 of HADCM3 results in the lowest total and yearly reliability at the Ste. Agathe. The results of the analysis show that the flood protection capacity is sufficient under low reliability criteria as established by KGS (2000).

Table 9. Flood protection system reliability – HADCM3 model

	Location	**Control**			**S1**		
		Min.	Max.	Mean	Min.	Max.	Mean
Assiniboine River	Shellmouth Reservoir	0.8417	0.9861	0.9834	0.8806	0.9806	0.9847
	Channel Capacity	0.8444	0.9944	0.9861	0.8833	0.9972	0.9879
	Russell	0.8472	0.9972	0.9862	0.8833	0.9917	0.9881
	St Lazare	0.8444	0.9944	0.9861	0.8833	0.9972	0.9879
	Miniota	0.9306	0.9722	0.9978	0.9472	0.9778	0.9984
	Griswold	0.9306	0.9722	0.9978	0.9472	0.9778	0.9984
	Brandon	0.9361	0.9806	0.9981	0.9528	0.9861	0.9986
	Holland	0.9333	0.9778	0.9980	0.9528	0.9833	0.9986
	Portage	0.9389	0.9833	0.9983	0.9556	0.9944	0.9988
Red River	Ste. Agathe	0.8972	0.9972	0.9727	0.8472	0.9917	0.9625
	Winnipeg	/	/	1.0000	0.9996*	0.9996*	0.9996*

*** Calculated with high reliability criteria (KGS, 2000)**

Table 10. Flood protection system reliability – ECHAM4 and CGCM1 models

	Location	**ECHAM4**			**CGCM2**		
				S1			S2
		Min.	Max.	Mean	Min.	Max.	Mean
Assiniboine River	Shellmouth Reservoir	0.7972	0.9861	0.9754	0.7014	0.9836	0.9599
	Channel Capacity	0.8000	0.9944	0.9774	0.7479	0.9945	0.9650
	Russell	0.8000	0.9917	0.9776	0.7507	0.9945	0.9653
	St Lazare	0.8000	0.9944	0.9774	0.7479	0.9945	0.9650
	Miniota	0.9417	0.9806	0.9982	0.9151	0.9918	0.9938
	Griswold	0.9417	0.9806	0.9982	0.9151	0.9918	0.9938
	Brandon	0.9472	0.9917	0.9984	0.9178	0.9781	0.9944
	Holland	0.9472	0.9889	0.9984	0.9205	0.9753	0.9944
	Portage	0.9694	0.9806	0.9989	0.9205	0.9863	0.9951
Red River	Ste. Agathe	0.8889	0.9944	0.9949	0.8795	0.9945	0.9865
	Winnipeg	/	/	1.0000	/	/	1.0000

Vulnerability

Vulnerability is the measure of flood severity. Table 11 compares the frequency of floods calculated for different climate change scenarios. In the Assiniboine River basin, the

scenario S2 of CGCM1 generated 40 flood evens at the Shellmouth dam and its neighboring towns. This number exceeds those from the scenario S1 of ECHAM4 model and two scenarios of HADCM3 model. Scenario S1 of HADCM3 generated 23 events at the Shellmouth dam and the control scenario generated 26 events. In the Red River basin, a significantly different result have been obtained. Scenario S1 and control scenario of HADCM3 resulted in 65 and 59 flood events at the Ste. Agathe, respectively. Scenario S2 of CGCM1 generated 29 flood events, and the scenario S1 of ECHAM4 model generated only 12 flood events. The results show that the mechanisms of flood generation under climate change in two river basins are different, because the Assiniboine River flows from west to east, while the Red River flows from south to north.

Table 11. Number of flood events generated by different GCM models

	Location	**HADCM3 Model**		**ECHAM4**	**CGCM1**
		Control	S1	S1	S2
Assiniboine River	Shellmouth Reservoir	26	23	33	40
	Channel Capacity	25	23	32	40
	Russell	25	22	32	40
	St Lazare	25	23	32	40
	Miniota	5	4	5	14
	Griswold	5	4	5	14
	Brandon	5	4	5	13
	Holland	5	4	5	13
	Portage	5	4	4	13
Red River	Ste. Agathe	59	65	12	29
	Winnipeg*	0	1	0	0

*** Calculated with high reliability criteria (KGS, 2000)**

Table 12. Mean vulnerability - HADCM3 model

	Location	**Control**			**S1**		
		Min.	Max.	Mean	Min.	Max.	Mean
Assiniboine River	Upstream flooded area	44.77	727.00	639.57	27.29	727.00	682.25
	Shellmouth Reservoir (m)	0.07	12.77	3.43	0.08	11.56	3.23
	Downstream flooded area	257.02	61497.24	7676.92	26.68	55111.16	6294.81
	Channel Capacity	1055.54	14199.80	2366.63	1054.88	10817.07	2093.93
	Russell	1091.19	15161.99	2493.19	1092.83	11481.82	2248.53
	St Lazare	267.65	16441.65	1880.94	266.83	12279.20	1545.38
	Miniota	2218.34	17666.11	7679.64	1180.83	12799.09	6790.34
	Griswold	2410.17	19402.72	8417.60	1268.92	14049.00	7439.38
	Brandon	2071.19	20763.00	8679.36	815.81	14873.89	7603.31
	Holland	2899.41	27168.97	11487.47	1259.76	19639.32	10127.09
	Portage	1970.80	28700.08	11420.49	175.61	20278.67	9881.74
Red River	Ste. Agathe (m^3/s)	3.22	1452.64	429.53	13.45	2588.38	457.59
	Winnipeg* (m^3/s)				682.86	682.86	682.86

*** Calculated with high reliability criteria (KGS, 2000)**

Table 13. Mean vulnerability – ECHAM4 and CGCM1 models

	Location	ECHAM4			CGCM1		
		S1			S2		
		Min.	Max.	Mean	Min.	Max.	Mean
	Upstream flooded area	37.50	600.00	535.71	116.89	727.00	556.62
	Shellmouth Reservoir (m)	0.08	8.93	3.43	0.09	14.37	5.30
	Downstream flooded area	283.54	28466.98	3191.50	283.72	85028.70	12848.34
	Channel Capacity	1055.81	4709.89	1579.36	1055.51	19655.03	3315.03
	Russell	1091.60	5012.38	1653.79	1091.44	20978.12	3511.70
	St Lazare	267.97	4764.31	912.20	267.61	23154.31	3047.94
	Miniota	631.61	4243.25	2731.78	73.86	25357.94	7773.52
	Griswold	664.77	4637.57	2974.96	51.25	27863.73	8520.87
Assiniboine River	Brandon	151.25	4521.33	2692.45	1088.99	30070.10	9509.62
	Holland	397.68	6045.26	3664.30	1601.64	39311.84	12535.74
	Portage	1793.67	5474.51	3767.69	566.25	42009.25	12607.76
Red River	Ste. Agathe (m^3/s)	9.97	1113.92	281.71	8.48	1823.03	480.98
	Winnipeg (m^3/s)						

Table 14. Comparison of normalized system vulnerability

	Location	HADCM3		ECHAM4	CGCM1
		Control	S1	S1	S2
	Shellmouth Reservoir	0.0024	0.0023	0.0024	0.0038
	Channel Capacity	1.4791	1.3087	0.9871	2.0719
	Russell	1.4247	1.2849	0.9450	2.0067
	St Lazare	0.6270	0.5151	0.3041	1.0160
	Miniota	1.6340	1.4448	0.5812	1.6539
	Griswold	1.6188	1.4306	0.5721	1.6386
Assiniboine River	Brandon	1.3777	1.2069	0.4274	1.5095
	Holland	1.4359	1.2659	0.4580	1.5670
	Portage	1.1420	0.9882	0.3768	1.2608
Red River	Ste. Agathe	0.3068	0.3268	0.2012	0.3436
	Winnipeg*		0.3397		

*** Calculated with high reliability criteria (KGS, 2000)**

Flood severity was assessed using vulnerability indicator. Tables 12 and 13 present the mean vulnerability for flood events, while Table 14 shows the mean vulnerability normalized by the failure flow at each location.

A number of physical indicators were used to assess the system vulnerability as discussed in the section 4.2 of this report. In the Shellmouth Reservoir, the scenario S2 of CGCM1 generated the highest reservoir water level of 14.37 m and the mean vulnerability of 5.3 m, while other scenarios did not show a significant difference in the maximum reservoir water level and the mean vulnerability. For the current reservoir operation rules, control and S1 scenarios of HADCM3 resulted in larger upstream flooding area than the scenario S1 of ECHAM4 model and the scenario S2 of CGCM1 model. Scenario S2 of CGCM1

however generated the largest downstream flooding. For downstream locations along the Assiniboine River, the mean and normalized vulnerabilities generated by the scenario S1 of HADCM3 are lower than those generated by the control scenario.

In Red River basin, the scenario S1 of HADCM3 results in the higher mean and normalized vulnerabilities at the Ste. Agathe than the control scenario. Of the four scenarios of three GCM models, the scenario S1 of ECHAM4 model generated the lowest average and normalized vulnerability at the Ste. Agathe, while the scenario S2 of CGCM1 resulted in the largest. In Winnipeg, scenario S1 of HADCM3 generated one flood event under high reliability. Peak flood flow of 5,668 m^3/s exceeds the reliability flow by 682.86 m^3/s, but is still 391 m^3/s smaller than the low reliability flow as established by KGS (2000). The results are demonstrating that that the current capacity of flood protection system for the City of Winnipeg is sufficient under the low reliability criteria, but there is some risk under the high reliability criteria.

Resiliency

Resiliency represents the ability of flood protection system to return to a satisfactory state when a failure has occurred. Mean, yearly minimum and maximum resiliency are presented in Tables 15-16. At the Shellmouth dam, the mean resiliency and the range of yearly resiliency generated for the control scenario of HADCM3 are greater than those obtained by the scenario S1 of HADCM3. This is the indication that, under the climate change conditions, the ability of the reservoir to return to a satisfactory state will decline. However, the same scenario S1 of HADCM3 compared to the control scenario results in a much higher mean resiliency and minimum yearly resiliency at the downstream locations from the reservoir. When comparing all four scenarios from the three GCM models, the scenario S2 of CGCM1 results in the lowest mean resiliency and yearly minimum resiliency. Results from all scenarios also show that the mean resiliency and the minimum yearly resiliency at downstream locations are higher than those at the reservoir location. The firm conclusion is that the Shellmouth reservoir greatly increases the resiliency of flood protection at the downstream locations along the Assiniboine River.

In the Red River basin, the scenario S1 of HADCM3 generates lower mean resiliency and minimum yearly resiliency at Ste. Agathe than the control scenario as shown in Table 15. Of the four scenarios from the three GCM models, the scenario S1 of ECHAM4 model and the scenario S2 of CGCM1 generated greater mean resiliency than two scenarios of HADCM3 did. The scenario S1 of ECHAM4 model generated the greatest mean resiliency value of 46.81. At the Winnipeg, only the scenario S1 of HADCM3 resulted in one flood with the resiliency of 24 under the high reliable criteria (KGS, 2000).

Summary

The climate variability and change may cause an increase in annual discharge in the Red River basin, and shift ahead in flood starting time and peak occurrence time in both, the Assiniboine and the Red River basins. Four scenarios of the three GCM models did not produce a significant difference in the distribution of flood peak values in the Assiniboine

River upstream from the Shellmouth Reservoir. The two scenarios of HADCM3 model show higher flood peak values than other scenarios of ECHAM4 and CGCM1 models.

Table 15. Comparison of resiliency calculated using the HADCM3 model

	Location	**HADCM3 Model**					
		Control			S1		
		Min.	Max.	Mean	Min.	Max.	Mean
	Shellmouth Reservoir	6.32	72.00	23.20	8.37	51.43	19.53
	Channel Capacity	6.43	180.00	41.62	8.57	360.00	48.10
	Russell	6.55	360.00	46.44	8.57	120.00	30.93
	St Lazare	6.43	180.00	41.62	8.57	360.00	48.10
	Miniota	14.40	36.00	26.02	18.95	45.00	27.91
	Griswold	14.40	36.00	26.02	18.95	45.00	28.20
	Brandon	15.65	51.43	31.72	21.18	72.00	37.10
Assiniboine River	Holland	15.00	45.00	29.64	21.18	60.00	33.42
	Portage	16.36	60.00	35.90	22.50	180.00	66.05
Red River	Ste. Agathe	9.73	360.00	34.33	6.55	120.00	26.09
	Winnipeg*				24.00	24.00	24.00

*** Calculated with high reliability criteria (KGS, 2000)**

Table 16. Comparison of resiliency - ECHAM4 and CGCM1 models

	Location	**ECHAM4 Model**			**CGCM1 Model**		
		S1			S2		
		Min.	Max.	Mean	Min.	Max.	Mean
	Shellmouth Reservoir	4.93	72.00	21.29	3.35	60.83	15.37
	Channel Capacity	5.00	180.00	31.20	3.97	182.50	27.18
	Russell	5.00	120.00	29.57	4.01	182.50	27.64
	St Lazare	5.00	180.00	31.20	3.97	182.50	27.18
	Miniota	17.14	51.43	31.25	11.77	121.67	30.50
	Griswold	17.14	51.43	31.25	11.77	121.67	30.77
	Brandon	30.00	120.00	47.33	12.17	45.63	27.03
Assiniboine River	Holland	18.95	90.00	40.47	12.59	40.56	26.80
	Portage	32.73	51.43	38.22	12.59	73.00	33.61
Red River	Ste. Agathe	9.00	180.00	46.81	8.30	182.50	40.92
	Winnipeg						

The results are confirming that the different mechanisms drive the flood generation in these two rivers. Analysis of reliability shows that the Shellmouth Reservoir increases downstream reliability. The present level of flood protection for the city of Winnipeg is sufficient under the low reliability (KGS, 2000) even that the scenario S1 of HADCM3 resulted in one flood larger than that of 1997.

6. Conclusions

6.1 Methodology

Climate variability and change may result in serious consequences for large-scale flood protection systems (Klemes, 1985; Burn and Simonovic, 1996). It is necessary to use reliable hydroclimatologic information for evaluating the impact of changing climatic conditions on existing flood protection systems. This study provided a framework for investigating the effectiveness of large-scale flood protection system under changing climatic conditions, and developed a regional dynamic hydroclimatologic assessment model for determining the impact of climate variability and change on flood protection system in the Red River basin. The model involves projected climate variability and change scenarios; hydrologic processes modeling; and the assessment of the performance of flood protection system using statistical indicators of reliability, vulnerability and resiliency.

The global circulation model, as a digital analogue to the real climatic system, is the most comprehensive way to predict a change in climate. Although the realistic simulation of climatic phenomena is limited due to their coarse grids and the assumptions of static or unchanging boundary conditions (Cubasch and Cess, 1990), existing GCMs still could provide the clearest picture of climate change at large scale and generate daily and monthly climate change data under different climate variability and change scenarios.

Hydrologic processes' modeling is based on the use of System Dynamics approach. System dynamics provides an effective modeling methodology for organizing and integrating existing information available on hydrologic processes in a watershed system, especially temperature and precipitation data available from observation and prediction of global climate models. Hydrologic model proposed in this study closely follows the dynamic processes of hydrologic cycling in a watershed. The model clarifies both, the interactions among surface-subsurface storage and the role of temperature change on canopy size, soil physical state and flood generation. The model has defined a clear boundary, *i.e*. the model explained key variables for generating the hydrologic system behavior. Dynamic behavior of streamflow is generated by the internal feedback structure and the strong external disturbance. Calibration and verification of the hydrologic model show that simulated streamflow responds appropriately to the disturbance in temperature and precipitation patterns as well as the moisture interaction among surface storage, subsurface soil storage and groundwater storage. The comparison of results from simulation and observation indicates that the model can well reproduce the observed flood starting time, peak time and peak duration. The model can be used to make a long-term prediction of streamflow under different climate change scenarios.

Three measures of effectiveness of flood protection systems used in this study include reliability, vulnerability and resiliency. Those measures describe system failure frequency (reliability), severity (vulnerability), and system effectiveness to recover from a failure

state (resiliency). These criteria are used to assist in evaluating the performance of large-scale flood protection system under climate variability and change.

The original modeling framework (DYHAM) for assessment of climate variation and change impacts on the performance of complex flood protection system has been tested using the Red River basin as a case study. The modeling framework developed herein could be readily employed to conduct the assessment of effectiveness of flood protection system under climate variability and change. The DYHAM provides an environment for assessing the impacts of climate variability and change on the effectiveness of large-scale flood protection system. It allows for a long-term evaluation of different climate change scenarios generated by GCM models. The methodological aspect of this modeling framework can be applied to the broad range of water resources management problems.

6.2 Impact of climate variability and change on the flood protection in the Red River basin

This study has generated a number of very important conclusions that are of relevance for the flood protection in the Red River basin:

(i) Use of three different GCM models results in different patterns of temperature and precipitation in the Red River basin. There is no clear indication which model should be used in order to predict future climate state in the basin. Considerable research is still required in order to bring GCM models to the level to be of real value in predicting future hydrological conditions on the watershed scale. Coarse grid and the lumped hydrologic model structure of GCM models ignoring the regional variation of climate, mantle and soil properties, warrants further work to improve their ability to predict future flood events.

(ii) Use of three different GCM models and four climate scenarios generated different output in the Red River basin. However, despite the differences between the models and the scenarios, the application of DYHAM revealed with consensus that the annual precipitation and the annual streamflow volume in the Red River basin might increase under the future climate change scenarios. Flood starting time and peak time might also shift earlier under the future climate change scenarios. In other words, the possible increase in temperature predicted by almost all GCM models will provide favorable hydrometeorological conditions in the Red River basin that will result in smaller floods occurring earlier in the year.

(iii) The results of this study indicate that the capacity of existing Red River flood protection system including: Shellmouth Reservoir; Portage Diversion; Red River Floodway; and the diking system along the both rivers; is sufficient to accommodate future climate variability and change if the low reliability criteria (KGS, 2000) is used. In the case of the application of high reliability criteria, future increase of flood protection capacity is warranted.

Acknowledgements

This work was made possible by a financial support from the Natural Resources Canada through the Climate Change Action Fund. The authors would like to thank Environment Canada for providing climate and streamflow records for both, the Assiniboine River basin and the lower reaches of the Red River; Department of Water Resource, Manitoba Conservation for providing watershed characteristics; the Minnesota Climatologic Working Group creating a gateway to access the National Weather Service databanks and retrieve the climate data for the Red River basin; the USGS for offering real streamflow records in lower reaches of the Red River; and the Hadley Centre of UK, Canadian Centre for Climate Modelling and Analysis, and the Max-Planck-Institut für Meteorologie (MPI) and Deutsches Klimatechenzentrum (DKRZ) of Germany for providing predicted daily climate change data.

All the data used in this research are available on the CD ROM upon request.

References

Ahmad, S. and S. Simonovic, 2000. 'System Dynamics of Reservoir Operations for Flood Management', *Journal of Computing in Civil Engineering*, 14(3):190-198.

Aitken, A.P., 1973. 'Assessing systematic errors in rainfall-runoff models', *Journal of Hydrology*, 20:121-136.

Anderson, E.A., 1973. 'National weather service river forecast system—snow accumulation and ablation model'. *NOAA Tech. Memo*. NWS HYDRO-17, US Dept. Commer., Washington, DC, USA.

Arp, P. A. and X. Yin, 1992. 'Prediction water fluxes throughout forests from monthly precipitation mean monthly air temperature records'. *Canadian Journal of Forest Research*, 22:864-877.

Bicknell, B.R., Imhoff, J.C., Kittle, J.L., Jr., Donigian, A.S., Jr., and Johanson, R.C., 1997, 'Hydrologic Simulation Program—Fortran', *User's manual* version 11: U.S. Environmental Protection Agency, National Exposure Research Laboratory, Athens, Ga., EPA/600/R-97/080, 755 p.

Bobba, A.G. and D.C.L. Lam, 1990. 'Hydrologic modeling of acidified Canadian watersheds'. *Ecological Modeling*, 50:5-32.

Brent, F. and Z. Yu. 1999. 'An Evaluation of Two Hydrologic models for Climate Change Scenarios'. *Journal of the American Water Resources Association*, 35(6):1351-1363.

Burn D. H., and S. P. Simonovic, 1986. 'Sensitivity of reservoir operation performance to climatic change'. *Water Resources Management*, 10:463-478.

Burn, D.H., H.D. Venema, and S.P. Simonovic 1991. 'Risk-Based Performance Criteria for Real-Time Reservoir Operation', *Canadian Journal of Civil Engineering*, 18(1):36-42.

Cubasch, U. and R.D. Cess. 1990. 'Processes and modeling'. In: *Climate Change: The IPCC Scientific Assessment*. (Eds) J.T. Houghton, G.J. Jenkins and J. J. Ephraums, Cambridge University Press, Combridge, UK.

Ehrman, J.M., K. Higuchi and T.A. Clair, 2000. 'Backcasting to test the use of neural networks for predicting runoff in Canadian rivers'. *Canadian Water Resources Journals*, 25(30):279-291.

Fletcher, E. J., 1998. 'The use of system dynamics as a decision support tool for the management of surface water resources'. *Proceedings* of the 1st International conference on new information technology for decision-making in Civil Engineering, University of Quebec, Montreal, Canada, 909-920.

Forester, J. W., 1968. *Principles of Systems*. 2nd edit. Productivity Press, MA.

Gleick, P. H. 1989. 'Climate change, hydrology, and water resources'. *Reviews of Geophysics*. 27(3):329-344.

Gray, D. M. and D. H. Male, 1981. *Handbook of snow*. Pergamon Press, New York.

Gutierrez, L. T. and W. R. Fey, 1980. *Ecosystem succession: A general hypothesis and test model of a grassland*. MIT press, Cambridge, MA.

Hashimoto, T., Stedinger, J. R. and Loucks, D. P. 1982. 'Reliability, resiliency and vulnerability criteria for water resources systems performance evaluation', *Water Resources Research*, 18(1):14-20.

High Performance System, Inc., 1997. *Technical Documentation*—STELLA, 255p.

Houghton, J. J., L. G. Meiro Fihlo, B. A. Callander. N. Harris, A. Kattenberg, And K. Maskell (Editors), 1996. *Climate Change 1995*: The Science of Climate Change. Contribution of Working Group I to the Second Assessment Report of the Intergovernmental Panel on Climate Chang (IPCC). Cambridge University Press, Port Chester, New York.

Hsu, K-L., H.V. Gupta and S. Sorooshian, 1995. 'Artificial neural network modeling of the rainfall-runoff process'. *Water Resources Bulletin*, 25:483-490.

International Joint Commission, 1999. *Flood Protection for Winnipeg*, A report to the Government of Canada and the United States on reducing flood impacts in the Red River Basin, Ottawa and Washington, 186p.

International Joint Commission, 2000. *Living with the Red*, A report to the Government of Canada and the United States on reducing flood impacts in the Red River Basin, Ottawa and Washington, 273p.

Karl, T. R., R. W. Knight, D.R. Easterling, and R.G. Quayle, 1996, 'Indices of Climate Change for the United States'. *Bulletin of the American Meteorological Society* 77:279-292.

Keys, A. M., and Palmer, R. 1993. 'The role of object oriented simulation models in the drought preparedness studies'. *Proceedings*, 20th Ann. Nat. Conf., Water Resources Planning and Management Div., ASCE, New York, 479-472.

Kite, G. W., 1998. *Manual for the SLURP Hydrologic Model*, V. 11. National Hydrology Research Institute, Saskatoon, 159pp.

Kite, G. W., A Dalton and K. Dion, 1994. 'Simulation of streamflow in a macroscale watershed using general circulation model data'. *Water Resources Research*, 30:1547-1559.

Klemes, V. 1985. 'Sensitivity of water resources systems to climate variations'. *World Climate Problem Report*. WCP-98, World Meteorological Organization, pp.115.

Kontzamanis-Graumann-Smith-MacMillan Inc. (KGS Group), 1999. *Red River Basin: Stage- Damage Curves Update and Preparation of Flood Damage Map*s. Winnipeg, Manitoba, January.

Kontzamanis-Graumann-Smith-MacMillan Inc. (KGS Group), 2000. *Flood Protection for Winnipeg, Part III - Prefeasibility Study*. Winnipeg, Manitoba, March 2000.

Leavesley, G.H., Lichty, R.W., Troutman, B.M., and Saindon, L.G., 1983, 'Precipitation-Runoff Modeling System', *User's Manual*: U.S. Geological Survey Water-Resources Investigations Report 83-4238, 207 p.

Lettenmaier, D.P, E. F. Wood, and J. R. Wallis, 1994. 'Hydro-climatological Trends in the Continental United States, 1948-1998'. *Journal of Climate*, 7:586-607.

Lewis, J. E. 1989. 'Climate Change and Its effects on Water Resources for Canada: A Review'. *Canadian Water Resources Journal*, 14(1):34-55.

Manley, R. E., 1982. *HYSIM - a general purpose hydrologic model*, Pisa Symposium in 1978. Pergamon Press.

Martinec, J., 1960. 'The degree-day factor for snowmelt runoff forecasting', *IAHS Publication* No. 51, 468-477.

Martinec, J., 1970. 'Study of snowmelt runoff process in two representative watersheds with different elevation range', *IAHS- Unesco Symposium*, Wellington, N.Z., IAHS Publ. No. 96, 29-39.

Martinec, J., 1975. 'Snowmelt-Runoff Model for stream flow forecasts', *Nordic Hydrology*, 6(3):145-154.

Martinec, J., Rango, A. and Major, E., 1983. 'The Snowmelt-Runoff Model (SRM)' *User's Manual*, NASA Reference Publication 1100, Washington, D.C., 118 pp.

Moy, W.S., Cohon, J. L. and ReVelle, C. S. 1986. 'A programming model for the analysis of the reliability, resiliency and vulnerability of a water supply reservoir'. *Water Resources Research*, 22:489-498.

Palmer, R., Hilton, K., and M. Hahn, 1995. 'Wilamette river basin reauthorization feasibility study'. (http://maximus.ce.washington.edu/~willamet/).

Palmer, R., Keyes, A/ M/, and Fisher, S., 1993. 'Empowering stakeholders through simulation in water resources planning'. *Proceedings* of Water management for the '90s. ASCE, New York, 451-454.

Palmer, R.. 1994. (ACT-ACF) 'River basin planning study'. (http://maximus.ce.washington.edu/~actacf/).

Putty, M.R.Y. and R. Prasad, 2000. 'Understanding runoff processes using a watershed model—a case study in the Western Ghats in South India'. *Journal of Hydrology*,.. 228:215-227.

Richardson, G. P., 1991. *Feedback thought in social science and systems theory*. University of Pennsylvania Press. Philadephia. PA.

Rumelhardt, D.E. and J. L McLelland. 1986. *Parallel distributed processing explorations in the microstructure of cognition*. MIT Press. Cambridge, MA.

Senge, P. M., 1990. *The fifth discipline*, Doubleday, New York.

Simonovic, S. P. 1992. 'Reservoir Systems Analysis: closing gap between theory and practice'. *Journal of Water Resources Planning and Management, ASCE*, 118 (3): 262-280.

Simonovic, S. P. and Fahmy, H. 1999. 'A New modeling approach for water resources policy analysis'. *Water Resources Research*. 35(1):295-304.

Simonovic, S. P., Fahmy, H. and El-Shorbagy, A. 1997. 'The use of object oriented modeling for water resources planning in Egypt'. *Water Resources Management*. 11(4):243-261.

Simonovic, S. P., H. D. Venema and D. H. Burn. 1992. 'Risk-based parameter selection for short-term reservoir operation'. *Journal of Hydrology*, 131:269-291.

Singh, P. and N., Kumar, 1996. 'Determination of snowmelt factor in the Himalayan region'. *Hydrologic Sciences Journal*, 41:301-310.

Thomas, R. B. and W.F. Megahan, 1998. 'Peak flow responses to clear-cutting and roads in small and large basins, Western Cascades, Oregon: a second opinion'. *Water Resources Research*, 34:3393-3403.

Zealand, C.M., D.H. Burn, and S.P. Simonovic, 1999. 'Short-term Streamflow Forecasting Using Artificial Neural Networks', *Journal of Hydrology*, .214(1-4):32-48.

US Army Corps of Engineers, 1971. *Runoff eveluation and streamflow simulation by computer*. Part-II, US Army Corps of Engineers. North Pacific Division, Portland, Oregon, USA.

Warkentin, A.A., 1999. *Hydrometeorologic Parameter Generated Floods for Design Purposes*, Manitoba Department of Natural Resources

World Meteorological Organization, 1970. *Guide to hydrometeorological practices*. WMO-No. 168. TP.82, Geneva, Switzerland.